JOURNAL OF PROTEOMICS 110 (2014) 93–106

Available online at www.sciencedirect.com

ScienceDirect

www.elsevier.com/locate/jprot

SKIP and BIR-1/Survivin have potential to integrate proteome status with gene expression

David Kostrouch[a], *Markéta Kostrouchová*[a], *Petr Yilma*[a], *Ahmed Ali Chughtai*[a], *Jan Philipp Novotný*[a], *Petr Novák*[b], *Veronika Kostrouchová*[a], *Marta Kostrouchová*[c], *Zdeněk Kostrouch*[a,*]

[a]*Laboratory of Molecular Pathology, Institute of Cellular Biology and Pathology, First Faculty of Medicine, Charles University in Prague, Czech Republic*
[b]*Laboratory of Structure Biology and Cell Signaling, Institute of Microbiology, Czech Academy of Sciences, Vídeňská 1083, Prague, Czech Republic*
[c]*Laboratory of Molecular Biology and Genetics, Institute of Cellular Biology and Pathology, First Faculty of Medicine, Charles University in Prague, Czech Republic*

ARTICLE INFO

Article history:
Received 12 May 2014
Accepted 22 July 2014

Keywords:
BIR-1
Gene expression
Ribosomal stress
SKIP
Survivin
Proteome

ABSTRACT

SKIP and BIR are evolutionarily conserved proteins; SKIP (SKP-1) is a known transcription and splicing cofactor while BIR-1/Survivin regulates cell division, gene expression and development. Their loss of function induces overlapping developmental phenotypes. We searched for SKP-1 and BIR-1 interaction on protein level using yeast two-hybrid screens and identified partially overlapping categories of proteins as SKIP-1 and BIR-1 interactors. The interacting proteins included ribosomal proteins, transcription factors, translation factors and cytoskeletal and motor proteins suggesting involvement in multiple protein complexes. To visualize the effect of BIR-1 on the proteome in *Caenorhabditis elegans* we induced a short time pulse BIR-1 overexpression in synchronized L1 larvae. This led to a dramatic alteration of the whole proteome pattern indicating that BIR-1 alone has the capacity to alter the chromatographic profile of many target proteins including proteins found to be interactors in yeast two hybrid screens. The results were validated for ribosomal proteins RPS3 and RPL5, non-muscle myosin and TAC-1, a transcription cofactor and a centrosome associated protein. Together, these results suggest that SKP-1 and BIR-1 are multifunctional proteins that form multiple protein complexes in both shared and distinct pathways and have the potential to connect proteome signals with the regulation of gene expression.

Biological significance
The genomic organization of the genes encoding BIR-1 and SKIP (SKP-1) in *C. elegans* have suggested that these two factors, each evolutionarily conserved, have related functions. However, these functional connections have remained elusive and underappreciated in light of limited information from *C. elegans* and other biological systems. Our results provide further evidence for a functional link between these two factors and suggest they may transmit proteome signals towards the regulation of gene expression.

* *Corresponding author at:* Laboratory of Molecular Pathology, Institute of Cellular Biology and Pathology, First Faculty of Medicine, Charles University in Prague, Ke Karlovu 2, 128 00 Prague 2, Czech Republic. Tel.: +420 22496 7090; fax: +420 22496 7092.
E-mail address: zdenek.kostrouch@lf1.cuni.cz (Z. Kostrouch).

http://dx.doi.org/10.1016/j.jprot.2014.07.023
1874-3919/

1. Introduction

Regulation of gene expression is the basis of proper function of organisms, their development and metabolism. It is executed at the level of chromatin by transcription factors, which recognize and bind specific regions in promoters of genes, and in cooperation with transcription cofactors attract and activate Polymerase II complex proteins. Further, downstream mechanisms then modulate gene expression at the level of RNA splicing and mRNA processing, nuclear export and translation into proteins. Tissue and metabolic state specific transcription factors and cofactors that are expressed in response to specific developmental and metabolic stimuli direct proper gene expression to cope with particular developmental and metabolic needs at the level of cells, tissues and whole organisms. This basic regulatory network is likely to include additional mechanisms that sense the functional and structural cellular states and link them with gene expression regulation for achievement of a precise and fast regulatory response.

SKIP is an ancient transcription cofactor found in all multicellular organisms as well as in yeast. It was originally identified as BX42, a *Drosophila* nuclear protein associated with active transcription (puffs) on polytene chromosomes [1,2] and later found in many species including *Dictyostelium discoideum* [3] and yeast [4]. SKIP interacts with several transcription factors including nuclear receptors [5–8], Notch [9], Wnt/beta catenin [10], TGF beta and Smad protein complexes [11] and it was also identified as a component of splicing machinery in yeast, mammals [12] and plants [13]. It was identified in both transcription activating as well as transcription inhibiting complexes [14]. In *Caenorhabditis elegans*, SKIP is indispensable for normal development and its inhibition results in multiple phenotypes including larval transition and molting that is dependent on NHR-23 [15].

In *C. elegans*, SKIP (SKP-1) is organized in an operon together with a mitotic and microtubule organizing protein BIR-1 [15], a homologue of the vertebrate protein Survivin that is expressed predominantly in fast dividing cells and is found upregulated in most if not all human cancers [16]. Since operons ensure that co-organized genes are co-expressed, at least at the transcriptional level, we hypothesized that these two proteins may be linked functionally. We previously showed in *C. elegans* that both BIR-1 and SKIP are involved in the regulation of gene expression and development. Moreover, in a heterologous transfection system with thyroid receptor/tri-iodothyronine, these factors act cooperatively in activating expression [17].

In this study, we sought to identify SKP-1 and BIR-1 involvement in a protein regulatory network by searching for their interacting proteins using yeast two-hybrid screens. Surprisingly, this strategy indicated that SKP-1 and BIR-1 interact with a wide variety of partially overlapping categories of proteins but not directly with each other. The regulatory potential of BIR-1 was visualized using a short time overproduction of BIR-1 in synchronized *C. elegans* larvae and by a whole proteome differential display. This confirmed that elevated levels of BIR-1 project to immediate whole proteome changes. The results were validated for ribosomal proteins RPS3 and RPL5, non-muscle myosin and TAC-1, a transcription cofactor and a centrosome associated protein implicated in cancer. Our results show that SKP-1 and BIR-1 are linked more than previously thought. They have potential to link the proteome status with major cellular regulatory pathways including gene expression, ribosomal stress pathway, apoptosis and cell division. SKP-1 and BIR-1 may be regarded as proteome sensors.

2. Materials and methods

2.1. Experimental design

Screening for interacting proteins of BIR-1 and SKP-1 was performed using the ProQuest Two-Hybrid System with Gateway Technology purchased from Invitrogen (Carlsbad, California, USA). Potential direct interactions between BIR-1 and SKP-1 were analyzed using the same system. The effect of a short-time forced expression of BIR-1 on the near-complete proteome of nondividing cells of *C. elegans* L1 larvae was visualized by two dimensional comparative chromatography using the Proteome fractionation system from Beckman Coulter (Brea, CA, USA) and fractions with differential protein content were visualized by DeltaVue software and were further examined by mass spectrometry. Selected proteins identified as BIR-1 and SKP-1 interacting proteins or proteomic targets of BIR-1 were analyzed in pull-down experiments using BIR-1 and SKP-1 GST-fusion proteins. Analyzed target proteins were expressed in vitro using the reticulocyte TNT system from Promega (Fitchburg, WI, USA) and labeled by ^{35}S-methionine (Institute of Isotopes Co., Budapest, Hungary). Bound interacting proteins were detected by Liquid scintillation analyzer Tri-Carb 1600TR Packard (Meriden, CT, USA). The effect of BIR-1 short-time overexpression on selected candidate interacting proteins was visualized using immunohistochemistry or by functional studies of cell cycle and apoptosis (employing immunohistochemistry and lines carrying integrated GFP fusion transgenes).

2.1.1. Strains used in the study

The *C. elegans* Bristol N2 strain was used whenever not specifically stated and was maintained as described [18]. For visualization of chromatin structure, the line AZ212 expressing Histone H2B::GFP was used.

BIR-1 overexpressing worms were created as lines expressing *bir-1* mRNA from heat-shock regulated promoter and were prepared by amplifying *bir-1* cDNA from wild-type mRNA. Sub-cloned and sequence verified constructs were cloned into the heat-shock promoter vector pPD49.83. 100 ng/μl of plasmid DNA was microinjected along with a marker plasmid pPRF4, *rol-6* (*su10060*) using an Olympus IX70 inverted microscope (Olympus, Tokyo, Japan) equipped with a PC-10 Narishige Microinjection System (Narishige, Tokyo, Japan).

2.2. Yeast two-hybrid screens

To identify BIR-1 and SKP-1 interacting proteins, we used the ProQuest Two-Hybrid System with Gateway Technology purchased from Invitrogen. The *C. elegans* mixed stages (Bristol N2) library (originally made by Monique A. Kreutzer and Sander van den Heuvel) was purchased from Invitrogen (Cat. No. 11288-016). *bir-1* and *skp-1* cDNAs were amplified

from N2 mixed stages cDNA using primers having flanking sequences ATT and ligated into the pENTRY vector. After cloning the cDNAs, the inserts containing complete coding regions were transferred into pDEST™32 vector using Clonase leading to DBX constructs (bait vectors) creating BIR-1 and SKP-1 fused to GAL4 DNA binding domain. These vectors were used for screening of the *C. elegans* cDNA library after testing for self activation of both *bir-1* and *skp-1* bait vectors.

The vector pDEST 32 includes the GAL DNA binding domain, the ARS/CEN6 sequence for replication and maintenance of low copy numbers in yeast, the LEU2 gene for selection in yeast on medium lacking leucine, the constitutive moderate-strength promoter and transcription terminator of the yeast Alcohol Dehydrogenase gene (ADH1) to drive expression of the GAL4 DBD bait fusion, the dominant CYH 2S allele that confers sensitivity to cycloheximide in yeast for plasmid shuffling, a pUC-based replication origin and gentamicin resistance gene (Gmr) for replication and maintenance in *Escherichia coli*.

For the analysis of BIR-1 binding to SKP-1, pDEST™22 vector containing a GAL4 Activation Domain (GAL4 AD) containing Gateway® Destination Vector was used.

Similarly, the constructs for SKP-1 were prepared using the same vectors. To reduce false positive interactants, the "Three Reporter Genes" system was used (HIS3, URA3 and lacZ stably integrated in the yeast genome). Additional controls included yeast control strains A to E, a self-activation test of the bait constructs, and a test of growth on histidine deficient media. For both BIR-1 and SKP-1 interacting proteins a total of 250 μl of competent cells containing more than 10^6 transformants were acquired. Screening yielded 54 colonies for SKP-1 and approximately 30 for BIR-1 that were prepared as yeast minipreps, screened by PCR using primers 5036 and 5037 (derived from pPC86 vector) and sequenced. All sequences were controlled for proper frame ligation of the insert by sequencing.

2.3. Two-dimensional comparative chromatography

Two-dimensional chromatographic separation of worm lysates was performed on the ProteomeLab PF 2D Protein Fractionation System (Beckman Coulter, Inc., Fullerton, CA) as recommended by the manufacturer. The chromatograms were analyzed using computer software provided by the manufacturer.

In order to detect differences in proteomes of mutant and wild-type larvae we prepared total protein from synchronized, bleached N2 L1 worms and homozygous *bir-1* animals. Proteomes were then analyzed using PF2D. In the first dimension all proteins were separated into 37 fractions by chromatofocusing, according to their isoelectric point, and eluted by a pH gradient. Proteins with an isoelectric point below pH 4.0 were then eluted by a rising concentration of NaCl (by rising ionic strength). Each of the 37 fractions was then further separated into an additional 35 fractions in the second dimension according to hydrophobicity by reversed-phase chromatography.

2.3.1. Preparation of protein lysates

In order to prepare larvae overexpressing *bir-1* in a short time period, we prepared embryos from transgenic hermaphrodites carrying *bir-1* gene regulated by hear-shock responding promoter. Synchronized L1 larvae were prepared by food deprivation. Control larvae were prepared in the same way. Larvae were then exposed to 37 °C for 20 min, left for 20 min at room temperature to recover and incubated for an additional 30 min at 37 °C. Larvae were than pelleted by centrifugation and frozen in aliquots. In order to obtain sufficient amount of material, these experiments had to be repeated 20 times over the period of 3 month. Control larvae were prepared in parallel in the same number of individual experiments. For preparation of protein lysates, frozen samples were melted on wet ice, pooled in 0.2 ml of 50 mM Tris–HCL (pH 8.0) and vortexed. The samples were then mixed with 1.6 ml of lysis buffer (7.5 M urea, 2.5 M thiourea, 12.5% glycerol, 50 mM Tris, 2.5% n-octylglucoside, 6.25 mM Tris-(carboxyethyl) phosphine hydrochloride containing 1× Protease Inhibitor Cocktail (Boehringer Mannheim, Mannheim, Germany)). The suspensions were incubated on ice for 10 min and sonicated in five cycles, each consisting of four times 10 s sonication/10 s interruption (20 kHz, amplitude 20 μm, 60 W) (Ultrasonic Processor (Cole-Parmers Instruments, Vernon Hills, IL)) using the internal sonication rod. The suspension was cleared from the non-soluble material by centrifugation at 20,000 ×*g* for 60 min at 4 °C and the supernatants were harvested. For subsequent first and second dimension chromatographic separations, the Beckman ProteomeLab PF 2D kit (part No. 380977) (Beckman Coulter, Inc., Fullerton, CA) was used. The sample was supplemented with Start Buffer to a final volume of 2.5 ml. The lysis buffer was then exchanged for the Start Buffer supplied by Beckman using the PD10 column (Amersham Pharmacia Biosciences, Uppsala, Sweden) equilibrated with Start Buffer for the first dimension separation (pH 8.5 ± 0.1, pH adjusted with iminodiacetic acid and ammonium hydroxide). The samples were loaded onto the PD10 columns, the first eluents were discarded. Start Buffer was used to elute the proteins that were collected in the first 3.5 ml fractions. The protein content was estimated using a BCA kit (Pierce, Rockford, IL) (C = 0.62 μg/μl for *bir-1* overexpression and C = 1.06 μg/μl for controls). 1.2 mg of total protein was loaded into the First Dimension Module in a total volume of 2 ml (the volume for control protein lysate was increased to 2 ml using 1× Start Buffer).

2.3.2. First dimension — chromatofocusing HPLC (HPCF)

For the chromatofocusing separation, the first module of the Beckman Coulter ProteomeLab PF 2D system was used (Beckman Coulter, Inc., Fullerton, CA). The HPCF column was equilibrated with 25 column volumes of Start Buffer. The pH gradient was based on the buffers supplied by the manufacturer, the Start Buffer and the Elution Buffer (Beckman Coulter, Inc.; pH adjusted with iminodiacetic acid and ammonium hydroxide). The upper limit of the pH gradient was set by the Start Buffer (pH 8.5) and the lower limit was set by the Elution Buffer (pH 4.0). The pH was monitored using a flow-through on-line probe. Following the pH gradient elution, the proteins remaining in the column were eluted by increasing ionic strength gradient (based on 1 M and 5 M NaCl). Protein content in eluates was determined by UV absorbance at 280 nm. Fractions were collected in 96 well plates (2 ml well capacity). The chromatofocusing fractionation was based on first on time for the first 9 fractions (5 minute intervals), then on pH (in the range of pH 8.5 to 4.0, 17 fractions, steps of pH approximately 0.27) and finally on

ionic strength (1 M NaCl to 5 M NaCl) for the last 14 fractions. The fractions were collected by Beckman Coulter FC/I Module (Fraction collector/injector). The reproducibility of the first (and the second dimension) separation was tested using control material assayed by Western blots for selected nuclear hormone receptors and was satisfactory for both dimensions. A ProteomeLab PF 2D kit containing new buffers and columns was used for the first dimension separation of control proteome and BIR-1 overexpression proteome and both analyses were done in the same day after careful wash and equilibration of the first dimension chromatofocusing HPLC (HPCF) system in an air-conditioned laboratory at 23 °C.

2.3.3. Second dimension — reversed phase HPLC (HPRP — High Performance Reversed Phase Chromatography)

The second module of Beckman Coulter ProteomeLab PF 2D system was used for the separation of proteins according to the surface hydrophobicity with two solvents. Solvent A was 0.1% trifluoroacetic acid (TFA) in water and solvent B was 0.08% TFA in acetonitrile. The aliquots of first dimension fractions were separated on HPRP columns packed with nonporous silica beads at 50 °C. The module was equilibrated with solvent A for 10 min. The gradient was run from 0 to 100% of solvent B for 35 min, followed by an elution with solvent B for 5 min to elute the remaining proteins from the column. The fractions were collected at 1 minute intervals (at the flow rate 0.2 ml/min) into 96 well plates (2 ml well capacity) using Fraction collector FC 204 (Gilson, Inc., Middleton, WI, USA). The module was then washed and equilibrated with solvent A by a 10 minute run and prepared for second dimension separation of another first dimension separation fraction. Fractions were frozen before following mass spectrometry analysis. A total of 1260 fractions were collected for each control proteome and the proteome of BIR-1 overexpressing larvae.

Chromatograms from corresponding paired fractions were then analyzed using 32Karat software. ProteoVue and DeltaVue software enabled us to represent differentially the entire proteome and also individual fractions. Some paired samples required manual compensation for a higher baseline.

The 98 paired fractions that showed prominent differences in major chromatographic peaks were selected for further analysis by mass spectrometry to identify their protein components. Chromatographic fractions that corresponded to identified peaks of paired fractions were prepared and analyzed using liquid chromatography–tandem mass spectrometry (LC/MS/MS) to identify present proteins by peptide microsequencing to derive sequences of individual proteins.

Specific fractions that were chosen for further analysis by mass spectrometry were prepared in the following manner — fractions were dried down into pellets (speed vac), these pellets were then dissolved in 15 μl of cleavage buffer which contained 0.01% 2-mercaptoethanol (Sigma Aldrich, St. Louis, MO, USA), 0.05 M 4-ethylmorpholine acetate pH 8.1 (Fluka (Sigma Aldrich)), 5% MeCN (Merck, Whitehouse Station, NJ, USA), and 10 ng/μl of sequencing grade trypsin (Promega). Digestion was carried out at 37 °C overnight and the resultant peptides were subjected to analysis by mass spectrometry.

Five microliters of the mixture was applied on a Magic-C18 column, (0.180 × 150 mm, 200 Å, 5 μm — Michrom Bioresources, Auburn, CA) and separated by gradient elution. The column was connected to a LCQ^{DECA} ion trap mass spectrometer (ThermoQuest, San Jose, CA) and equipped with a nanoelectrospray ion source. Spectrum analysis was done using SEQUEST™ software against the SwissProt database. SEQUEST results were processed with BioWorks Browser software [19] using the following criteria: XCorr values were 1.7 for singly charged, 2.2 for doubly charged and 3.0 for triply charged peptides [20].

2.4. Bioinformatic analysis

Bioinformatic analysis was done using NCBI bioinformatic tools BLAST [21], gene ontology tool DAVID (http://david.abcc.ncifcrf.gov/) [22,23] and Wormbase WS242 (http://www.wormbase.org). GO terms with the enrichment factor bigger than 2 were considered as significant. Curated GO terms keeping with known functions of either BIR-1 of SKP-1 were considered as criteria of shared functions.

2.5. Pull-down experiments for selected proteins

The complete cDNA of BIR-1 and SKP-1 (not including the first methionine codon) was amplified by PCR and cloned into the pGEX-2T vector (Amersham Pharmacia Biotech, Amsterdam, UK) and sequenced. The GST fusion proteins (Glutathione-S-transferase) were expressed in the BL-21 strain of *E. coli*. Empty pGEX-2T vectors expressing the protein domain of GST were used for control experiments. Cultures of transformed bacteria that were obtained from single bacterial colonies were grown overnight at 37 °C in 400 ml of Luria–Broth medium with 100 μg/ml of Ampicillin. Cultures were grown to an O.D. (600 nm) of 0.8 and subsequently induced by 1 mM isopropyl-thiogalactopyranoside (IPTG), incubated at 20 °C for 5 h and centrifuged to pellets at 3300 ×*g* at 4 °C for 10 min. The pellets were washed twice in LB medium and then resuspended in 6 ml of phosphate-buffered saline (PBS). Cell lysis of bacteria was performed in 6 ml of Lysis buffer (Biorad — 2× Native lysis buffer, CA), that was supplemented with protease inhibitors (1× Complete, Roche, Penzberg, Germany). The samples were incubated on ice for 10 min with intermittent vortexing and sonication (4× for 10 s at 80% intensity) — (Sonicator UP 100 H, Hielscher, Teltow, Germany). The lysates were centrifuged at 10,000 RPM for 5 min. at 4 °C. The supernatant was removed and filtered by ROTH 0.22 μm filter (Carl Roth GmbH, Karlsruhe, Germany). Glutathione–agarose (Sigma-Aldrich, St. Louis, Mo) was used for the binding of GST, GST-SKIP and GST-BIR and was prepared by swelling 0.01 g of beads in 1 ml of PBS, which were then collected by sedimentation and then resuspended in 100 μl of PBS. Purification of fusion proteins and control was done in 100 μl of slurry, 300 μl of bacterial lysates that were incubated for 30 min at 4 °C, and mixed intermittently (every 4 min). Next the beads were washed 4 times in 1 ml of PBS Triton X-100 (1%). Beads were collected by sedimentation and resuspended in 500 μl of PBS. Elution was done in 10 mM reduced glutathione and 50 mM Tris–HCL, pH 9.5 (all chemicals were obtained from Sigma-Aldrich).

The TNT T7/T3 coupled reticulocyte lysate system (Promega) was used to prepare ^{35}S-radiolabeled proteins with 1.48 MBq of ^{35}S-Methionine (37 TBq/mmol) in the final volume of 50 μl (Institute of Isotopes, Budapest, Hungary). Binding was done at 22 °C for 30 min using 10 μl of the TNT

product — mixing every 4 min and then the samples were washed 3× in 1 ml of PBS and resuspended in 40 μl of PBS. Afterwards 5 μl of 2× Laemmli Buffer and 1 μl of β-mercaptoethanol were added. The samples were boiled for 5 min. 35 μl of the sample was used for polyacrylamide gel electrophoresis and autoradiography. 10 μl of supernatant was analyzed using the Liquid Scintillation Analyzer Tri-Carb 1600 TR (Packard, Meriden, CT) and Ultima-Gold scintillation cocktail (Perkin-Elmer, Watham, MA). For determination of input in binding experiments, 2 μl of in-vitro transcribed — translated product was resolved using polyacrylamide gel electrophoresis, transferred on Whitman 3M paper, dried and radioactivity determined in cut strips containing the translated proteins but not the unincorporated ^{35}S-Methionine.

2.6. *skp-1* reduction-of-function effect

The knockdown of *skp-1* was induced by injecting *skp-1* specific dsRNA directly into the gonads of adult wild type N2 hermaphrodites. The progeny was harvested and stained with DAPI and by antibody staining (9 v 5 LA) against SPD-2 that localizes to centrosomes (denominated 9 v 5, LA) (a kind gift of Dr. O'Connell) [24] and used diluted 1:100. We searched for phenotypic changes described earlier [15] and we added screening for cell cycle arrest phenotypes.

2.7. Antibody staining

Antibody experiments (for NMY-2) were done on transgenic embryos and larvae (expressing *bir-1* from heat shock regulated promoter) that were bleached, heated for 30 min at 34 °C and allowed 1 h for recovery at room temperature. Controls were wild type N2 embryos and larvae prepared and heated in parallel to experimental embryos. Embryos and larvae were put on poly-L-lysine-coated slides and fixed by adding 10μl of 5% paraformaldehyde to embryos and larvae that were in 5 μl of water, incubated for 30 min in a wet chamber at room temperature and frozen on a chilled aluminum block for 5 min. After freeze cracking, the samples were placed in cold methanol (−20 °C) and cold acetone (−20 °C) for ten minutes. Rehydratation was done in a series of rehydratation buffers in ethanol (10 min in 90% cold ethanol, 60% cold ethanol, 30% ethanol at room temperature, and 1 h in TTBS — Tris-Tween-buffered saline). The NMY-2 antibody () was then applied in a 1:50 dilution and the slides kept in a wet chamber overnight at 4 °C. The next day the slides were washed 3× in TTBS and a secondary antibody (goat anti rabbit IgG AF 488 antibody, goat anti mouse IgM AF 488 antibody — diluted 1:100) was added. The slides were incubated for 2 h at room temperature, washed 3× in TTBS and mounted in 10 μl of mounting medium.

3. Results

3.1. Yeast two hybrid screens identified transcription and translation regulating proteins as well as structural proteins and ribosomal proteins as BIR-1 and SKP-1 interactors

Previous suggestions of functional connections between SKP-1 and BIR-1 [15,17,25], led us to determine if these two proteins may interact on the protein level, directly or indirectly. We screened for their interacting proteins using yeast two-hybrid screens for both *skp-1* and *bir-1* in a commercially available *C. elegans* library.

Table 1 – Proteins identified as SKP-1 interactors in a yeast two-hybrid screen.

No	Sequence	Gene/protein type
1	F11A3.2/C50F4, NM_073051.1	eIF-2B
2	Y54E2A.3	TAC-1
3	F57B9.6a	INF-1 (orthologous to mammalian eIF-4A)
4	K02F2 (WBGene00001075)	DPY-14
5	W10G6.3	IFA-2 (intermediate filament)
6	4F2011, R08C7.3	H2A.F HTZ-1
7	Y45F10D.13, F56F12.1	SORB-1
8	F54C9.5	RPL-5
9	4K941, K04D7.1	RACK-1
10	C10G11.9, T27A3.4	Mitochondrial protein
11	Y106G6H	PAB-1
12	1E420, T03F1.7	Mitochondrial transcription factor B1
13	T22F3.4 gi|17563233|ref|NM_071607.1|	RPL-11.1
14	gi|671714|gb|L39894.1|CELCPR6A	CPR-6
15	3L413, T07A5	Myosin heavy chain
16	C05C10.4	PHO-11, Intestinal acid phosphatase protein 4 member 2K223
17	4C397, Y41D4B.8	NHR-92 (HNF4-like)
18	W02D7.3	Similar to Ankyrin and KH repeat

The search for SKP-1 interacting proteins identified proteins involved in translation: translation initiation factors 2B and 4A, polyadenylate binding protein PAB-1, ribosomal protein RPL-5 and RPL-11, and transcription cofactor TAC-1, NHR-92 and Myosin Heavy Chain protein (Table 1).

BIR-1 interaction studies yielded NHR-6, acid ribosomal protein RLA-0 and PAL-1, and two Y-box containing cold shock proteins, CEY-1 and CEY-2, that are homologues of vertebrate proteins that regulate gene expression on the level of transcription as well as mRNA in the cytoplasm (Table 2). Neither screen identified a direct interaction between SKP-1 and BIR-1. We also directly tested their potential interaction using the yeast two-hybrid system by cloning BIR-1 in one vector and SKP-1 in the other vector. This system did not

Table 2 – Proteins identified as BIR-1 interactors in a yeast two-hybrid screen.

No	Sequence	Gene/protein type
1	B0546.1	MAI-1
2	ZK1240.9	Ubiquitin ligase
3	C48D5.1	NHR-6
4	T10E10.2	COL-167
5	F32B6.2	MCCC-1
6	C38D4.6	PAL-1
7	F46F11.2	CEY-2
8	D2096.3	Glycoside dehydrogenase
9	F33A8.3	CEY-1
10	F25H2.10	RLA-0

Table 3 – Proteins detected by MS in fractions with chromatographically altered pattern in two-dimensional comparative chromatography.

Protein	Gene	GO (WormBase WS243)
A. Proteins identified only in BIR-1 hyperinduction fractions		
40S ribosomal protein S3	*rps-3*	Apoptotic process, lifespan, embryo dev., molting, larval dev., reproduction, translation
Putative sideroflexin-like protein AH6.2	AH6.2	Cation transport
ATP synthase subunit alpha, mitochondrial precursor	H28O16.1	ATP binding, rotational mech.
60S ribosomal protein L5	*rpl-5*	Body morphogen., embryo and larval dev., reproduction, translation, (apoptosis in vertebrates)
Myosin-4 (UNC-54)	*unc-54*	Morphogen., locomotion, myosin assembly
Nuclear anchorage Protein1	*anc-1*	Cytoskeleton organization, pronuclear migration
B. Proteins identified only in wild type (N2) fractions		
Probable electron transfer flavoprotein subunit	F27D4.1	Embryo and larval dev., mitochondrial
Hit-like protein TAG-202	*tag-202*	Catalytic (tumor suppressor in vertebrates)
Triosephosphate isomerase	*tpi-1*	Catalytic
Uncharacterized protein B0303.3	B0303.3	Metabolic, mitochondrion
Probable 26S protease regulatory subunit S10	*rpt-4*	Morphogenesis, proteasome regulation
Probable ornithine aminotransferase, mitochondrial protein	C16A3.10	Catalytic, transaminase activity
Probable malate dehydrogenase mitochondrial protein	*mdh-1*	Catalytic
Probable prefoldin subunit 5	R151.9 *pfd-5*	Embryo dev., pronuclear migration, protein folding, locomotion
Superoxide dismutase [Cu–Zn]	*sod-1*	Metabolic, germ cell dev., striated muscle myosin thick filament assembly
Heat-shock protein Hsp-12.2	*hsp-12.2*	Reproduction, hsp binding
Glyceraldehyde-3-phosphate dehydrogenase 2	*gpd-2*	Metabolic, development
C. Proteins identified differentially in both N2 and BIR-1 hyperinduction fractions		
NHP2/L7aE family protein YEL026W homologue	M28.5	Morphogenesis, development
Protein UNC-87, a calponin-related protein	*unc-87*	Actin bundle assembly, morphogenesis
Transthyretin-like protein T07C4.5 precursor	T07C4.5	Extracellular (enriched in muscle)
Tropomyosin isoforms a/b/d/f + c/e	*lev-11*	Morphogenesis, development, cytokinesis, molting, negative regulation of actin filament depolymerization
Myosin, essential light chain	*mlc-3*	Locomotion, oviposition
Elongation factor 1-alpha	*eft-3*	Apoptosis, development, growth, translational elongation
Fructose-bisphosphate aldolase 2	F01F1.12	Catalytic, embryo dev., reproduction
40S ribosomal protein S8	*rps-8*	Apoptosis, development, translation
40S ribosomal protein S21	*rps-21*	Molting, development, translation

show direct interaction between BIR-1 and SKP-1 either (not shown).

3.2. *Short-time forced overproduction of BIR-1 induces chromatographic alterations of proteins functionally linked to SKP-1 interactors*

Since our yeast-two hybrid experiments indicated that SKP-1 and BIR-1 may influence gene expression through shared pathways, but did not show a direct interaction, we attempted to visualize the effect of BIR-1 short-time forced over expression on the whole proteome using a proteome differential display of *C. elegans* synchronized L1 larvae. We hypothesized that this experimental setting may help us visualize the involvement of BIR-1 on proteins functionally shared with SKP-1, which cannot be easily targeted in other ways.

To determine the time course of maximal expression, heat shock induced BIR-1 was monitored at the mRNA level by quantitative RT-PCR. This showed that at the time of harvesting larvae for the proteome study, the mRNA level of BIR-1

Fig. 1 – Two dimensional comparative chromatography of complete proteomes of control and BIR-1 overexpressing L1 Larvae. Panel A — first dimensional separation of protein lysates from wild type (N2) (red line) and *bir-1* overexpression samples (green line). Comparative analysis shows significant changes in the whole pI spectrum. The pH changes from pH 8.5 to pH 4 (arrowheads). In the last third of the chromatogram, proteins are eluted at pH 4 with an increasing concentration of NaCl to elute acidic proteins. Panel B — second dimension separation. A representative chromatogram of second dimension separation (fraction A2). The arrows indicate elevated absorbance (A_{214}) indicating higher protein content in the eluate in BIR-1 overexpressing larvae (green line) during the particular chromatographic time (arrows). Panel C — graphical representation of the differential proteome using the DeltaVue computer program. The protein content in particular chromatographic fractions is indicated in a gel-like pattern by red (for control proteome) and green colors (proteome of BIR-1 overexpressing larvae). The protein difference is indicated by the intensity of the color. Proteins constituting ninety eight paired fractions that showed a prominent difference in protein content were used for analysis by mass spectrometry. The arrow in panel C indicates a fraction containing elevated amount of protein in BIR-1 overexpressing larvae corresponding to the peak visible in the second dimension chromatogram (panel B, left arrow). There are clearly visible dramatic differences in the differential display of both proteomes across the pH spectrum.

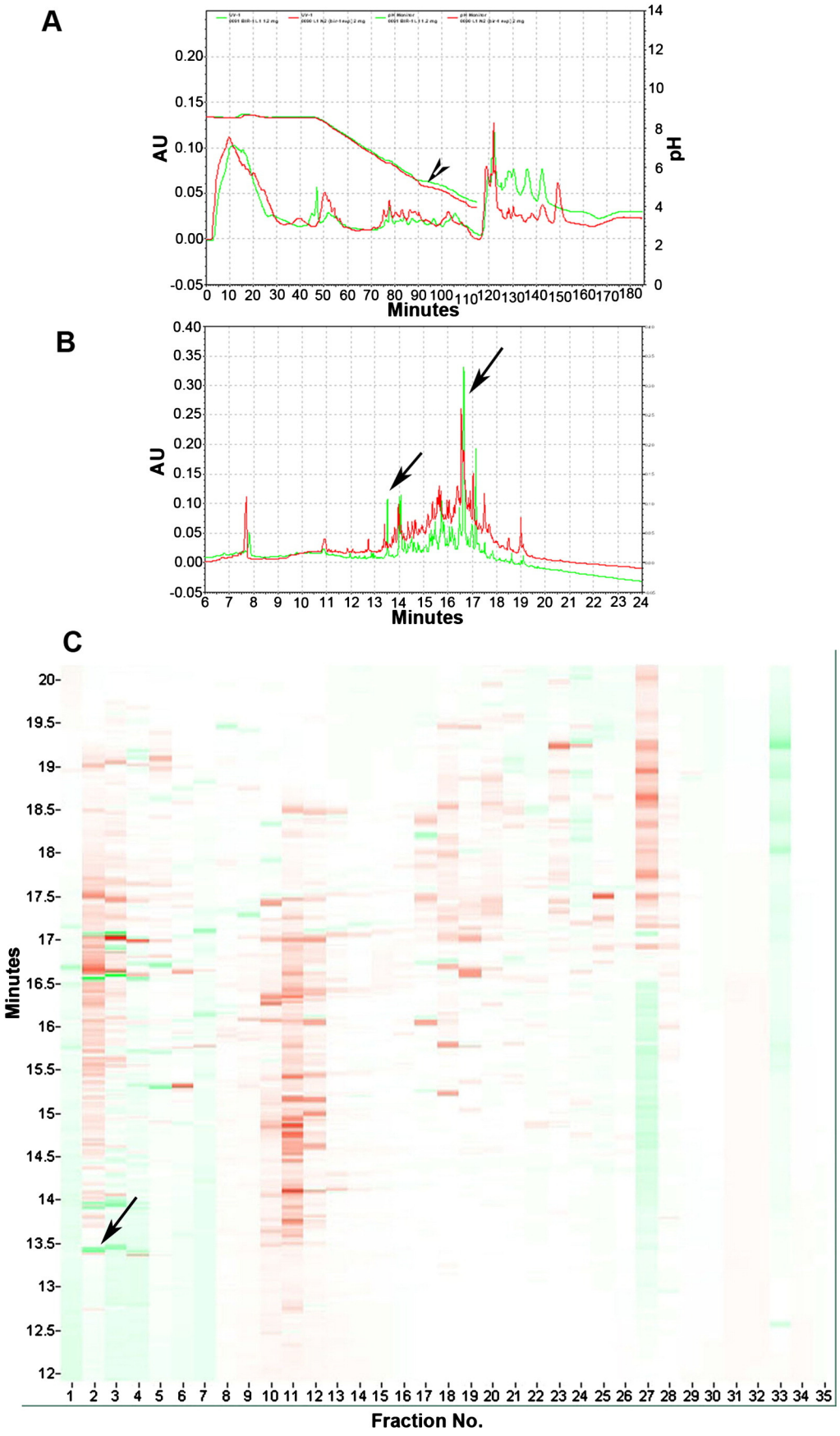
A
AU
pH
Minutes
B
AU
Minutes
C
Minutes
Fraction No.

was approximately 20 times higher than in control animals. Experiments for detection of a possible adverse effect of forced expression of BIR-1 were also conducted. As in previous experiments, we did not observe any developmental phenotype or defects of mitoses in larvae expressing increased levels of *bir-1* even after prolonged exposures.

For the comparative near-whole proteome analysis, we used the Proteome Lab Protein fractionation system (Beckman-Coulter, Brea, CA, USA). Protein lysates from synchronized *C. elegans* larvae with heat shock induced BIR-1 and wild type controls were obtained and small proteins eliminated together with salts on PD10 columns (with the fractionation range Mr 5000) thus eliminating proteins smaller than approximately 45 AA. The complete proteomes were separated using pH/NaCl gradient in the first dimension and stored in 40 fractions for each proteome (Supplementary Table S1).

Chromatographic profiles obtained from these samples clearly differed in specific regions between BIR-1 overproduction and the control proteomes (Fig. 1 A). In the second dimension chromatographic analysis (protein separation by hydrophobicity) approximately 1200 fractions were obtained from each control and experimental proteome. As shown on a representative chromatogram, BIR-1 hyperinduction leads to specific increases and decreases of protein content in fractions collected during the chromatographic elution. Differential display of the control and BIR-1 induction proteomes was obtained using DeltaVue software provided by the manufacturer (Fig. 2 B). The two dimensional comparative chromatography showed, to our surprise, that short time-forced expression of *bir-1* led to complex proteome changes in approximately 100 chromatographic fractions. 98 fractions were selected for further analysis by mass spectrometry. Spectrum analysis by SEQUEST™ software against the SwissProt database identified numerous *C. elegans* proteins together with proteins assigned to other species including bacteria and vertebrates. Filtering against confidence criteria (score, number of peptides) and selecting only *C. elegans* proteins yielded 24 proteins that were detected in 8 fractions (Supplementary Table S2). Seventeen proteins showed clear differences between larvae expressing large levels of BIR-1 and controls (Table 3A and B). These proteins were detected by mass spectrometry with high confidence only in fractions from BIR-1 overexpressing larvae (Table 3A) or only in the paired fraction from control larvae (Table 3B and Supplementary Tables S2 to S9). Nine proteins were detected with high confidence in both paired fractions (Table 3 C) including myosine and tropomyosin in acidic fraction (fraction 27) and elongation factor EF1 alpha. Interestingly, these proteins are likely to be shifted in BIR-1 overproducing larvae to more acidic fractions (Fig. 1 C, first dimension fraction No. 33) (but were not confirmed by mass spectrometry). These proteins were considered as candidate differential proteins. Their likely shift to more acidic fractions (especially fraction No. 33) can be seen in the chromatograms shown in Supplementary Figures S1 to S9. In addition to proteins with high confidence score, mass spectrometry detected many proteins with lower confidence scores. These proteins were not included in further analyses.

Gene ontology analysis of proteins identified as differentially expressed in BIR-1 overexpressing larvae compared to control N2 larvae using David Ontology Tool indicated BIR-1 involvement in the regulation of growth, embryonic development, molting cycle and cuticle formation, larval morphogenesis, locomotion, larval development, translational elongation and translation and gamete generation.

The set of proteins clearly affected by BIR-1 induction included ribosomal proteins RPS-3 and RPL-5 and myosin. These proteins were further analyzed functionally for a possible connection with BIR-1 and SKP-1 together with interacting proteins identified by yeast two-hybrid screens which were indicating shared involvement of BIR-1 and SKP-1 in the ribosomal stress pathway, in apoptosis and in the regulation of cytoskeleton during mitosis.

3.3. *Analyses targeted at selected proteins validate regulatory roles of SKP-1 and BIR-1 proteome interactions*

The protein interactions identified in yeast two hybrid screens indicated that SKP-1 and BIR-1 may be part of functionally linked protein complexes. The variability and expected cellular localizations of identified protein interactors led us to conclude that the interactions are likely to occur in separate cellular compartments and at specific conditions. We have chosen selected proteins for additional studies for validation of proteomic data.

Because the yeast two-hybrid screens demonstrated that TAC-1 interacts with SKP-1, we wondered if these two proteins are related functionally. TAC-1, a transforming coiled coil protein, is a known cofactor of nuclear receptors and is indispensable for normal centrosomal functions, centrosome migration and mitosis [26]. Therefore, we studied the effects of SKP-1 inhibition on mitosis in detail (Fig. 2) specifically assaying for the characteristic TAC-1 reduction-of-function phenotypes in centrosome migration during G2 phase. Staining of SKP-1 inhibited embryos with an antibody against SPD-2 [24] showed that SKP-1 inhibition led to serious defects of mitoses including endomitoses and defects of centrosome migration in the G2 phase (Fig. 2 F), similar to those previously shown following TAC-1 inhibition [27].

A protein category that is clearly represented in our yeast two-hybrid screen for SKP-1 interactome, as well as in BIR-1 hyperinduction, is ribosomal proteins. Interestingly, three specific proteins found in our study are ribosomal proteins involved in the ribosomal stress pathway [28–31]. We have therefore searched if the proteins that were identified in our experiments may interact with BIR-1 and SKP-1 in a GST fusion system. We prepared GST-fusion proteins and precipitated in vitro transcribed ribosomal proteins labeled with ^{35}S-methionine. Both GST-BIR-1 and GST-SKP-1, but not GST alone, showed binding to RPS-3 and RPL-5 (Fig. 3).

Since three myosin-related proteins were identified as protein species with an altered chromatographic pattern in BIR-1 hyperinduced larvae compared to controls, we searched if BIR-1 overproduction alters the immunocytochemical pattern of non-muscle myosin. As shown in Fig. 4 B, forced expression of *bir-1* leads to more prominent staining of NMY-2 at the cellular peripheries.

We also searched if the short exposure of *C. elegans* larvae to high levels of BIR-1 may affect organization of intermediate filaments in epidermis using a monoclonal antibody MH27 that specifically recognizes the MH-27 protein, which is similar to human trichohyalin, and is likely to be involved in organizing intermediate filaments in the hypodermis. As shown in Fig. 4 D, larvae that developed in the presence of

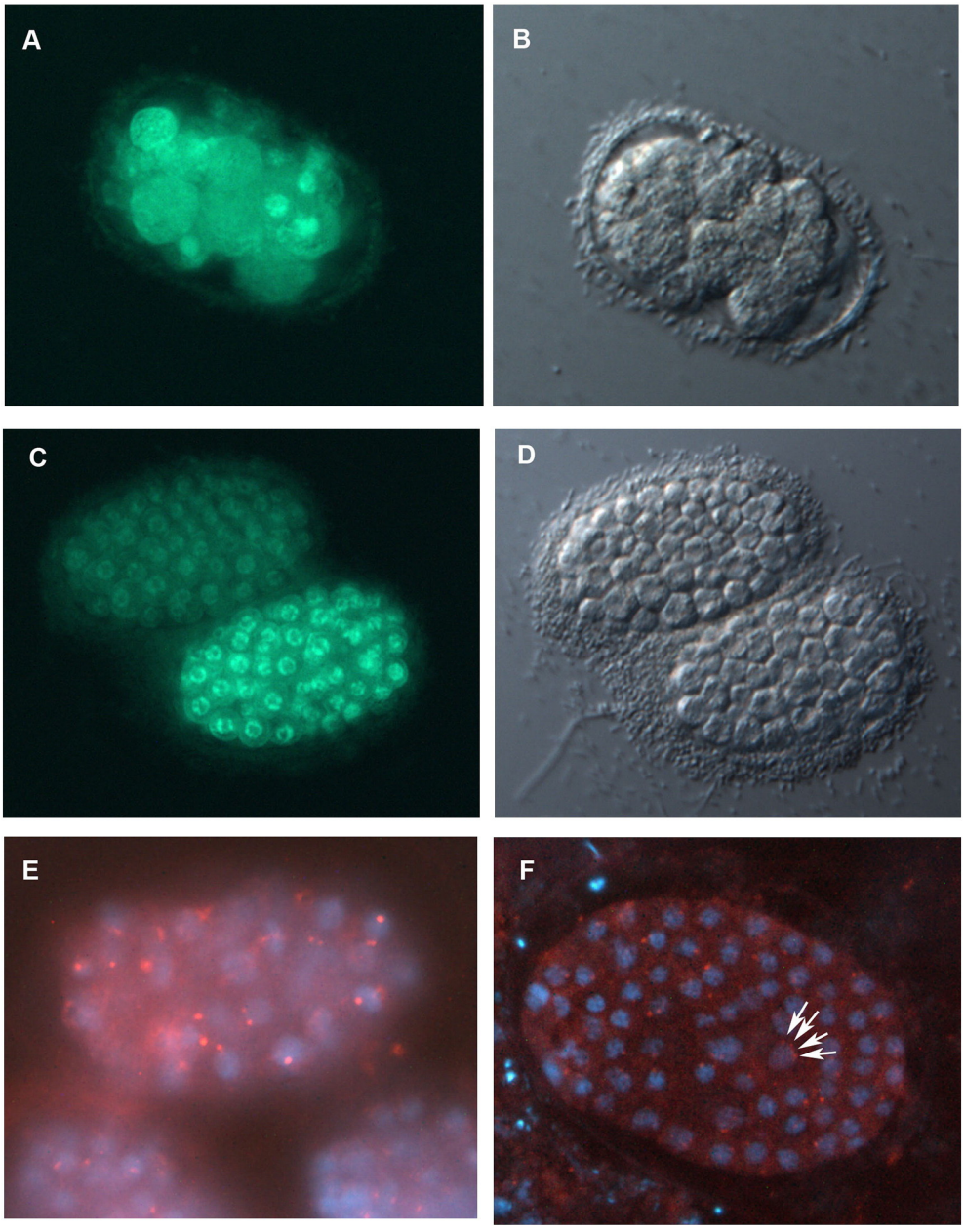

Fig. 2 – Inhibition of SKP-1 induces cell division arrest and endomitoses. Panels A and C show Histone H2::GFP expressing embryos. B and D are corresponding views in Nomarski optics. A and B show mitotic defects of *skp-1* RNAi embryos. The nuclei lost their regular architecture and the embryo arrested at approximately the 20 cell stage of development. Panel E shows a control embryo stained for DAPI and centrosomes. An embryo treated with *skp-1* RNAi (panel F) stained in the same way is arrested in development and contains cells that underwent endomitotic divisions with twice duplicated centrosomes with defective migration (arrows).

high expression of *bir-1* had higher levels of MH-27 localized at cellular borders of seam cells compared to controls. This supports the relevance of cytoskeletal and motor proteins detected as targets of BIR-1 at the protein level.

4. Discussion

In this study, we searched for possible links between SKP-1 and BIR-1. These proteins are coexpressed from one operon and their loss of function phenotypes was shown to be linked to the regulation of gene expression and development [15,17]. Both SKIP and BIR-1/Survivin are evolutionarily old highly conserved proteins that may be expected to be important for fundamental regulatory events. In this work, we searched for immediate protein functions that may transmit their cellular roles. We searched for interactors of SKP-1 and BIR-1 and identified proteins with overlapping and complementary functions as SKP-1 and BIR-1 interactors in yeast two hybrid screens. However, we did not observe a direct interaction

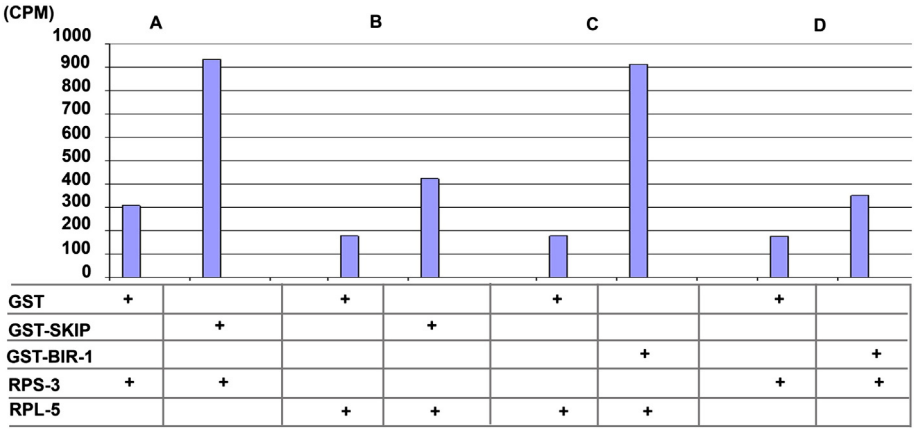

Fig. 3 – SKP-1 and BIR-1 interact with RPS-3 and RPL-5. Panels A to D show interactions of SKP-1 (panels A and B) with RPS-3 and RPL-5 (panels A and B, respectively) and interactions of BIR-1 with RPL5 and RPS-3 (panels C and D).

between SKP-1 and BIR-1. The character of processes in which SKP-1 and BIR-1 are involved, the regulation of gene expression and cell division makes their analysis difficult. Mitosis itself has profound effect on the proteome and this effect has to be distinguished from proteome states caused by specific developmental or metabolic regulators. *C. elegans* is a suitable system for combined functional and proteomic studies focused at proteins that function in interphase as well as in mitosis. In *C. elegans*, cell divisions occur in embryonic and larval stages in a precisely timed way and it is possible to obtain synchronized larval cultures that contain almost exclusively non-dividing cells. During larval stages (L1, L2) only a few cells divide and the growing gonad is small and does not affect significantly the complete proteome. This opens a wealth of possibilities for experimental functional analyses for proteins with multiple roles.

In our case, we studied the effect of short time BIR-1 hyperinduction on the *C. elegans* proteome in non-dividing cells. This approach identified several proteins found by yeast two-hybrid screens as SKP-1 and BIR-1 interactors also as targets of BIR-1 hyperinduction on the proteomic level. The wide range of proteins identified as SKP-1 and BIR-1 interactors by both approaches included cytoskeletal and motor proteins, ribosomal proteins known to be active in the ribosomal stress pathway and transcription and translation regulating proteins. The BIR-1 hyperinduction had a profound effect on the composition of the whole proteome in non-dividing cells. This indicated that BIR-1 hyperinduction may influence a wide spectrum of target proteins and/or regulates proteins that affect other proteins. Some proteins found by our screens fulfill these criteria: protein involved in the proteasome pathway, enzymes, and transcription and translation regulators.

Selected proteins that were studied functionally supported the concept that incorporation of BIR-1 and SKP-1 in cellular mechanistic events may be linked to their regulatory roles in major cellular events: cell cycle progression and mitosis, ribosomal stress, (and apoptosis) and gene expression.

Some connections were expected from known functions of BIR-1 or its vertebrate homologue Survivin. The connection between BIR-1 and non-muscle myosin is in agreement with the Survivin role in cytokinesis revealed by a separation-of-function mutant [32].

Identification of ribosomal proteins as both SKP-1 and BIR-1 interactors and targets of BIR-1 hyperinduction was unexpected but it further supports the functional connections between these two factors. The direct binding of SKP-1 and BIR-1 to RPS-3 and RPL-5 was confirmed by pull-down experiments. The physical interaction between SKP-1 and BIR-1 with ribosomal proteins that are known to participate in the ribosomal stress pathway opens a possibility that both SKP-1 and BIR-1 may be or their evolutionary ancestors were involved in ribosomal stress and apoptosis. Although *C. elegans* doesn't have a known MDM2 ortholog, it is likely that a protein that is still not recognized in the *C. elegans* genome supports this function. MDM2-p53 is a very ancient regulatory pathway that is already functional in a basal Metazoan — *Trichoplax adhaerens* [33,34]. MDM2 can reversely bind ribosomal proteins RPS3 [31], RPL5 [29,35,36], RPL11 [28,30,37,38], and RPS28 [39]. Additional proteins were shown to participate in the regulation of p53 pathway, including RPL37, RPS15, and RPS20 [39]. Various ribosomal proteins in the p53 pathway may function through multiple mechanisms, as was recently shown for ribosomal protein S26 [40]. SKP-1 and BIR-1 are thus likely to be functionally linked on multiple levels in the regulation of apoptosis, stress pathways and gene expression. Keeping with this, SKP-1 counteracts p53-regulated apoptosis through regulation of p21Cip1 mRNA splicing [41]. It seems likely, that SKP-1 and BIR-1's role in the regulation of apoptosis through interaction with ribosomal proteins may be more ancient than the role of Survivin in inhibition of apoptosis through the direct binding and inactivation of caspases. In *C. elegans*, BIR-1 doesn't regulate apoptosis through inactivation of caspases but its role in apoptosis induced by ribosomal stress was not yet tested. This Survivin's capacity may have evolved later in evolution on the basis of BIR/Survivin ability to physically interact with variable proteins.

There are additional lines of evidence indicating that SKP-1 and BIR-1 may be functionally linked at the proteome level. BIR-1 is a regulator of microtubule attachment to chromosomes in anaphase and progression of mitosis. TAC-1 that

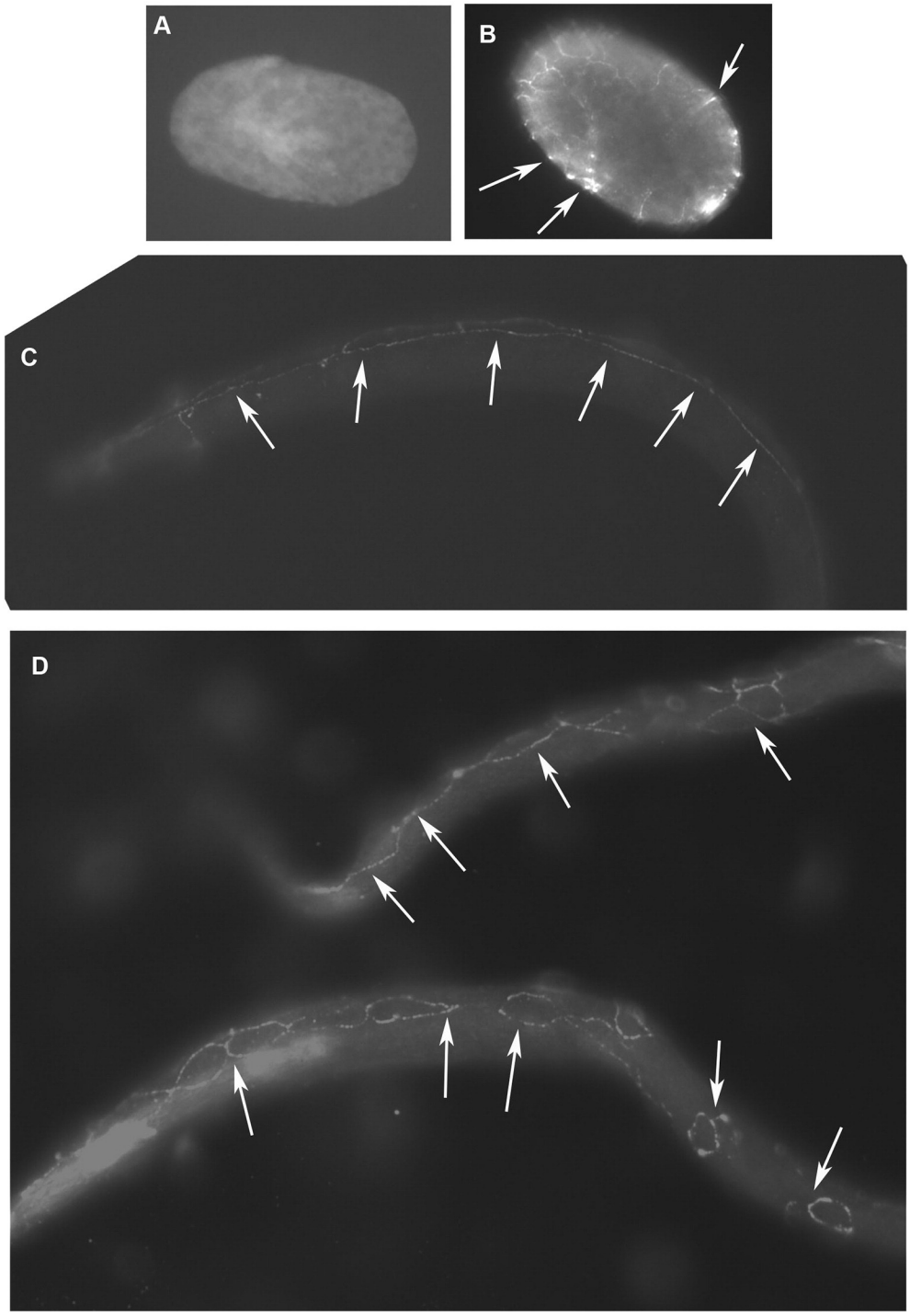

Fig. 4 – The effect of short term overexpression of *bir*-1 on non-muscle myosin localization in *C. elegans* embryos and development of seam cells. Panels A and B show *C. elegans* embryos stained for NMY-2. A) Control wild type (N2) embryo (containing control transgene consisting of empty vector), B) Embryo overexpressing *bir*-1 from a transgene regulated by heat shock promoter. Arrows indicate accumulation of NMY-2 at the cell borders. Panels C and D show L1 larvae stained for MH27 antigen. Panel C shows a control larva with regularly developed seam cells forming a ribbon of rectangular cells along the length and side of the animal. Panel D shows a L1 larva that developed from embryos affected by short term *bir*-1 overexpression. Arrows indicate seam cells that are bigger than in wild type controls, not properly connected to each other, and that often have an irregular shape.

was found as SKP-1 interactor has a critical role in mitosis specifically in the relocation of ZYG-9 to centrosomes. TAC-1 is found localized on centrosomes as well as in the nucleus where it plays critical roles in gene expression regulation. Interestingly, SKP-1 inhibition results in the same cellular event — G2 arrest and failure of centrosome migration as is known for TAC-1 [26]. A possibility of direct centrosomal localization and function of SKIP is keeping with the centrosomal localization and mitotic function of SKI [42,43], a protein which is interacting physically and functionally with SKIP [44].

Taken together, the protein interactions of SKP-1 and BIR-1 meet in major cellular events: cell division, ribosomal stress and apoptosis and gene expression.

Our results suggest that BIR-1 and SKP-1 are part of a larger network that is likely to participate not only on the same mechanistic events but that this network also has a potential to connect proteome signals with the regulation of gene expression on multiple levels. Several lines of evidence indicate that this network is real and functionally important. For example, SKIP is known to be a multifunctional protein involved in the regulation of transcription and is a co-activator for nuclear receptors [5,6,8]. SKIP also interacts with nuclear receptor co-repressor SMRT and functions in the Notch pathway through binding of Notch IC that is required for Notch biological activity [9]. SKIP also directly binds the retinoblastoma tumor suppressor protein pRb and, in co-operation with Ski, overcomes the G1 arrest induced by pRb [45]. SKIP is also involved in regulation of splicing [12,13,46,47]. Thus, SKIP has a well-documented role in the regulation of transcription and cell cycle.

It may be hypothesized that the pleiotropic protein interactions that we have identified for SKP-1 and BIR-1 are part of a proteome regulatory network with the capacity to project proteomic states towards gene expression regulation. Our data further link functionally SKP-1 and BIR-1. Both proteins bind proteins of the ribosomal stress pathway and possibly other stress pathways. SKIP was shown to be affecting stress related genes in plants. In rice and in *Arabidopsis*, it regulates stress related genes [48,49]. The ribosomal stress pathway thus may represent a special case of the cytoplasmic proteomic signals towards gene expression. If such proteomic signaling would be proved as a more general mechanism by which proteome composition projects directly towards gene expression, it may be considered as a proteome code. Such regulatory loops should include proteins that are localized in specific cellular structures and when liberated or synthesized in excess of cellular needs assume their additional regulatory roles. In fact, such inhibition of gene expression was shown to be the autoregulatory mechanism for RPL-12, which was shown to affect its own splicing most likely through a sensor affecting transcription [50]. SKP-1 and/or BIR-1 may be the sensor(s) in ribosomal protein transcription and in the ribosomal stress pathway.

5. Conclusion

Our proteomic analyses further support the functional links between SKP-1 and BIR-1 with connected and overlapping roles in the ribosomal stress pathway and transcriptional regulation. It seems likely, that SKP-1 and BIR-1/Survivin are involved in the ribosomal stress pathway and are possibly components of complexes connecting cellular needs with the regulation of gene expression at the level of transcription and translation.

Supplementary data to this article can be found online at http://dx.doi.org/10.1016/j.jprot.2014.07.023.

Transparency document

The Transparency document associated with this article can be found, in the online version.

Acknowledgments

DK, MK Jr. (Markéta Kostrouchová), PY, AC, JPN, PN, VK, MK, and ZK performed the experiments, participated on planning of experiments and wrote the manuscript; DK, MK Jr., PY, AC, JPN, VK, MK, and ZK were supported by grant PRVOUK-P27/LF1/1 from the Charles University in Prague, DK, MK Jr., PY, AC, JPN were supported by SVV 266505/2013 and SVV 260023/2014, PN was supported by the Institutional Research Concept RVO 61388971 (P.N.); DK, MK Jr., PY, AC, JPN, PN, VK, MK, and ZK are supported by the European Regional Development Fund "BIOCEV — Biotechnology and Biomedicine Centre of the Academy of Sciences and Charles University in Vestec" (CZ.1.05/1.1.00/02.0109); ZK, MK, MK Jr, and DK were supported by the Intramural Research Program of the National Institute of Diabetes and Digestive and Kidney Diseases (NIDDK) of the National Institutes of Health, USA. ZK and MK contributed with personal funds to this work. The authors are very grateful to Dr. Michael W. Krause, NIDDK, NIH, Bethesda for his support and help during all stages of the work connected with this project and preparation of the manuscript. The authors thank WormBase for bioinformatic support. No additional external funding was received for this study. The funders had no role in the study design, data collection and analysis, decision to publish, or preparation of the manuscript.

REFERENCES

[1] Saumweber H, Frasch M, Korge G. Two puff-specific proteins bind within the 2.5 kb upstream region of the *Drosophila melanogaster* Sgs-4 gene. Chromosoma 1990; 99:52–60.
[2] Wieland C, Mann S, von Besser H, Saumweber H. The *Drosophila* nuclear protein Bx42, which is found in many puffs on polytene chromosomes, is highly charged. Chromosoma 1992;101:517–25.
[3] Folk P, Puta F, Krpejsova L, Blahuskova A, Markos A, Rabino M, et al. The homolog of chromatin binding protein Bx42 identified in Dictyostelium. Gene 1996;181:229–31.
[4] Martinkova K, Lebduska P, Skruzny M, Folk P, Puta F. Functional mapping of *Saccharomyces cerevisiae* Prp45 identifies the SNW domain as essential for viability. J Biochem 2002;132:557–63.
[5] Baudino TA, Kraichely DM, Jefcoat Jr SC, Winchester SK, Partridge NC, MacDonald PN. Isolation and characterization

of a novel coactivator protein, NCoA-62, involved in vitamin D-mediated transcription. J Biol Chem 1998;273:16434–41.
[6] Barry JB, Leong GM, Church WB, Issa LL, Eisman JA, Gardiner EM. Interactions of SKIP/NCoA-62, TFIIB, and retinoid X receptor with vitamin D receptor helix H10 residues. J Biol Chem 2003;278:8224–8.
[7] Fantappie MR, de Oliveira FM Bastos, de Moraes Maciel R, Rumjanek FD, Wu W, Loverde PT. Cloning of SmNCoA-62, a novel nuclear receptor co-activator from *Schistosoma mansoni*: assembly of a complex with a SmRXR1/SmNR1 heterodimer, SmGCN5 and SmCBP1. Int J Parasitol 2008;38:1133–47.
[8] Abankwa D, Millard SM, Martel N, Choong CS, Yang M, Butler LM, et al. Ski-interacting protein (SKIP) interacts with androgen receptor in the nucleus and modulates androgen-dependent transcription. BMC Biochem 2013;14:10.
[9] Zhou S, Fujimuro M, Hsieh JJ, Chen L, Miyamoto A, Weinmaster G, et al. SKIP, a CBF1-associated protein, interacts with the ankyrin repeat domain of NotchIC To facilitate NotchIC function. Mol Cell Biol 2000;20:2400–10.
[10] Wang Y, Fu Y, Gao L, Zhu G, Liang J, Gao C, et al. Xenopus skip modulates Wnt/beta-catenin signaling and functions in neural crest induction. J Biol Chem 2010;285:10890–901.
[11] Leong GM, Subramaniam N, Figueroa J, Flanagan JL, Hayman MJ, Eisman JA, et al. Ski-interacting protein interacts with Smad proteins to augment transforming growth factor-beta-dependent transcription. J Biol Chem 2001; 276:18243–8.
[12] Zhang C, Dowd DR, Staal A, Gu C, Lian JB, van Wijnen AJ, et al. Nuclear coactivator-62 kDa/Ski-interacting protein is a nuclear matrix-associated coactivator that may couple vitamin D receptor-mediated transcription and RNA splicing. J Biol Chem 2003;278:35325–36.
[13] Wang X, Wu F, Xie Q, Wang H, Wang Y, Yue Y, et al. SKIP is a component of the spliceosome linking alternative splicing and the circadian clock in *Arabidopsis*. Plant Cell 2012; 24:3278–95.
[14] Leong GM, Subramaniam N, Issa LL, Barry JB, Kino T, Driggers PH, et al. Ski-interacting protein, a bifunctional nuclear receptor coregulator that interacts with N-CoR/SMRT and p300. Biochem Biophys Res Commun 2004;315:1070–6.
[15] Kostrouchova M, Housa D, Kostrouch Z, Saudek V, Rall JE. SKIP is an indispensable factor for *Caenorhabditis elegans* development. Proc Natl Acad Sci U S A 2002;99:9254–9.
[16] Li F, Ambrosini G, Chu EY, Plescia J, Tognin S, Marchisio PC, et al. Control of apoptosis and mitotic spindle checkpoint by survivin. Nature 1998;396:580–4.
[17] Kostrouchova M, Kostrouch Z, Saudek V, Piatigorsky J, Rall JE. BIR-1, a *Caenorhabditis elegans* homologue of Survivin, regulates transcription and development. Proc Natl Acad Sci U S A 2003;100:5240–5.
[18] Brenner S. The genetics of *Caenorhabditis elegans*. Genetics 1974;77:71–94.
[19] Tabb DL, McDonald WH, Yates III JR. DTASelect and Contrast: tools for assembling and comparing protein identifications from shotgun proteomics. J Proteome Res 2002;1:21–6.
[20] Pohludka M, Simeckova K, Vohanka J, Yilma P, Novak P, Krause MW, et al. Proteomic analysis uncovers a metabolic phenotype in *C. elegans* after nhr-40 reduction of function. Biochem Biophys Res Commun 2008;374:49–54.
[21] Altschul SF, Gish W, Miller W, Myers EW, Lipman DJ. Basic local alignment search tool. J Mol Biol 1990;215:403–10.
[22] Huang DW, Sherman BT, Lempicki RA. Systematic and integrative analysis of large gene lists using DAVID bioinformatics resources. Nat Protoc 2009;4:44–57.
[23] Huang DW, Sherman BT, Lempicki RA. Bioinformatics enrichment tools: paths toward the comprehensive functional analysis of large gene lists. Nucleic Acids Res 2009;37:1–13.
[24] Kemp CA, Kopish KR, Zipperlen P, Ahringer J, O'Connell KF. Centrosome maturation and duplication in *C. elegans* require the coiled-coil protein SPD-2. Dev Cell 2004;6:511–23.
[25] Liby P, Pohludka M, Vohanka J, Kostrouchova M, Kostrouch D, Rall JE, et al. BIR-1, the homologue of human Survivin, regulates expression of developmentally active collagen genes in *C. elegans*. Folia Biol (Praha) 2006;52:101–8.
[26] Bellanger JM, Carter JC, Phillips JB, Canard C, Bowerman B, Gonczy P. ZYG-9, TAC-1 and ZYG-8 together ensure correct microtubule function throughout the cell cycle of *C. elegans* embryos. J Cell Sci 2007;120:2963–73.
[27] Srayko M, Quintin S, Schwager A, Hyman AA. *Caenorhabditis elegans* TAC-1 and ZYG-9 form a complex that is essential for long astral and spindle microtubules. Curr Biol 2003;13:1506–11.
[28] Zhang Y, Wolf GW, Bhat K, Jin A, Allio T, Burkhart WA, et al. Ribosomal protein L11 negatively regulates oncoprotein MDM2 and mediates a p53-dependent ribosomal-stress checkpoint pathway. Mol Cell Biol 2003;23:8902–12.
[29] Horn HF, Vousden KH. Cooperation between the ribosomal proteins L5 and L11 in the p53 pathway. Oncogene 2008; 27:5774–84.
[30] Dai MS, Shi D, Jin Y, Sun XX, Zhang Y, Grossman SR, et al. Regulation of the MDM2-p53 pathway by ribosomal protein L11 involves a post-ubiquitination mechanism. J Biol Chem 2006;281:24304–13.
[31] Yadavilli S, Mayo LD, Higgins M, Lain S, Hegde V, Deutsch WA. Ribosomal protein S3: a multi-functional protein that interacts with both p53 and MDM2 through its KH domain. DNA Repair (Amst) 2009;8:1215–24.
[32] Szafer-Glusman E, Fuller MT, Giansanti MG. Role of Survivin in cytokinesis revealed by a separation-of-function allele. Mol Biol Cell 2011;22:3779–90.
[33] Lane DP, Cheok CF, Brown C, Madhumalar A, Ghadessy FJ, Verma C. Mdm2 and p53 are highly conserved from placozoans to man. Cell Cycle 2010;9:540–7.
[34] von der Chevallerie K, Rolfes S, Schierwater B. Inhibitors of the p53-Mdm2 interaction increase programmed cell death and produce abnormal phenotypes in the placozoon *Trichoplax adhaerens* (F.E. Schulze). Dev Genes Evol 2014;224:79–85.
[35] Dai MS, Lu H. Inhibition of MDM2-mediated p53 ubiquitination and degradation by ribosomal protein L5. J Biol Chem 2004;279:44475–82.
[36] Marechal V, Elenbaas B, Piette J, Nicolas JC, Levine AJ. The ribosomal L5 protein is associated with mdm-2 and mdm-2-p53 complexes. Mol Cell Biol 1994;14:7414–20.
[37] Lohrum MA, Ludwig RL, Kubbutat MH, Hanlon M, Vousden KH. Regulation of HDM2 activity by the ribosomal protein L11. Cancer Cell 2003;3:577–87.
[38] Morgado-Palacin L, Llanos S, Serrano M. Ribosomal stress induces L11- and p53-dependent apoptosis in mouse pluripotent stem cells. Cell Cycle 2012;11:503–10.
[39] Daftuar L, Zhu Y, Jacq X, Prives C. Ribosomal proteins RPL37, RPS15 and RPS20 regulate the Mdm2-p53-MdmX network. PLoS One 2013;8:e68667.
[40] Cui D, Li L, Lou H, Sun H, Ngai SM, Shao G, et al. The ribosomal protein S26 regulates p53 activity in response to DNA damage. Oncogene 2013;33:2225–35.
[41] Chen Y, Zhang L, Jones KA. SKIP counteracts p53-mediated apoptosis via selective regulation of p21Cip1 mRNA splicing. Genes Dev 2011;25:701–16.
[42] Mosquera J, Armisen R, Zhao H, Rojas DA, Maldonado E, Tapia JC, et al. Identification of Ski as a target for Aurora A kinase. Biochem Biophys Res Commun 2011;409:539–43.
[43] Marcelain K, Hayman MJ. The Ski oncoprotein is upregulated and localized at the centrosomes and mitotic spindle during mitosis. Oncogene 2005;24:4321–9.
[44] Prathapam T, Kuhne C, Hayman M, Banks L. Ski interacts with the evolutionarily conserved SNW domain of Skip. Nucleic Acids Res 2001;29:3469–76.

[45] Prathapam T, Kuhne C, Banks L. Skip interacts with the retinoblastoma tumor suppressor and inhibits its transcriptional repression activity. Nucleic Acids Res 2002; 30:5261–8.
[46] Figueroa JD, Hayman MJ. The human Ski-interacting protein functionally substitutes for the yeast PRP45 gene. Biochem Biophys Res Commun 2004;319:1105–9.
[47] Bres V, Gomes N, Pickle L, Jones KA. A human splicing factor, SKIP, associates with P-TEFb and enhances transcription elongation by HIV-1 Tat. Genes Dev 2005;19:1211–26.
[48] Hou X, Xie K, Yao J, Qi Z, Xiong L. A homolog of human ski-interacting protein in rice positively regulates cell viability and stress tolerance. Proc Natl Acad Sci U S A 2009;106:6410–5.
[49] Zhang Y, Zhao L, Li H, Gao Y, Li Y, Wu X, et al. GmGBP1, a homolog of human ski interacting protein in soybean, regulates flowering and stress tolerance in *Arabidopsis*. BMC Plant Biol 2013;13:21.
[50] Mitrovich QM, Anderson P. Unproductively spliced ribosomal protein mRNAs are natural targets of mRNA surveillance in *C. elegans*. Genes Dev 2000;14:2173–84.

Perilipin-related protein regulates lipid metabolism in *C. elegans*

Ahmed Ali Chughtai[1], Filip Kaššák[1], Markéta Kostrouchová[1,2], Jan Philipp Novotný[1], Michael W. Krause[3], Vladimír Saudek[4], Zdenek Kostrouch[1] and Marta Kostrouchová[1]

[1] Institute of Cellular Biology and Pathology, First Faculty of Medicine, Charles University in Prague, Albertov, Prague, Czech Republic
[2] Department of Pathology, Third Faculty of Medicine, Charles University in Prague, Ruská, Prague, Czech Republic
[3] Laboratory of Molecular Biology, National Institute of Diabetes and Digestive and Kidney Diseases, National Institutes of Health, Bethesda, MD, USA
[4] University of Cambridge Metabolic Research Laboratories, Wellcome Trust—Medical Research Council, Institute of Metabolic Science, Cambridge, UK

ABSTRACT

Perilipins are lipid droplet surface proteins that contribute to fat metabolism by controlling the access of lipids to lipolytic enzymes. Perilipins have been identified in organisms as diverse as metazoa, fungi, and amoebas but strikingly not in nematodes. Here we identify the protein encoded by the *W01A8.1* gene in *Caenorhabditis elegans* as the closest homologue and likely orthologue of metazoan perilipin. We demonstrate that nematode *W01A8.1* is a cytoplasmic protein residing on lipid droplets similarly as human perilipins 1 and 2. Downregulation or elimination of *W01A8.1* affects the appearance of lipid droplets resulting in the formation of large lipid droplets localized around the dividing nucleus during the early zygotic divisions. Visualization of lipid containing structures by CARS microscopy *in vivo* showed that lipid-containing structures become gradually enlarged during oogenesis and relocate during the first zygotic division around the dividing nucleus. In mutant embryos, the lipid containing structures show defective intracellular distribution in subsequent embryonic divisions and become gradually smaller during further development. In contrast to embryos, lipid-containing structures in enterocytes and in epidermal cells of adult animals are smaller in mutants than in wild type animals. Our results demonstrate the existence of a perilipin-related regulation of fat metabolism in nematodes and provide new possibilities for functional studies of lipid metabolism.

Subjects Bioinformatics, Cell Biology, Genomics
Keywords Perilipin, Perilipin-related protein in *C. elegans*, *Caenorhabditis elegans*, Lipid droplets, Fat metabolism

Submitted 17 March 2015
Accepted 5 August 2015
Published 1 September 2015

Corresponding authors
Vladimír Saudek, vs317@cam.ac.uk
Marta Kostrouchová, marta.kostrouchova@lf1.cuni.cz

Academic editor
Natascia Ventura

Additional Information and Declarations can be found on page 19

DOI **10.7717/peerj.1213**

INTRODUCTION

Perilipins are regulatory proteins targeted to the surface of fat storage organelles called lipid dropplets (LDs) where they contribute to the regulation of lipid metabolism (*Brasaemle, 2007*). Functional perilipins (PLIN proteins encoded by the *PLIN* genes) (*Lu et al., 2001*) have been identified in very diverse organisms such as *Drosophila* (*Teixeira et al., 2003*), *Dictyostelium* (*Du et al., 2013*) and fungi (*Wang & St Leger, 2007*) and protein databases

list clear orthologues in diverse, non-plant eukaryota, including the simplest metazoan *Trichoplax adherens*, sponges, crustaceans, and choanoflagelates (UniProt proteins B3RRM2, I1GA14, G5DCP6, F2UJD9, respectively). In humans and other mammals, the PLIN family consists of five members (*Kimmel et al., 2010*) (Perilipin 1–5) with diverse tissue distribution, specificity, and partially redundant functions. Strikingly, no perilipin othologue has been identified in *C. elegans*, suggesting that nematode-specific lipid regulatory pathways might exist in this phylum and perhaps in others as well.

This unusual evolutionary gap in the perilipins prompted us to re-examine the *C. elegans* genome for a gene related to mammalian perilipin. We identify *W01A8.1* as the likely *C. elegans* orthologue of mammalian perilipin genes. We show that W01A8.1 is the previously unrecognized *C. elegans* homologue of vertebrate perilipins that possesses all functional domains characteristic for perilipins and functions in lipid metabolism at the level of lipid droplets.

The protein encoded by W01A8.1 in *C. elegans* is identified as Mediator Complex subunit 28 (MDT-28) in many protein databases (e.g., Pfam, UniProt, PIR, WormPep) (accessed on March 14, 2015), but the bioinformatics analysis reveals that this is a misannotation. We observe that protein isoforms expressed from *W01A8.1* are cytoplasmic proteins, residing predominantly on membranous structures of enterocytes and epidermal cells that have the characteristics of lipid droplets. We also show that transgene-encoded GFP fusion proteins of human Perilipins 1 and 2 localize in *C. elegans* similarly as W01A8.1::GFP on vesicular structures that are positive for lipid content. Furthermore, down regulation of *W01A8.1* by RNAi or its elimination lead to an altered appearance and behavior of lipid droplets prominently observed in the germline and in early embryos. Our results indicate that *C. elegans* can compensate for the loss of *W01A8.1* in all developmental stages except early embryos likely by additional fat degradation mechanisms.

Our data demonstrates that the perilipin-related regulation of fat metabolism is conserved in *C. elegans*, and provides a novel insight into early embryonic lipid management. This discovery offers promising possibilities for functional studies of lipid metabolism in a nematode model system.

MATERIALS AND METHODS

Sequence analysis

Perilipin orthologues and W01A8.1 sequences were extracted from UniProt, NCBI and OMA (omabrowser.org) databases. Chordate and nematode sequences were aligned separately using the T-Coffee algorithm (*Notredame, Higgins & Heringa, 2000*) (server tcoffee.crg.cat) and submitted to PSI-BLAST (*Altschul et al., 1997*) (E-value inclusion threshold $<10^{-3}$, 5 iterations) and HHpred (*Remmert et al., 2011*; *Biegert & Soding, 2008*) searches as implemented in MPItoolkit (toolkit.tuebingen.mpg.de). Repeat detection used HHrepID module in MPItoolkit. Alignments were displayed and analyzed in Jalview app (www.jalview.org).

Strains, transgenic lines and genome editing

Wild type animals, N2 (var. Bristol), were used unless otherwise noted and all strains were maintained as described (*Brenner, 1974*). Transgenic lines were prepared using microinjections into gonads of young adult N2 hermaphrodites as described (*Tabara et al., 1999*; *Timmons, Court & Fire, 2001*; *Vohanka et al., 2010*). All injections also included mCherry co-injection markers: pCFJ90, pCJ104 and pGH8 (*Dickinson et al., 2013*).

To create mutants, we employed CRISPR/Cas9 system as described (*Dickinson et al., 2013*). The following plasmids were constructed: pCK001 targeting the sgRNA (+323) to the second exon of the *W01A8.1* gene (forward primer #7992), and pCK023 targeting the sgRNA (+1,372) to the sixth exon (forward primer #8078). The reverse primer was #7993. A scheme of known expressed isoforms listed in WormBase WS246 and the strategy for the disruption of *W01A8.1* gene is shown in Figs. S1 and S2. Primers used in this study are listed in Table S1.

The following transgenic lines regulated by *W01A8.1* natural promoter were prepared: *W01A8.1a/c::gfp* and *W01A8.1b::gfp* (containing the whole coding sequence of isoforms a and b). *W01A8.1* isoforms a and c have identical 3′ ends which both could be expressed from *W01A8.1a/c::gfp*. This construct also includes complete untagged isoform b. The GFP-tagged isoform a (plasmid pCK28 {$P_{W01A8.1}$::*W01A8.1(a)synth::gfp::unc-54 3′ UTR*}) was constructed by synthesizing the *W01A8.1a* sequence with modified codons to allow protection from CRISPR/Cas9 targeted sgRNA and prepared as a GeneArt® Strings™ DNA Fragment from Invitrogen (Invitrogen, Carlsbad, California, USA) and cloned using GeneArt® Seamless Cloning System (Invitrogen) into pPD95.75(NeoR). Schemes for isoforms expressed from *W01A8.1* gene and preparation of GFP tagged transgenes are given in Figs. S1 and S2.

Human *PLIN2* and *PLIN3* were cloned from a collection of anonymous unmarked samples (*PLIN2*), and from human peripheral lymphocytes (*PLIN3*) donated by a volunteer with a written consent in compliance with the legislation of the Czech Republic and European Union (Act No 372/2011 of 11. 11. 2011 on Health Care Services, Coll., Paragraph 81, section 1a and section 4a, which is in accordance with the declaration of Helsinki) and was approved by the Ethics Committee of the First Faculty of Medicine, Charles University in Prague (Ref. No. MZ13-UK1LF-KostrouchZdenek). Human PLIN1 optimized for *C. elegans* was prepared as a synthetic sequence requested as a GeneArt® Strings™ DNA Fragment from Invitrogen™.

Transgenic lines expressing human *PLIN1*, *PLIN2*, *PLIN3* tagged by GFP under *W01A8.1* natural promoter were prepared using N2 animals and animals with disrupted *W01A8.1*. Primers used for cloning *PLIN2* and *PLIN3* are listed in Table S1.

Downregulation of gene expression by RNA interference

Downregulation of *W01A8.1* expression used the RNAi protocol of injection of dsRNA into gonads of young adult hermaphrodites as well as RNAi through feeding animals bacteria producing dsRNA as previously described (*Tabara et al., 1999*; *Timmons, Court & Fire, 2001*; *Vohanka et al., 2010*).

Injection RNAi protocol

Double stranded RNA (dsRNA) was prepared for injection by *in vitro* transcription reactions (SP6/T7 Riboprobe® *in vitro* Transcription Systems; Promega, Madison, Wisconsin, USA) from opposing promoters and subsequent annealing of each single stranded RNA (ssRNA) product prior to injection. For RNAi directed against *W01A8.1*, BamHI or ApaI linearized pCK014 plasmid preparations were used in separate reactions to generate complementary ssRNA. After linearization, the DNA was phenol-chloroform extracted and ethanol precipitated. BamHI linearized DNA was transcribed using T7 RNA Polymerase while ApaI linearized DNA with SP6 RNA Polymerase. After *in vitro* transcription (∼2 h), equal volumes of sense and antisense RNA were incubated at 75 °C for 10 min and then cooled at room temperature for 30 min. Control RNAi was prepared from the promoter region of *nhr-60* as previously described (*Simeckova et al., 2007*). The dsRNA concentration was measured using a UV spectrophotometer and ∼1 μg/μl was used for injections.

Feeding RNAi protocol

Nematode Growth Medium (NGM) agar plates were prepared according to standard protocols and were supplemented with Ampicillin (100 μg/ml final concentration) and isopropyl β-D-1-thiogalactopyranoside (IPTG) (1.5 mM final concentration). *E. coli* strain HT115 was transformed with pCK015 and control L4440 vector. After transformation, a single colony from each was used to inoculate LB medium with Ampicillin (100 μg/ml final concentration). The culture was grown to $OD_{600} \approx 1.0$; 900 μl of culture was poured onto NGM agar plates to completely cover the surface and 750 μl of the suspension was removed to leave 150 μl of the suspension on the plates. The bacteria were allowed to grow and were induced overnight at room temperate (∼22 °C).

Fecundity and brood size assay

Fecundity measurement following RNAi (injection method) was conducted using a total of 50 young adult worms (25 control and 25 inhibited by RNAi specific for *W01A8.1*). Progeny was counted 24 h and again 48 h after injections. Brood size assay was performed for W01A8.1 disrupted animals and controls ($n = 15$ for each group). The progeny was determined during 6 days. The experiments were conducted at room temperature ∼22 °C.

Fecundity measurement after RNAi using feeding protocol was performed over two generations to maximize the effect of knockdown. For this, a semi-synchronized population was isolated using standard WormBook (http://www.wormbook.org/) bleaching protocol. Hatched L1 stage worms were placed on NGM agar RNAi (*W01A8.1* specific and control) plates at ∼22 °C. Small, synchronized populations, of parents (P0) were transferred to fresh RNAi plates and allowed to lay progeny (F1). F1 generation animals were transferred to new RNAi plates and F2 generation was scored for a total of 21 F1 parents in each group. The experiment was repeated twice to confirm the results.

RNA isolation and cDNA synthesis

Total RNA was extracted as previously described (*Vohanka et al., 2010*). Briefly, *C. elegans* washed, pelleted and re-suspended in re-suspension buffer with proteinase K. After lysis

TRIzol® Reagent (Invitrogen) was added to the mixture and the standard manufacturer's protocol was followed to obtain total RNA. Samples were then treated with DNaseI (New England Biolabs, Ipswich, Massachusetts, USA) and again TRIzol-chloroform extracted (Invitrogen) to obtain DNA free total RNA.

Human total RNA was also extracted using TRIzol® Reagent (Invitrogen) from peripheral blood lymphocytes and fat tissue. cDNA was prepared from total RNA by reverse transcription using standard protocols for the SuperScript® III First-Strand Synthesis System (Invitrogen) and oligo(dT) priming.

Transcript quantification

Quantitative polymerase chain reaction (qPCR) was performed with cDNA prepared from total RNA isolated as described above, using the Roche Universal Probe Library technique (Hoffmann-La Roche, Basel, Switzerland). Primers and probes for determination of number of transcripts of *W01A8.1* are given in Table S1. Levels of *W01A8.1* expression were normalized against *ama-1*.

Single worm PCR

Single animals were placed into 5 µl of worm lysis buffer (10 mM Tris–HCl pH 8.3, 50 mM KCl, 2.5 mM MgCl2, 0.45% NP-40, 0.45% Tween 20, 0.01% Gelatin and 500 µg/ml fresh proteinase K) in a PCR tube. Animals were frozen at −80 °C for 5 min before placing the tube into a thermal cycler and run under the following conditions: heat to 60 °C for 60 min followed by inactivation of proteinase K by heating to 95 °C for 20 min. Post-lysis, a PCR reaction mix (45 µl) targeting the template of choice was added and cycled for ∼35 times with Q5® Hot Start DNA polymerase (New England Biolabs).

LipidTox staining

The lipid staining protocol was done as described (*O'Rourke et al., 2009*) with modifications. Approximately 200–500 animals were harvested from NGM plates with 1X PBS and washed several times to remove *E. coli* and pelleted at 1,500 × g. To the pellet, 500 µl 2X MRWB (160 mM KCl, 40 mM NaCl, 14 mM Na_2EGTA, 1 mM Spermidine 3HCl, 0.4 mM Spermine, 30 mM NaPIPES pH 7.4, 0.2% beta-ME) and 100 µl 20% paraformaldehyde were added and the volume was adjusted up to 1 ml with 1X PBS. Inverting the tube several times mixed the worms in solution after which it was allowed to fix for ∼60 min at room temperature with gentle shaking.

After fixation, animals were pelleted at 1,500 × g and washed 3 times with 1 ml Tris–HCl buffer (100 mM, pH 7.4). After the third wash, the supernatant was discarded down to 100 µl and 650 µl of Tris-HCL buffer was added followed by 250 µl of fresh/frozen reduction buffer (100 mM Tris-Cl pH 7.4, 40 mM DTT). Worms were then left shaking for ∼30 min at room temperature. After reduction, worms were washed 3 times in 1X PBS. After the final PBS wash, the volume was brought up to 500 µl and then 500 µl of LipidTox (Red) (1:500 dilution) (Invitrogen) was added to make a final volume of 1 ml. The final concentration of 1:1,000 dilution of LipidTox was used. The worms were left in the dark for at least 60 min with shaking before viewing.

Microinjections

Microinjections of plasmids, DNA amplicons or dsRNA into gonads of young adult hermaphrodites were done using an Olympus IX70 microscope equipped with a Narishige microinjection system (Olympus, Tokyo, Japan).

Microscopy

Fluorescence microscopy and Nomarski optics microscopy were done using an Olympus BX60 microscope equipped with DP30BW CD camera (Olympus, Tokyo, Japan).

Coherent Anti-Stokes Raman Scattering microscopy (CARS)

For label-free CARS imaging the worms were anesthetized with levamisole and placed on a cover glass with a thin layer of 2% agarose. The CARS images were acquired with a Leica TCS SP8 CARS system (Leica Microsystems, Mannheim, Germany) consisting of a TCS SP8 confocal microscope combined with a picoEmerald laser (APE, Berlin, Germany) offering a fixed Stokes laser line of 1064.5 nm and a tuneable Pump line from an optical parametric oscillator (780 nm–940 nm). A HC PL IRAPO 40x water immersion objective was used for the imaging and CARS signal was detected with a non-descanned photon multiplier tube detector at the transmitted light side. For imaging of CH_2 vibration with Raman shift of 2,868 cm^{-1} pump wavelength of 815.5 nm was used. The CARS signal was selected with a CARS2000 filter cube placed in front of the detector. Adult animals and embryos were completely scanned and recorded as stacks of focal planes. Recordings for quantitative analysis were done at fixed settings for mutant and wild type.

Image analysis

Single focal planes (containing the highest number of CARS positive structures) from stacks of representative embryos and adult hermaphrodites were selected and analyzed using ImageJ computer program (http://imagej.nih.gov/ij/). Analysis for embryos was done on images of seven different embryos (seven mutant and seven wild type embryos) inside gravid hermaphrodites (only one and two cell early embryonic stages were chosen for comparison). Analysis of adult somatic tissue was performed on distal body region and we compared five different mutant adults with five different wild type adults. The images selected for analysis have been provided as supplement.

Automatic particle counting feature of ImageJ program was used for determination of the number and area of CARS positive structures with manual thresholding as described on http://imagej.net/Particle_Analysis. Image area required for analysis was first selected (the area outside the selected zone was cleared) then the image was converted to an 8-bit scale. Manual threshold was applied with settings yielding the biggest number of individually recognizable structures (adult tissue threshold setting range was 36–200 and for embryos 11–13 to 200). Overlapping structures were separated using the "Watershed" command and also by manual line draw feature. "Analyze particles" command generated data sets containing the number and area of particles. Microsoft Excel 2003 was used to perform statistical analysis and two-tailed Student's *t*-test for determining the *p*-value.

Raw data sets are provided as supplement and labels in the Excel tables correspond to the marked images also provided as supplement.

RESULTS

Identification of a perilipin orthologue in *C. elegans*

We performed BLASTp searches with individual protein sequences of human perilipins that generated no significant hits to Nematoda sequences in the UniProt database, consistent with previous efforts that failed to identify a perilipin-related protein in this phylum. However, when a sequence alignment of chordate perilipins 2 and 3 (OMA database) was submitted as query in PSI-BLAST, the *C. elegans* protein W01A8.1a (Q23095_CAEEL) was identified as a highly significant hit ($E = 3 \times 10^{-13}$). A reciprocal PSI-BLAST search with the aligned closest nematode homologues of W01A8.1a identified chordate perilipins as strong hits with human Perilipin 2 (significance score $E = 10^{-53}$) appearing in the second iteration of the search. Similarly, HHpred profile-to-profile searches with human perilipin sequences as a query of the *C. elegans* proteome identified proteins coded by W01A8.1 (a, b or c) and reciprocally W01A8.1a showed profile homology to all human perilipins and the corresponding Pfam (*Punta et al., 2012*) perilipin profile (PF03036). Each available nematode proteome contained only a single such perilipin-related sequence, in stark contrast to the insect and chordate proteomes that had 2–5 perilipin paralogues. A sequence alignment of Plin2 and 3 from two selected vertebrates is compared with their nematode homologues (Fig. 1). Although the sequence-to sequence comparisons are not sufficient to unravel the sequence homology between vertebrate and nematode Plins, the similarity appear clearly in the profile-to sequence (PSI-BLAST) and profile-to-profile (HHpred) searches. We conclude that vertebrate Plins and nematode W01A8.1 are statistically highly significant homologues.

The alignment encompasses a substantial part of *C. elegans* and human sequences (e.g., 90% of W01A8.1 and 87% of Perilipin 2) and covers all three domains characteristic for perilipins (N-terminal PAT, imperfect amphiphilic 11-mer repeat (*Brasaemle, 2007*) and C-terminal four-helix bundle (*Hickenbottom et al., 2004*)) covering approximately amino acids 10–100, 125–190 and 220–380 respectively in W01A8.1a. As W01A8.1 and human perilipins appear to be the best mutual reciprocal PSI-BLAST and HHpred hits, W01A8.1 is a very good candidate for a *C. elegans* orthologue of perilipin.

Protein databases annotate W01A8.1 as Mediator Complex subunit 28, hence the official protein name assignment of MDT-28 in WormBase (WS246). Pfam database (*Punta et al., 2012*) based the Mediator 28 Hidden Markov model profile on a seed alignment of bovine and mosquito Mediator 28 sequences with W01A8.1. This very profile was probably used subsequently in all automatic annotations of the nematode sequences. However, no substantial homology between W01A8.1 and Mediator 28 exists as shown in the above searches. Since using the WormBase name of W01A8.1 (MDT-28) would be misleading, the gene is referred here by the cosmid name *W01A8.1*, which gives rise to at least three protein isoforms designated W01A8.1a, W01A8.1b, and W01A8.1c from at least seven different transcripts (*W01A8.1a.1*, *W01A8.1a.2*, *W01A8.1b.1*, *W01A8.1b.2*, *W01A8.1b.3*,

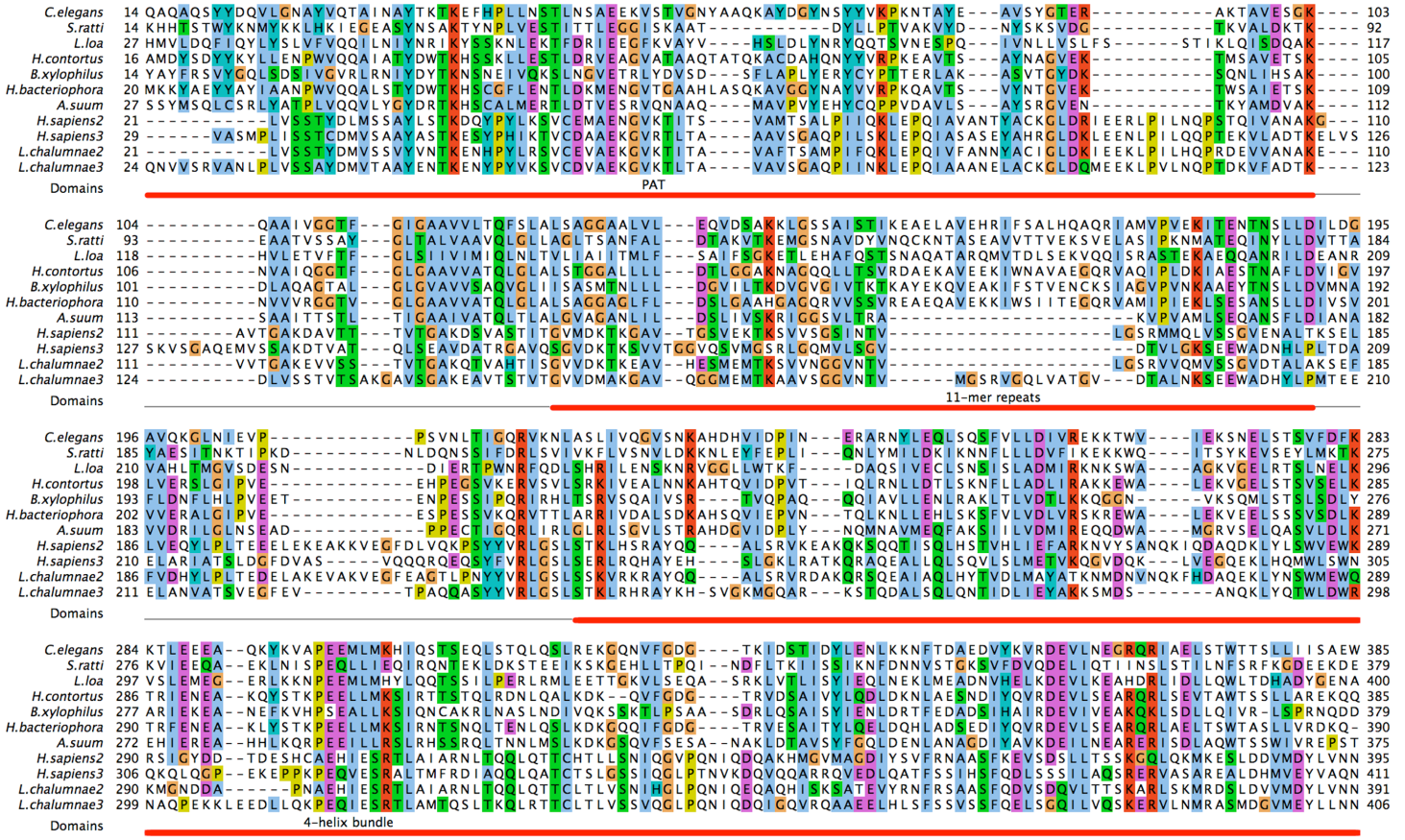

Figure 1 Identification of *C. elegans* protein W01A8.1a as a close homologue of vertebrate perilipin. *C. elegans* protein W01A8.1a is compared with nematode homologues of pairwise sequence identity lower then 70% and with Plin2 and 3 from two diverse vertebrates. The three perilipin specific domains (indicated in red) were identified through homology with human Plin3. The six 11-mer repeats in W01A8.1a (positions 126–136, 137–147, 148–158, 159–169, 170–180 and 181–191) were established with HHrepID algorithm (*Biegert & Soding, 2008*). The N-terminal PAT domain is thought to interact with HSL. The central domain consisting of imperfect 11-mer repeats forming amphipathic helices is responsible for the main affinity to LDs and the C-terminal domain containing an apolipoprotein-like 4-helix bundle probably plays an additional role in the affinity to LDs and is known to interact with ABHD5 in mammalian Plin1 and 3 (*Brasaemle, 2007*). Alignment was done using T-coffee alignment of all available nematode sequences aligned with vertebrate Plin2 and 3 sequences in three iterations using ProfileAlign routine in MyHits suite (myhits.isb-sib.ch). Selected sequences from top to bottom: (Species, database identifier): *Caenorhabditis elegans*, Q23095; *Strongyloides ratti*, CACX01001972.1; *Loa loa*, E1G5Y0 and ADBU02007219.1; *Haemonchus contortus*, CDJ80228.1; *Bursaphelenchus xylophilus*, CADV01008520.1; *Heterorhabditis bacteriophora*, ES742365.1 and ACKM01001830.1; *Ascaris suum*, U1NU60; *Homo sapiens* 2, PLIN2_HUMAN; *Homo sapiens* 3, PLIN3_HUMAN; *Latimeria chalumnae* 2, H3AYC0; *Latimeria chalumnae* 3, GAAA01019375.1. Nucleotide sequences were translated with Wise2 program (*Birney, Clamp & Durbin, 2004*). Amino acid types are colored according to the Clustal scheme (jalview.org/help/html/colourSchemes/clustal.html).

W01A8.1c.1, *W01A8.1c.2*). The three protein isoforms are 415, 385, and 418 amino acid residues in length for isoform a, b, and c, respectively (Fig. S1). According to the *C. elegans* nomenclature, we suggest to rename *W01A8.1* as *Cel-plin-1* (isoform a, b, and c) and proteins Cel-PLIN-1 (isoform a, b, and c).

W01A8.1 protein products are cytoplasmic and reside primarily on lipid droplets

If the proteins encoded by *W01A8.1* act as perilipins, they would be expected to be associated with lipid droplets (*Kozusko et al., 2015*). To test this, we created translational reporter transgenes regulated by the putative endogenous promoter expressing isoform b and lines in which the genomic locus was tagged by an in-frame C-terminal GFP cassette. The second transgene, *W01A8.1a/c::gfp*, is likely to express not only high levels of a and c tagged isoforms, but also the native isoform b (Fig. S1). The translational fusion constructs resulted in high levels of cytoplasmic proteins present in intestinal and epidermal cells on vesicular structures with the characteristic appearance of lipid droplets. This pattern of expression and cellular distribution was observed beginning at the three-fold embryonic stage and continued throughout development to adulthood (Fig. 2). To confirm that the observed GFP-associated vesicular structures were indeed lipid droplets, transgenic animals were stained with the lipophilic reagent LipidTox as previously described (*O'Rourke et al., 2009*). The translational GFP fusion protein reporters were localized at the periphery of fat droplets that were LipidTox positive (Fig. 2).

Human PLINs 1 and 2 label identical compartments as W01A8.1 proteins in *C. elegans*

We prepared transgenic *C. elegans* lines expressing human PLIN1, PLIN2 and PLIN3 fused to GFP and regulated by the *W01A8.1* promoter. PLIN1::GFP and PLIN2::GFP were localized on spherical cytoplasmic structures primarily in gut and epidermal cells (Figs. 3A, 3C, 3D and 3F) with identical appearance as W01A8.1 translational reporter GFP tagged proteins and *Drosophila* PLIN1::GFP expressed in *C. elegans* as reported by *Liu et al. (2014)*. PLIN3 expression was diffusely cytoplasmic and only faintly defined spherical structures (Figs. 3G and 3I). The structures clearly labeled with PLIN1::GFP and PLIN2::GFP were also positive in LipidTox staining (shown for PLIN2::GFP in Figs. 3J–3L). We conclude that W01A8.1 proteins are localized on the same structures as human PLIN1 and PLIN2.

W01A8.1 reduction-of-function alters the appearance of lipid droplets in early embryos and causes a reduction of brood size

To test the function of *W01A8.1*, we used RNAi done by germline injection and by feeding. *W01A8.1* RNAi made by microinjections and feeding resulted in a significantly smaller brood size, with approximately 30% less progeny. RNAi made by microinjections resulted in ∼52% reduced progeny laid in the first 24 h after microinjections and after 48 h ∼28% reduction in progeny laid compared to controls ($n = 260$, $n = 550$, for day one and $n = 1{,}000$, $n = 1{,}400$ for day two).

Repetition of knockdown by RNAi feeding over two generations confirmed this observation (Fig. S4). dsRNA feeding caused the *W01A8.1* specific group to produce ∼30% less larvae compared to controls, experiment was repeated twice independently with consistent findings. We confirmed, using RT-qPCR, that feeding based knockdown

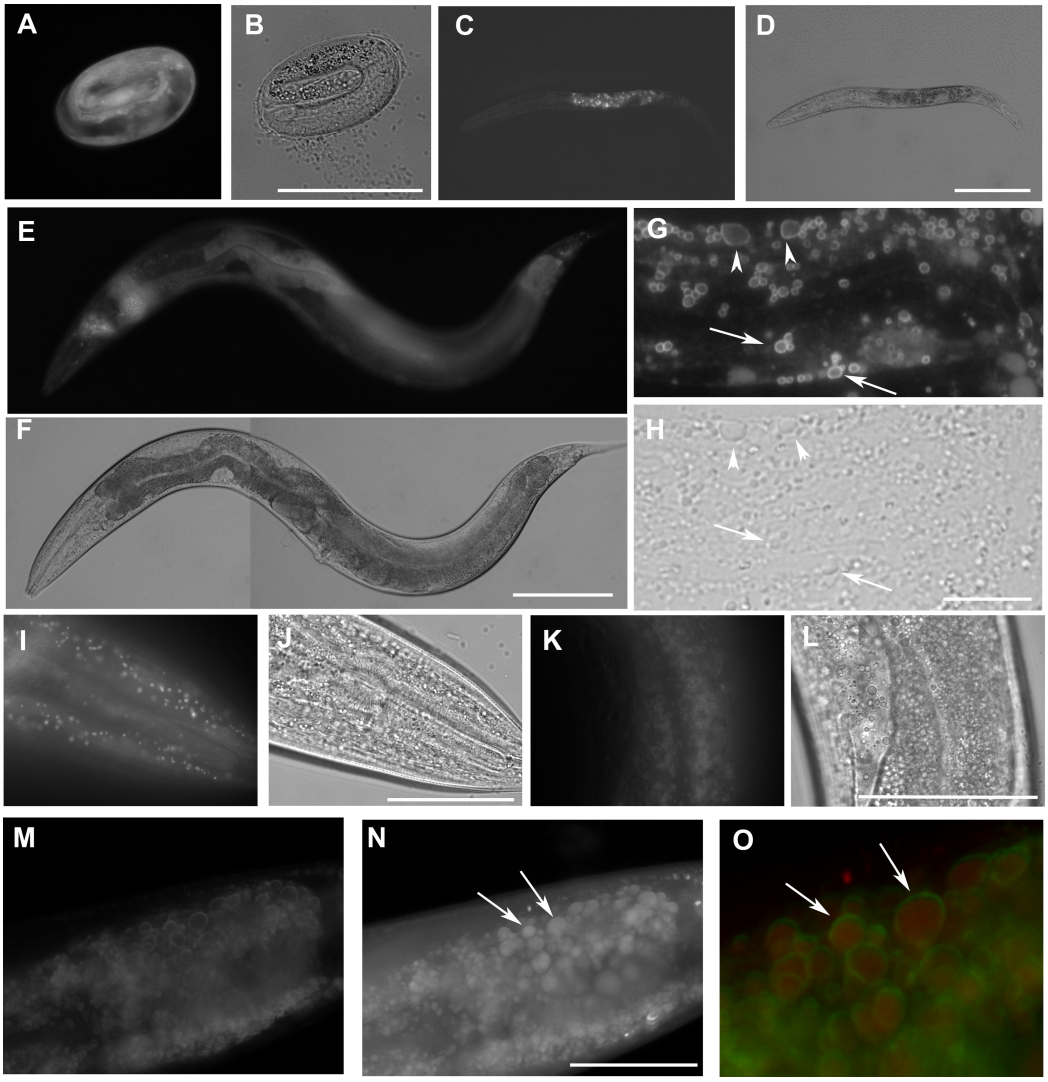

Figure 2 The expression *W01A8.1::gfp* reporter genes in transgenic strains. W01A8.1a/c::GFP is shown in (A, C, E, G), and (I), and corresponding areas in Nomarski optics are shown in (B, D, F, H) and (J). (A) The onset of expression of W01A8.1a/c::GFP in epidermal cells and in intestinal cells of three-fold embryo. (C) The expression of W01A8.1a/c::GFP in intestinal cells of an L2 larva. (E) and (G) W01A8.1a/c::GFP expression in epidermal cells and intestinal cells of a young adult hermaphrodite. (G) GFP fluorescence around lipid droplet-like structures in the intestine that are marked by arrows and arrowheads. Corresponding image in Nomarski optics is in (H). (I) A higher magnification the lipid droplet-like structures in epidermal cells labeled by W01A8.1a/c::GFP (shown in Nomarski optics in the J). (K) Lipid droplets of an unfixed intestine labeled by W01A8.1b::GFP (corresponding Nomarski image is in L). (M, N) and (O) Part of the intestine of an adult larva expressing W01A8.1b::GFP (M) with corresponding staining of lipid droplets by LipidTox (N). (O) LipidTox-positive lipid droplets (red) with W01A8.1b::GFP on the periphery (green) in this merged view. Bars represent 50 μm in (B, H, J, L) and (N) and 100 μm in (D) and (F).

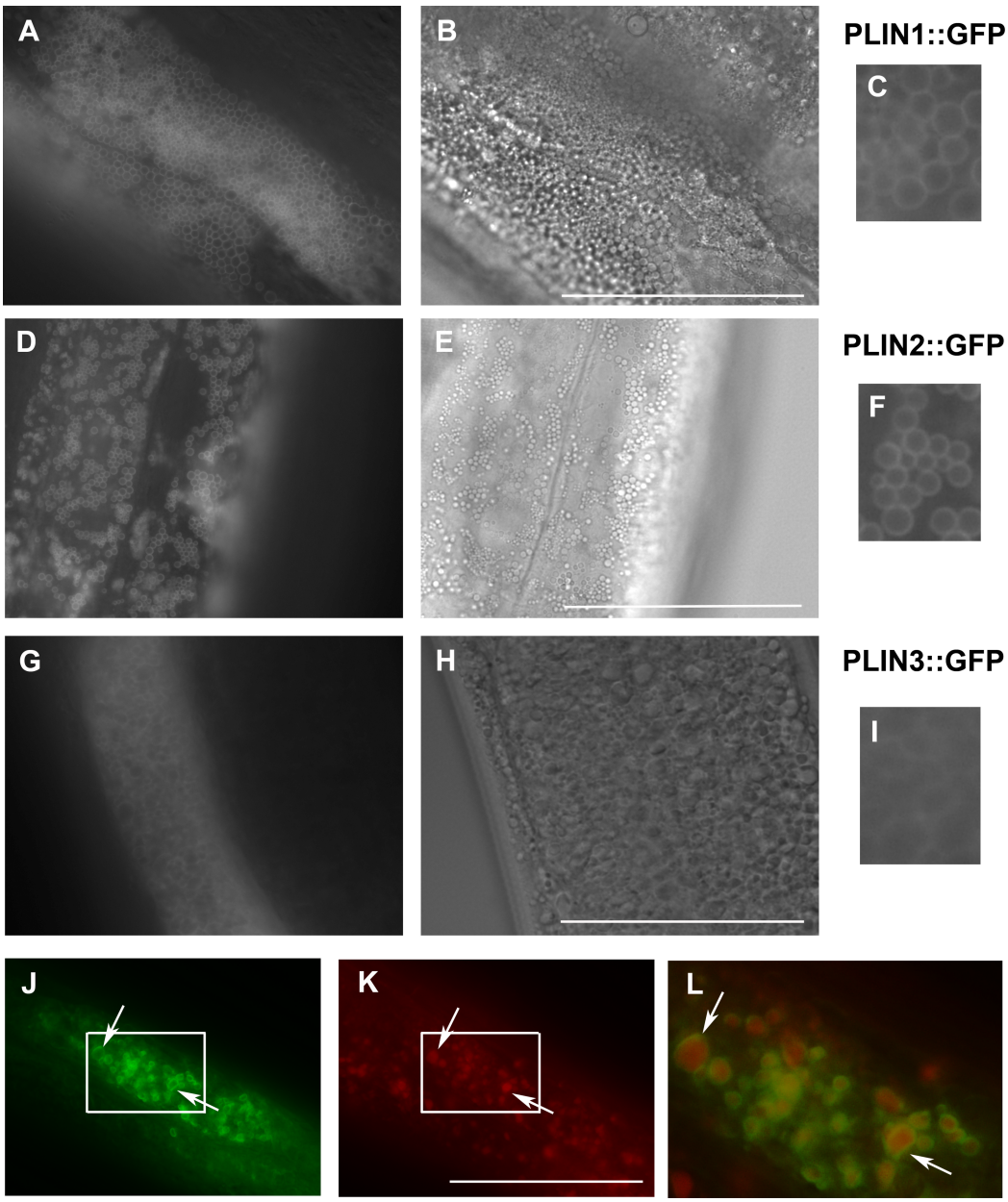

Figure 3 Expression of human perilipins fused to GFP in *C. elegans*. (A–C) Expression of human PLIN1::GFP in live transgenic *C. elegans*. PLIN1::GFP is localized on vesicles with an appearance of lipid droplets. PLIN2::GFP (D–F) is localized in transgenic animals on vesicular structures with an appearance of lipid droplets similarly as PLIN1::GFP. PLIN3::GFP (G, H and I) yields a more diffuse cytoplasmic pattern with faintly stained vesicular structures. (A, D) and (G) and details in (C, F) and (I) show GFP in fluorescence microscopy and (B, E) and (H) corresponding areas to (A, D) and (G) in Nomarski optics. (J, K) and (L) show PLIN2::GFP in fluorescence microscopy (J) in fixed *C. elegans* stained with LipidTox (K). The area indicated by the white rectangle in (J) and (K) is magnified and merged for co-localization of PLIN2::GFP (green) and LipidTox (red) in (L). Arrows indicate lipid droplets clearly marked by GFP with the LipidTox positive content. Bars represent 50 μm.

(represented in Fig. S4) resulted in approximately 45% decrease in *W01A8.1* transcripts (data not shown).

Staining of adult hermaphrodites with LipidTox (after formaldehyde fixation) revealed larger lipid droplets in early embryos derived from adults inhibited for *W01A8.1* (Figs. 4A and 4B) compared to controls (Figs. 4C and 4D).

Targeted disruption of *W01A8.1* results in early embryonic defects but not lethality

In order to eliminate the W01A8.1 function completely, we designed a CRISPR/Cas9-mediated gene editing approach to eliminate almost the entire coding region (Fig. S2). We also included a rescuing plasmid consisting of isoform a that was prepared as cDNA synthesized *in vitro* using synonymous codons (*W01A8.1(a)synth::gfp*) that is protected against CRISPR/Cas9 targeted editing but allows the production of the wild type isoform a at the protein level. Lines that expressed the GFP fusion transgene were morphologically normal and W01A8.1(a)synth::GFP was found on lipid droplet-like structures as expected (Figs. 4E and 4G) that also stained positive by LipidTox (Figs. 4F and 4G). This transgenic strain yielded lines either carrying or losing the rescuing transgene in the background of a disrupted endogenous *W01A8.1*. The elimination of W01A8.1 was easily monitored by PCR (Fig. S3). Surprisingly, animals with the deleted *W01A8.1* locus that lost the extra-chromosomal rescuing array were able to reproduce normally. From several lines that had a confirmed disruption of *W01A8.1* and a confirmed loss of the extrachromosomal array, the line CK123 (KV001) was selected and used for subsequent analyses. As was observed in *W01A8.1* RNAi embryos, loss of *W01A8.1* activity resulted in the formation of large LipidTox-positive structures (Figs. 4H and 4I) that were clearly bigger than droplets observed in control embryos using the same protocol (Figs. 4C and 4D). These large lipid-containing structures were observable in live mutant embryos (Fig. 4J) but not in wild type embryos (Fig. 4K) using Nomarski optics. Viewing through multiple focal planes in live, developing embryos lacking *W01A8.1* showed that these large lipid droplets are present in embryos during the early mitotic divisions and were localized around the nucleus. Staining with LipidTox (after fixation) confirmed the lipid content in the vesicular structures arranged around dividing nucleus (Figs. 4L and 4M). These large vesicles persist through the two-cell stage, disappearing in most embryos with more than 6 cells. On fixed embryos stained with LipidTox, larger than wild type lipid droplets are visible until late embryonic stages, including three fold embryos.

In order to visualize lipid-containing structures in *W01A8.1* null mutants and in controls *in vivo*, we used CARS microscopy (done with kind help from Dr. Zhongxiang Jiang, Leica Microsystems, Mannheim, Germany). The CARS systems allow visualization of lipids of specific categories by tuning into symmetric CH_2 vibrations of specific fat composing molecules (*Zumbusch, Langbein & Borri, 2013*). CARS microscopy clearly confirmed the formation of large lipid containing vesicles in early embryos and allowed detailed analysis of the *W01A8.1* null phenotype. CARS microscopy also confirmed the gradual increase of the size of lipid containing structures during oogenesis (Figs. 5A

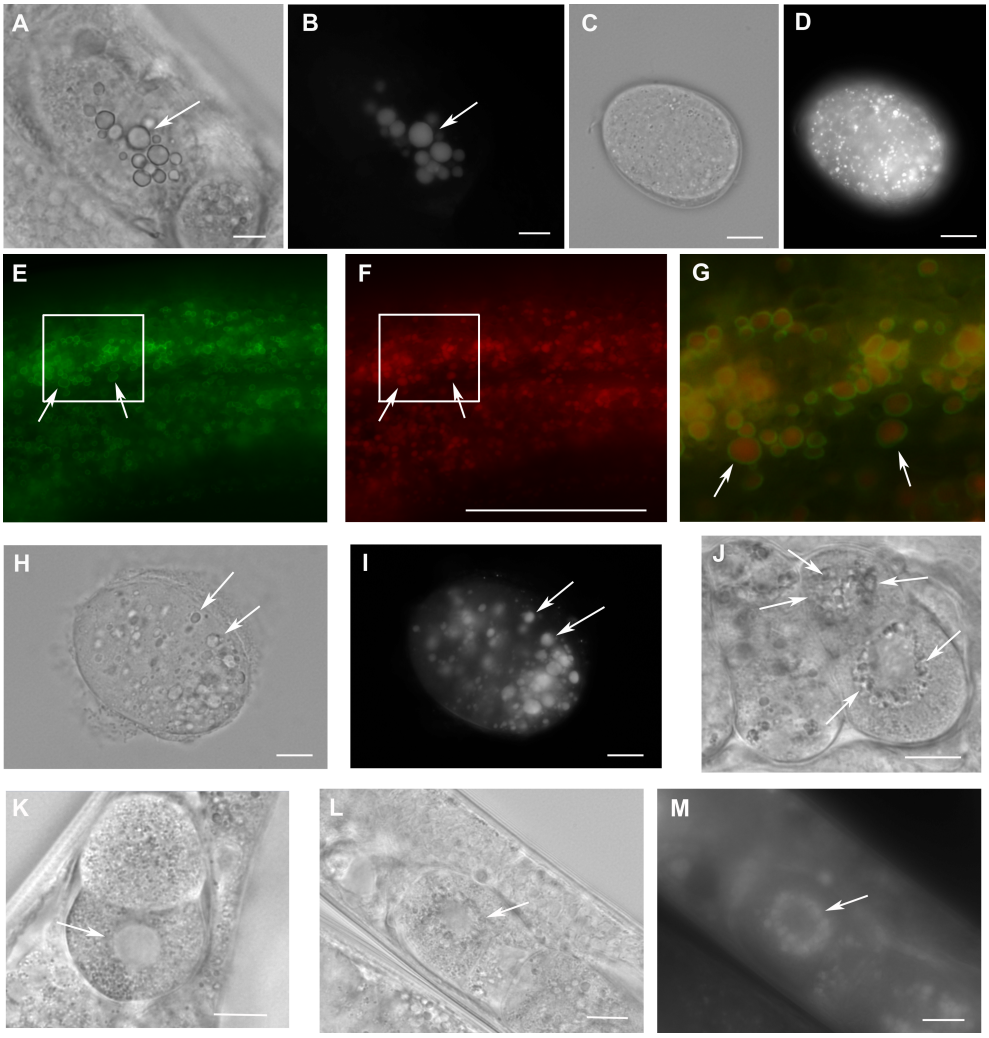

Figure 4 Loss of *W01A8.1* function results in abnormal lipid droplet appearance. (A) and (B) An embryo from a hermaphrodite inhibited for *W01A8.1* function by RNAi. Large lipid droplets stained by LipidTox (B) are visible also in Nomarski optics (A) in contrast with a control embryo that has only small and more evenly distributed lipid droplets (C—Nomarski optics and D—LipidTox staining). (E–J, L) and (M) Images of structures observed in animals with disrupted *W01A8.1*. (E) and (F) show structures with the appearance of lipid droplets in the intestine of an animal with disrupted W01A8.1 balanced with the synthetic transgene *W01A8.1(synth)::gfp*. GFP tagged synthetic W01A8.1a is localized on lipid droplets-like vesicular structures (E). (F) Shows the same area stained with LipidTox. (G) Shows in magnification a merged image of the area indicated by white rectangles in (E) and (F). Arrows indicate W01A8.1(synth)::GFP labeled lipid droplets (green) positive for lipids in LipidTox staining (red). (H) and (I) show an embryo of a parent with disrupted *W01A8.1* that had confirmed loss of the balancing transgene. Large LipidTox stained droplets are visible in Nomarski optics (H) as well as in LipidTox staining (I). Their enlargement is clearly visible in comparison with the wild type embryo shown in (C) and (D). (J) and (K) are images of live animals. (J) Shows an embryo with disrupted *W01A8.1* and confirmed loss of the balancing transgene. Large vesicular structures are formed around the dividing nucleus (arrows). (K) Shows a control embryo with normal appearance of the nuclear periphery (arrow). (L) and (M) show a one cell embryo from a parent with disrupted *W01A8.1* and confirmed loss of extrachromosomal array containing *W01A8.1(a)synth::gfp* after fixation and staining by LipidTox with large lipid droplets around the dividing nucleus visible in Nomarski optics (L) and positive for lipids in LipidTox staing (M) indicated by arrows. Bars represent 10 μm.

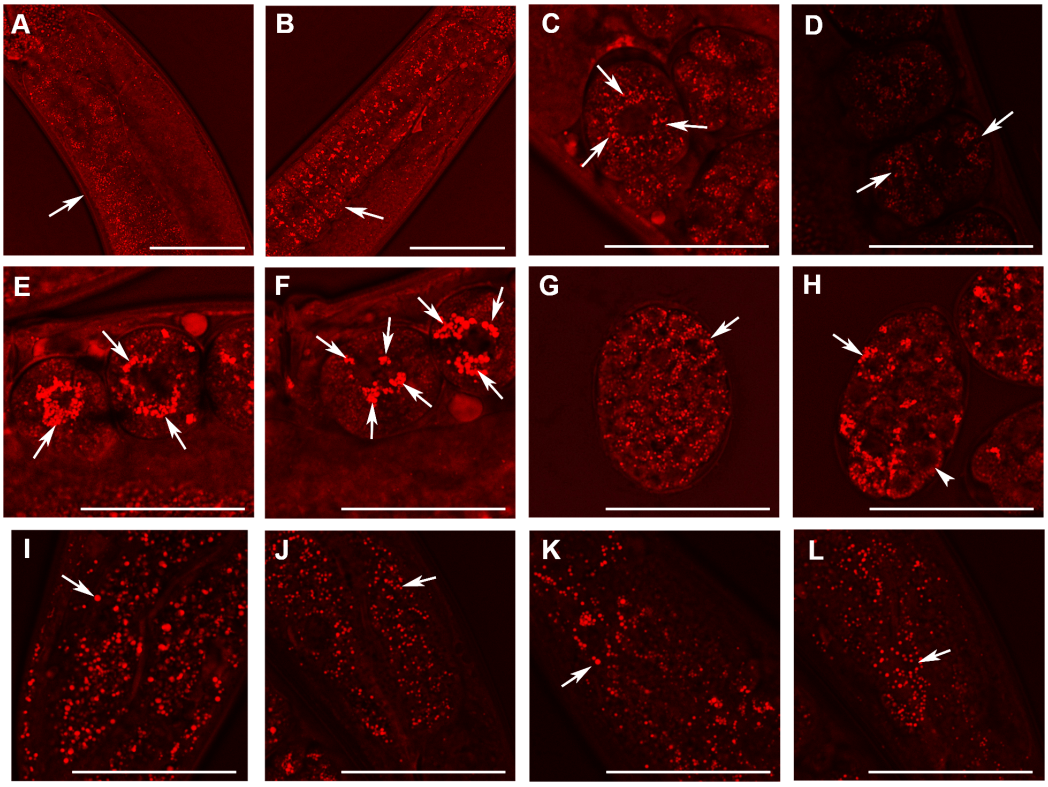

Figure 5 Analysis of lipid containing structures in live wild type animals and in animals with disrupted *W01A8.1* by CARS microscopy. CARS microscopy was performed using constant magnification and intensity settings (20% laser intensity) with the exception of control embryos (C and G) that were examined at 30% laser intensity since the lipid content was lower in wild type. The brightness of the entire figure was digitally enhanced using Adobe Photoshop brightness setting (+150 units) for better visibility of structures. Arrows indicate lipid containing structures in paired panels. (A) The germline of a wild type adult hermaphrodite animal with small lipid containing structures in oocytes and an increase in their number and size during oogenesis. (B) The germline of a mutant hermaphrodite animal. Lipid containing structures are bigger compared to the control animal yet distributed evenly in mutant oocytes. (C) Lipid containing structures localize around the nucleus in one cell wild type embryos. This tendency of the association of the lipid containing structures with nuclear periphery can be seen also during later developmental stages in wild type embryos (D). (E, F) and (H) Enlarged lipid containing structures arranged around the nuclei in mutant embryos. (F) The formation of clusters of lipid containing structures on the periphery of nuclei. (G) Shows a wild type embryo at later stage of the development. (H) The lipid containing structures progressively diminish in size in mutant embryos during later stages of embryonic development (arrowhead). (I) and (J) Lipid containing structures in enterocytes of wild type (I) and mutant (J) animals. In contrast to embryos, which exhibit higher CARS signal and bigger lipid containing structures in mutant animals, gut cells in adult animals show the opposite, that is, a reduced fat-related CARS signal and smaller lipid containing structures in mutant animals. Similarly, lipid containing structures in epidermal cells (K and L) are bigger in wild type animals as shown in the (K) and smaller in mutant animals (L). Bars represent 50 μm.

and 5B), the sudden re-localization of these structures to the periphery of the dividing nucleus in the first embryonic division (Fig. 5E), and the propagation of this phenotype, although with gradually diminishing appearance, throughout embryonic development (Figs. 5F and 5H). CARS microscopy detected this phenomenon also in wild type animals, although the size of lipid containing structures was smaller making the phenomenon of

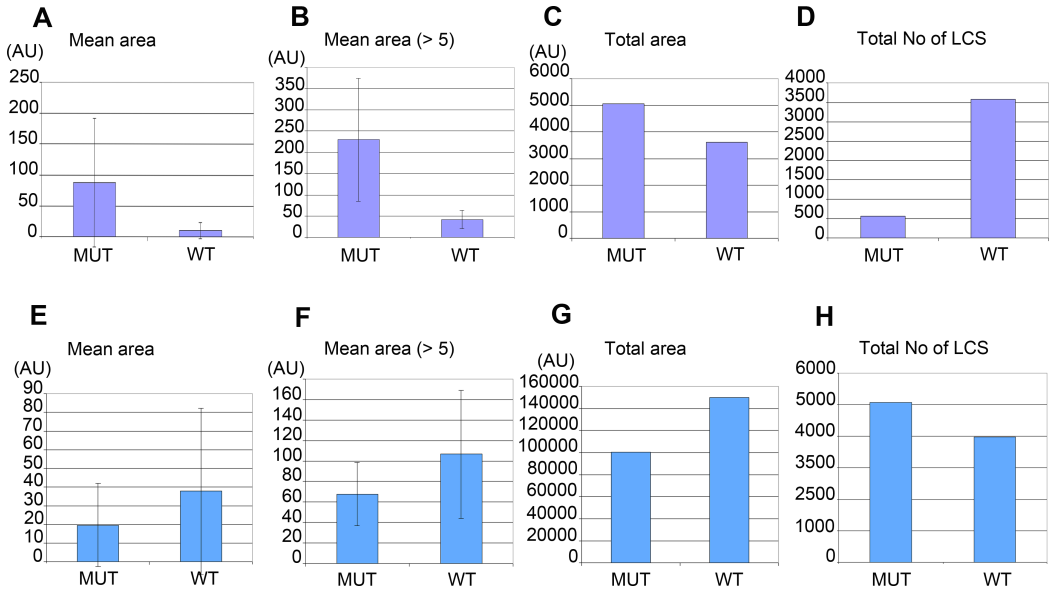

Figure 6 Morphometric analysis of lipid containing structures by CARS microscopy in wild type and *W01A8.1* null animals. Morphometric analysis was performed on CARS positive structures in single focal plane images acquired from representative mutant and wild type animal image stacks. (A–D) compare early embryos from mutant (MUT) and wild type (WT) animals using seven representative CARS images. (A) shows the mean area of all individually recognizable structures and (B) shows the mean area of all individually recognizable structures with an area bigger or equal to 5 arbitrary units (derived from pixels at the same settings). (C) compares the total area of all CARS positive structures in mutant and wild type embryos while (D) compares the total number of individually recognizable CARS positive structures (lipid containing structures—LCS) in the same embryos. (E–H) compare adult somatic tissue (tail region) from mutants and wild type hermaphrodites using five representative CARS images. (E) shows the mean area of all individually recognizable CARS positive structures and (F) shows the mean area of all individually recognizable structures with an area bigger or equal to 5 arbitrary units. (G) compares the total area of all CARS positive structures in mutant and wild type tail regions while (H) compares the total number of individually recognizable CARS positive structures (LCS) in the same regions. Vertical bars in (A, B, E) and (F) represent Standard Deviation. The results presented in (A, B, E) and (F) are statistically significant in two-tailed Student's *t*-test ($p < 0.0001$).

the sudden re-localization of lipid containing structures less obvious (Figs. 5C, 5D and 5G) than in *W01A8.1* null embryos. In contrast to embryos, lipid-containing structures in intestinal and epidermal cells of adult *W01A8.1* null mutants (Figs. 5J and 5L) were smaller than lipid-containing structures in control animals (Figs. 5I and 5K).

Morphometric analysis confirmed that *W01A8.1* null mutant embryos contained larger lipid positive structures recognized by CARS microscopy (Figs. 6A and 6B) that represent a larger total area (Fig. 6C), as determined by quantitating individual focal planes images. Morphometry revealed many small structures with area 1–4 AU (arbitrary units) with the provided threshold settings (Figs. 6A and 6E). There was a clear inverse relation in the number of large and small structures (with area <5 AU) for embryos as well as for adult tissues. The analysis in Figs. 6B and 6F shows that inclusion of small structures into analysis does not significantly affect the results but affects only standard deviation of the particle size distribution indicating that the results are independent on the setting of the limit for the size of lipid containing structures. The probability of the results were assayed using

Student's *t*-test and found to be statistically significant as the probability of this result, assuming the null hypothesis (no difference between control and experimental sets) was less than 0.0001.

Despite the fact that there were a larger number of individually recognizable lipid containing structures in wild type embryos (Fig. 6D), the mean area of these structures in mutants was considerably larger (Fig. 6C). In contrast, adult mutant animals contained smaller, more numerous lipid-containing structures (Figs. 6E, 6F and 6H) that covered a smaller total area (Fig. 6G) (and therefore volume) compared to wild type controls.

The morphometric analysis confirms that there is more CARS positive signal and therefore most likely more fat in *W01A8.1* null embryos (despite lower threshold used for analysis of wild type embryos) and less CARS positive signal (and less fat) in adult tissues of *W01A8.1* null animals compared to controls.

The analysis of the number of progeny laid by animals lacking W01A8.1 in comparison to wild type animals showed a decrease of progeny in mutant animals statistically significant on the day 3 (Fig. S5).

DISCUSSION

Lipolysis is a tightly regulated cellular process in which triacylglycerol fatty acids (TAG) are degraded into free fatty acids (FFA) and glycerol (G) with intermediates of diacylglycerol (DAG) and monoacylglycerol (MAG). The function and regulation of three key lipases (adipose triglyceride lipase (ATGL), hormone-sensitive lipase (HSL) and monoglyceride lipase (MGL) have been studied in great detail in mammalian adipocytes (reviewed in *Lass et al., 2011*). Multidomain and multifunctional LD coating proteins, the perilipins, mediate the access of ATGL and HSL to LDs. Briefly (Fig. 7), the phosphorylated N-terminal domain PAT in perilipin interacts with HSL and brings it in contact with lipid droplets (LDs) (*Shen et al., 2009*). At the same time, the C-terminal phosphorylation (controlled by the kinase PKA) releases a specific activator of ATGL named ABHD5 without which ATGL remains inactive in the cytoplasm. The final step of the glycolysis is catalyzed by MGL. Conversely, unphosphorylated perilipin blocks lipolysis in the basal fed state by blocking the access of lipolytic enzymes to the fat stored in LDs. Both HSL and ATGL are the rate-limiting enzymes needed for fatty acids mobilization (*Schweiger et al., 2006*). A variation of this regulatory process, although less well understood in detail, exists in other cells and organisms. Most organisms so far studied contain several perilipin genes, complicating the analysis of complete perilipin loss-of-function.

Clear orthologues of ATGL, HSL, MGL, ABHD5 and catalytic and regulatory subunits of PKA have been identified in *C. elegans* (ATGL-1, HOSL-1, LID-1, KIN-1, KIN-2 respectively (*Lee et al., 2014*; *Xie & Roy, 2015*) (Fig. 7). The MGL orthologue remains to be identified but several un-annotated homologous proteins exist (*Birsoy, Festuccia & Laplante, 2013*). A recent careful and elegant study of ATGL function and regulation (*Lee et al., 2014*) revealed that the process in *C. elegans* was almost identical to that found in mammalian adipocytes. Even the degradation of ABHD5 in the proteasome

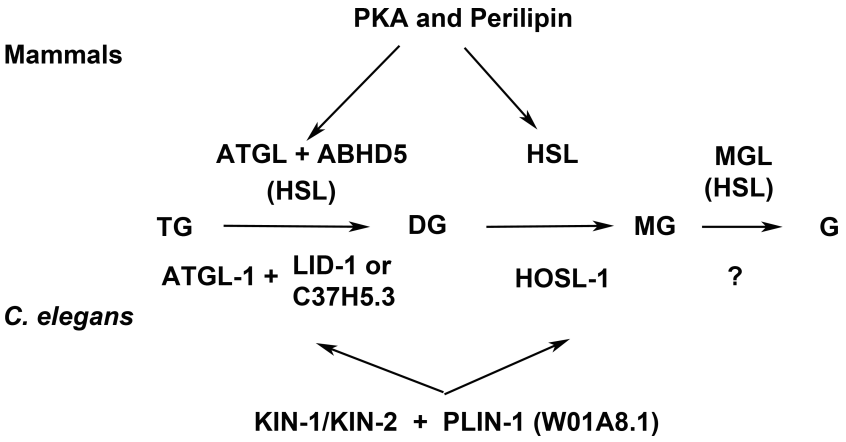

Figure 7 Enzymes and regulatory proteins involved in lipolysis (Adapted from *Lass et al., 2011*). Mammalian proteins are indicated above the arrows and their *C. elegans* orthologues (*Lee et al., 2014*) below. Triacylglycerol (TAG) is progressively hydrolysed to diacylglycerol (DAG), monoacylglycerol (MAG) and glycerol (G) by lipases specific for each of these steps: adipose triacylglycerol lipase (ATGL), hormone-sensitive lipase (HSL) and finally monoacylglycerol lipase (MGL). LID-1 and C37H5.3 were proposed to be orthologues of ABHD5/CGI58 in *C. elegans* (*Lee et al., 2014*; *Xie & Roy, 2015*). HSL also shows some activity in the first and third step. The access of ATGL and HSL to lipid droplets is regulated by perilipin, which is under the control of protein kinase A (PKA). W01A8.1 is proposed to be a perilipin orthologue in the present work.

(*Dai et al., 2013*) is mirrored in *C. elegans* (*Lee et al., 2014*). The glaring difference in fat storage and metabolism seemed to be the absence of perilipin in nematode genomes.

Here we have established that *C. elegans* possesses a close homologue of perilipin that is intimately involved in the regulation of lipid metabolism. Although the sequence alignment of *C. elegans* and human homologues of perilipin does not appear visually very informative, the underlying evolutionary conserved homology is statistically very significant. Perilipin is a scaffolding protein allowing co-evolution of interacting domains and divergence of non-docking sequences, thus the function can be conserved even with limited amino acid conservation across species. This evolutionary plasticity was already apparent in the alignment of the human perilipin paralogues where only the knowledge of the three-dimensional structure enabled observations of the similarities in the C-terminal domains (*Hickenbottom et al., 2004*). The nematode sequences have diverged beyond the point where pairwise comparisons used in routine searches can reveal homology, hence the difficulty in identifying the nematode orthologues. Only rigorous statistical analysis of the hidden Markov profiles of a great number of diverse sequences made it possible to identify the conserved domain composition.

The nematode perilipin-related protein W01A8.1 contains all three major perilipin features: N-terminal PAT domain, amphipathic region composed of imperfect helical repeats and C-terminal apolipoprotein-like four-helix bundle. In mammals, the first two domains are known to be responsible for the interaction with HSL and LDs respectively and the ATGL interaction region resides in the C-terminus following the bundle. The function of the bundle is still unclear but its stability probably fine-tunes the solubility and the affinity to LDs (*Brasaemle, 2007*). All these functions will have to

be investigated in the isoforms of W01A8.1 in the future. The repeats are confirmed by analysis of internal homology using the HHrepID algorithm and the helical composition by secondary structure prediction. The bundle appears not to be stabilized by β-sheets as in human Perilipin 3 as revealed by the absence of the homology in the C-terminal region; the β-sheets are similarly absent in Perilipin 1.

Our findings are consistent with a proteomic study that found that W01A8.1b is among the most abundant proteins associated with LDs (*Zhang et al., 2012*). Similarly, perilipins are abundant proteins on mammalian LDs, although the distribution and proportion of the individual isoforms changes depending on the cell type and metabolic state (*Brasaemle et al., 2004*). Perilipins are widely used as general markers of LDs and it seems that W01A8.1a or b can be exploited for the same purposes; human PLIN1 was recently proposed as a marker for LDs in *C. elegans* (*Liu et al., 2014*).

Surprisingly, in laboratory conditions *C. elegans* can overcome the complete loss of the perilipin-related protein W01A8.1, presumably by activating perilipin-independent lipid degradation. Previous work has shown that an additional lipid degradation pathway, autophagy, was important for lipid metabolism in *C. elegans* (*Lapierre et al., 2013*), mammals (*Singh et al., 2009*) as well as in yeast (*Van Zutphen et al., 2014*). Similarly in *Drosophila*, which has two perilipins (*plin1* and *plin2*), the double mutants are viable but have small lipid droplets. This suggests that perilipins are required for growth or maintenance of lipid droplets, but are dispensable for lipolysis (*Beller et al., 2010*; *Bi et al., 2012*). The abnormal LD behavior, but viability, of *W01A8.1* null animals strongly suggests a regulatory role for the nematode perilipin-related protein in the regulation of fat metabolism that is similar to perilipins in other phyla. Taking in account the opposing phenotypes of *Drosophila plin1* and *plin2* loss of function regarding to lipid droplet size, it is intriguing to speculate that individual W01A8.1 splice forms may support distinct functions as well. It is also possible that some functions of W01A8.1 protein forms may be related to a proposed ancestral protein acting differently than mammalian perilipins as was suggested by *Beller et al. (2010)*. A possibility of the existence of an ancestor protein with wider, less specific functionality may be also considered if such a parallel to enzymatic activities of ancestral proteins (*Hujova et al., 2005*) is taken in account.

CARS microscopy allowed a detailed analysis of lipid containing structures in wild type and in mutant animals *in vivo*. Detection of lipids *in vivo* showed that the lack of the perilipin homologue affects the intracellular distribution of lipid droplets, which is in agreement with the role of perilipin homologue LSD2 (PLIN2) in movement of lipid droplets in *Drosophila* (*Cohen, 2005*; *Welte et al., 2005*). Analysis of lipid-containing structures in developing embryos and in adult tissues suggested that W01A8.1 protein forms are likely to act differently in embryos than in adult tissues and lipid-containing structures in embryos are likely to differ from those of adult tissues. The characteristic aggregation of lipid-containing structures around the embryonic nuclei clearly detected in *C. elegans* embryos by CARS microscopy are reminiscent of lipid droplets recently reported to be a characteristic feature of cancer stem cells in colorectal carcinomas (*Tirinato et al., 2015*).

Our results suggest that the previously accepted view of a perilipin-independent nematode fatty acid flux of LDs needs to be revisited. Clearly we see evidence for perilipin-like LD regulation that is evolutionarily conserved. Based on the results reported here, *W01A8.1* is renamed with permission from WormBase as *plin-1* (*Cel-plin-1* with species identifier). With only a single gene and a toolbox of forward and reverse genetic approaches at hand, *C. elegans* offers an opportunity to explore the exact role of perlipin-related factors in fat regulation throughout development of many different somatic and germline cells. Exploitation of these opportunities will likely reveal new levels of regulation and novel players in the complex and vital regulation of fat in all organisms.

ACKNOWLEDGEMENTS

The authors thank WormBase and NCBI for accessibility of data and bioinformatics support and CGC for the N2 wild type strain. Authors thank Dr. Zhongxiang Jiang and Leica Microsystems CMS GmbH (Mannheim, Germany) for CARS microscopy. Authors thank Dr. Sebastian Honnen, and Reviewer 2 for valuable suggestions and corrections.

ADDITIONAL INFORMATION AND DECLARATIONS

Funding

This work was supported by the European Regional Development Fund "BIOCEV—Biotechnology and Biomedicine Centre of the Academy of Sciences and Charles University in Vestec" (CZ.1.05/1.1.00/02.0109); the grant PRVOUK-P27/LF1/1 from Charles University in Prague; the grants SVV 260023/2014 and SVV 260149/2015 from Charles University in Prague. MWK is supported by the Intramural Research Program of the National Institute of Diabetes and Digestive and Kidney Diseases (NIDDK) of the National Institutes of Health, USA. The authors received funds from MediCentrum Praha a.s. to support the work reported in this publication. ZK and MK contributed personal funds to this work. The funders (excluding the authors) had no role in study design, data collection and analysis, decision to publish, or preparation of the manuscript.

Grant Disclosures

The following grant information was disclosed by the authors:
European Regional Development Fund: CZ.1.05/1.1.00/02.0109.
Charles University in Prague: PRVOUK-P27/LF1/1, SVV 260023/2014, SVV 260149/2015.
National Institute of Diabetes and Digestive and Kidney Diseases (NIDDK).

Competing Interests

Marta Kostrouchová is an Academic Editor for PeerJ. The authors declare there are no competing interests.

Author Contributions

- Ahmed Ali Chughtai, Filip Kaššák and Markéta Kostrouchová conceived and designed the experiments, performed the experiments, analyzed the data, wrote the paper, prepared figures and/or tables, reviewed drafts of the paper.

- Jan Philipp Novotný conceived and designed the experiments, performed the experiments, analyzed the data, wrote the paper, reviewed drafts of the paper.
- Michael W. Krause conceived and designed the experiments, analyzed the data, wrote the paper, reviewed drafts of the paper.
- Vladimír Saudek conceived and designed the experiments, analyzed the data, wrote the paper, prepared figures and/or tables, reviewed drafts of the paper.
- Zdenek Kostrouch and Marta Kostrouchová conceived and designed the experiments, performed the experiments, analyzed the data, contributed reagents/materials/analysis tools, wrote the paper, prepared figures and/or tables, reviewed drafts of the paper.

Human Ethics

The following information was supplied relating to ethical approvals (i.e., approving body and any reference numbers):

Human PLIN2 and PLIN3 were cloned from a collection of anonymous unmarked samples (PLIN2), and from human peripheral lymphocytes (PLIN3) donated by a volunteer with a written consent in compliance with the legislation of the Czech Republic and European Union (Act No 372/2011 of 11. 11. 2011 on Health Care Services, Coll., Paragraph 81, section 1a and section 4a, which is in accordance with the declaration of Helsinki) and was approved by the Ethical Committee of the First Faculty of Medicine, Charles University in Prague (Ref. No. MZ13-UK1LF-KostrouchZdenek).

Supplemental Information

Supplemental information for this article can be found online at http://dx.doi.org/10.7717/peerj.1213#supplemental-information.

REFERENCES

Altschul SF, Madden TL, Schaffer AA, Zhang J, Zhang Z, Miller W, Lipman DJ. 1997. Gapped BLAST and PSI-BLAST: a new generation of protein database search programs. *Nucleic Acids Research* **25**:3389–3402 DOI 10.1093/nar/25.17.3389.

Beller M, Bulankina AV, Hsiao HH, Urlaub H, Jackle H, Kuhnlein RP. 2010. PERILIPIN-dependent control of lipid droplet structure and fat storage in *Drosophila*. *Cell Metabolism* **12**:521–532 DOI 10.1016/j.cmet.2010.10.001.

Bi J, Xiang Y, Chen H, Liu Z, Gronke S, Kuhnlein RP, Huang X. 2012. Opposite and redundant roles of the two *Drosophila* perilipins in lipid mobilization. *Journal of Cell Science* **125**:3568–3577 DOI 10.1242/jcs.101329.

Biegert A, Soding J. 2008. De novo identification of highly diverged protein repeats by probabilistic consistency. *Bioinformatics* **24**:807–814 DOI 10.1093/bioinformatics/btn039.

Birney E, Clamp M, Durbin R. 2004. GeneWise and Genomewise. *Genome Research* **14**:988–995 DOI 10.1101/gr.1865504.

Birsoy K, Festuccia WT, Laplante M. 2013. A comparative perspective on lipid storage in animals. *Journal of Cell Science* **126**:1541–1552 DOI 10.1242/jcs.104992.

Brasaemle DL. 2007. Thematic review series: adipocyte biology. The perilipin family of structural lipid droplet proteins: stabilization of lipid droplets and control of lipolysis. *Journal of Lipid Research* **48**:2547–2559 DOI 10.1194/jlr.R700014-JLR200.

Brasaemle DL, Dolios G, Shapiro L, Wang R. 2004. Proteomic analysis of proteins associated with lipid droplets of basal and lipolytically stimulated 3T3-L1 adipocytes. *Journal of Biological Chemistry* **279**:46835–46842 DOI 10.1074/jbc.M409340200.

Brenner S. 1974. The genetics of *Caenorhabditis elegans*. *Genetics* **77**:71–94.

Cohen RS. 2005. Microtubule motors: LSD2 trips the toggle. *Current Biology* **15**:R651–R653 DOI 10.1016/j.cub.2005.08.027.

Dai Z, Qi W, Li C, Lu J, Mao Y, Yao Y, Li L, Zhang T, Hong H, Li S, Zhou T, Yang Z, Yang X, Gao G, Cai W. 2013. Dual regulation of adipose triglyceride lipase by pigment epithelium-derived factor: a novel mechanistic insight into progressive obesity. *Molecular and Cellular Endocrinology* **377**:123–134 DOI 10.1016/j.mce.2013.07.001.

Dickinson DJ, Ward JD, Reiner DJ, Goldstein B. 2013. Engineering the Caenorhabditis elegans genome using Cas9-triggered homologous recombination. *Nature Methods* **10**:1028–1034 DOI 10.1038/nmeth.2641.

Du X, Barisch C, Paschke P, Herrfurth C, Bertinetti O, Pawolleck N, Otto H, Ruhling H, Feussner I, Herberg FW, Maniak M. 2013. Dictyostelium lipid droplets host novel proteins. *Eukaryotic Cell* **12**:1517–1529 DOI 10.1128/EC.00182-13.

Hickenbottom SJ, Kimmel AR, Londos C, Hurley JH. 2004. Structure of a lipid droplet protein; the PAT family member TIP47. *Structure* **12**:1199–1207 DOI 10.1016/j.str.2004.04.021.

Hujova J, Sikora J, Dobrovolny R, Poupetova H, Ledvinova J, Kostrouchova M, Hrebicek M. 2005. Characterization of gana-1, a *Caenorhabditis elegans* gene encoding a single ortholog of vertebrate alpha-galactosidase and alpha-N-acetylgalactosaminidase. *BMC Cell Biology* **6**:5 DOI 10.1186/1471-2121-6-5.

Kimmel AR, Brasaemle DL, McAndrews-Hill M, Sztalryd C. 2010. Adoption of PERILIPIN as a unifying nomenclature for the mammalian PAT-family of intracellular lipid storage droplet proteins. *Journal of Lipid Research* **51**:468–471 DOI 10.1194/jlr.R000034.

Kozusko K, Tsang VH, Bottomley W, Cho YH, Gandotra S, Mimmack M, Lim K, Isaac I, Patel S, Saudek V, O'Rahilly S, Srinivasan S, Greenfield JR, Barroso I, Campbell LV, Savage DB. 2015. Clinical and molecular characterization of a novel PLIN1 frameshift mutation identified in patients with familial partial lipodystrophy. *Diabetes* **64**:299–310 DOI 10.2337/db14-0104.

Lapierre LR, Silvestrini MJ, Nunez L, Ames K, Wong S, Le TT, Hansen M, Melendez A. 2013. Autophagy genes are required for normal lipid levels in *C. elegans*. *Autophagy* **9**:278–286 DOI 10.4161/auto.22930.

Lass A, Zimmermann R, Oberer M, Zechner R. 2011. Lipolysis—a highly regulated multi-enzyme complex mediates the catabolism of cellular fat stores. *Progress in Lipid Research* **50**:14–27 DOI 10.1016/j.plipres.2010.10.004.

Lee JH, Kong J, Jang JY, Han JS, Ji Y, Lee J, Kim JB. 2014. Lipid droplet protein LID-1 mediates ATGL-1-dependent lipolysis during fasting in *Caenorhabditis elegans*. *Molecular and Cellular Biology* **34**:4165–4176 DOI 10.1128/MCB.00722-14.

Liu Z, Li X, Ge Q, Ding M, Huang X. 2014. A lipid droplet-associated GFP reporter-based screen identifies new fat storage regulators in *C. elegans*. *Journal of Genetics and Genomics* **41**:305–313 DOI 10.1016/j.jgg.2014.03.002.

Lu X, Gruia-Gray J, Copeland NG, Gilbert DJ, Jenkins NA, Londos C, Kimmel AR. 2001. The murine perilipin gene: the lipid droplet-associated perilipins derive from tissue-specific, mRNA splice variants and define a gene family of ancient origin. *Mammalian Genome* **12**:741–749 DOI 10.1007/s00335-01-2055-5.

Notredame C, Higgins DG, Heringa J. 2000. T-Coffee: a novel method for fast and accurate multiple sequence alignment. *Journal of Molecular Biology* **302**:205–217 DOI 10.1006/jmbi.2000.4042.

O'Rourke EJ, Soukas AA, Carr CE, Ruvkun G. 2009. *C. elegans* major fats are stored in vesicles distinct from lysosome-related organelles. *Cell Metabolism* **10**:430–435 DOI 10.1016/j.cmet.2009.10.002.

Punta M, Coggill PC, Eberhardt RY, Mistry J, Tate J, Boursnell C, Pang N, Forslund K, Ceric G, Clements J, Heger A, Holm L, Sonnhammer EL, Eddy SR, Bateman A, Finn RD. 2012. The Pfam protein families database. *Nucleic Acids Research* **40**:D290–D301 DOI 10.1093/nar/gkr1065.

Remmert M, Biegert A, Hauser A, Soding J. 2011. HHblits: lightning-fast iterative protein sequence searching by HMM-HMM alignment. *Nature Methods* **9**:173–175 DOI 10.1038/nmeth.1818.

Schweiger M, Schreiber R, Haemmerle G, Lass A, Fledelius C, Jacobsen P, Tornqvist H, Zechner R, Zimmermann R. 2006. Adipose triglyceride lipase and hormone-sensitive lipase are the major enzymes in adipose tissue triacylglycerol catabolism. *Journal of Biological Chemistry* **281**:40236–40241 DOI 10.1074/jbc.M608048200.

Shen WJ, Patel S, Miyoshi H, Greenberg AS, Kraemer FB. 2009. Functional interaction of hormone-sensitive lipase and perilipin in lipolysis. *Journal of Lipid Research* **50**:2306–2313 DOI 10.1194/jlr.M900176-JLR200.

Simeckova K, Brozova E, Vohanka J, Pohludka M, Kostrouch Z, Krause MW, Rall JE, Kostrouchova M. 2007. Supplementary nuclear receptor NHR-60 is required for normal embryonic and early larval development of *Caenorhabditis elegans*. *Folia Biolica* **53**:85–96.

Singh R, Kaushik S, Wang Y, Xiang Y, Novak I, Komatsu M, Tanaka K, Cuervo AM, Czaja MJ. 2009. Autophagy regulates lipid metabolism. *Nature* **458**:1131–1135 DOI 10.1038/nature07976.

Tabara H, Sarkissian M, Kelly WG, Fleenor J, Grishok A, Timmons L, Fire A, Mello CC. 1999. The rde-1 gene, RNA interference, and transposon silencing in *C. elegans*. *Cell* **99**:123–132 DOI 10.1016/S0092-8674(00)81644-X.

Teixeira L, Rabouille C, Rorth P, Ephrussi A, Vanzo NF. 2003. *Drosophila* Perilipin/ADRP homologue Lsd2 regulates lipid metabolism. *Mechanisms of Development* **120**:1071–1081 DOI 10.1016/S0925-4773(03)00158-8.

Timmons L, Court DL, Fire A. 2001. Ingestion of bacterially expressed dsRNAs can produce specific and potent genetic interference in *Caenorhabditis elegans*. *Gene* **263**:103–112 DOI 10.1016/S0378-1119(00)00579-5.

Tirinato L, Liberale C, Di Franco S, Candeloro P, Benfante A, La Rocca R, Potze L, Marotta R, Ruffilli R, Rajamanickam VP, Malerba M, De Angelis F, Falqui A, Carbone E, Todaro M, Medema JP, Stassi G, Di Fabrizio E. 2015. Lipid droplets: a new player in colorectal cancer stem cells unveiled by spectroscopic imaging. *Stem Cells* **33**:35–44 DOI 10.1002/stem.1837.

Van Zutphen T, Todde V, De Boer R, Kreim M, Hofbauer HF, Wolinski H, Veenhuis M, Van der Klei IJ, Kohlwein SD. 2014. Lipid droplet autophagy in the yeast Saccharomyces cerevisiae. *Molecular Biology of the Cell* **25**:290–301 DOI 10.1091/mbc.E13-08-0448.

Vohanka J, Simeckova K, Machalova E, Behensky F, Krause MW, Kostrouch Z, Kostrouchova M. 2010. Diversification of fasting regulated transcription in a cluster of duplicated nuclear hormone receptors in *C. elegans*. *Gene Expression Patterns* **10**:227–236 DOI 10.1016/j.gep.2010.05.001.

Wang C, St Leger RJ. 2007. The Metarhizium anisopliae perilipin homolog MPL1 regulates lipid metabolism, appressorial turgor pressure, and virulence. *Journal of Biological Chemistry* **282**:21110–21115 DOI 10.1074/jbc.M609592200.

Welte MA, Cermelli S, Griner J, Viera A, Guo Y, Kim DH, Gindhart JG, Gross SP. 2005. Regulation of lipid-droplet transport by the perilipin homolog LSD2. *Current Biology* **15**:1266–1275 DOI 10.1016/j.cub.2005.06.062.

Xie M, Roy R. 2015. The causative gene in chanarian dorfman syndrome regulates lipid droplet homeostasis in *C. elegans*. *PLoS Genetics* **11**:e1005284 DOI 10.1371/journal.pgen.1005284.

Zhang P, Na H, Liu Z, Zhang S, Xue P, Chen Y, Pu J, Peng G, Huang X, Yang F, Xie Z, Xu T, Xu P, Ou G, Zhang SO, Liu P. 2012. Proteomic study and marker protein identification of *Caenorhabditis elegans* lipid droplets. *Mol Cell Proteomics* **11**:317–328 DOI 10.1074/mcp.M111.016345.

Zumbusch A, Langbein W, Borri P. 2013. Nonlinear vibrational microscopy applied to lipid biology. *Progress in Lipid Research* **52**:615–632 DOI 10.1016/j.plipres.2013.07.003.

The nematode homologue of Mediator complex subunit 28, F28F8.5, is a critical regulator of *C. elegans* development

Markéta Kostrouchová[1,2], David Kostrouch[1], Ahmed A. Chughtai[1], Filip Kaššák[1], Jan P. Novotný[1], Veronika Kostrouchová[1], Aleš Benda[3], Michael W. Krause[4], Vladimír Saudek[5], Marta Kostrouchová[1] and Zdeněk Kostrouch[1]

[1] Biocev, First Faculty of Medicine, Charles University, Prague, Czech Republic
[2] Department of Pathology, Third Faculty of Medicine, Charles University, Prague, Czech Republic
[3] Imaging Methods Core Facility, BIOCEV, Faculty of Science, Charles University, Prague, Czech Republic
[4] Laboratory of Molecular Biology, National Institute of Diabetes and Digestive and Kidney Diseases, National Institutes of Health, Bethesda, MD, USA
[5] Metabolic Research Laboratories, Wellcome Trust-Medical Research Council Institute of Metabolic Science, University of Cambridge, Cambridge, UK

ABSTRACT

The evolutionarily conserved Mediator complex is a critical player in regulating transcription. Comprised of approximately two dozen proteins, the Mediator integrates diverse regulatory signals through direct protein-protein interactions that, in turn, modulate the influence of Mediator on RNA Polymerase II activity. One Mediator subunit, MED28, is known to interact with cytoplasmic structural proteins, providing a potential direct link between cytoplasmic dynamics and the control of gene transcription. Although identified in many animals and plants, MED28 is not present in yeast; no bona fide MED28 has been described previously in *Caenorhabditis elegans*. Here, we identify bioinformatically F28F8.5, an uncharacterized predicted protein, as the nematode homologue of MED28. As in other Metazoa, F28F8.5 has dual nuclear and cytoplasmic localization and plays critical roles in the regulation of development. *F28F8.5* is a vital gene and its null mutants have severely malformed gonads and do not reproduce. F28F8.5 interacts on the protein level with the Mediator subunits MDT-6 and MDT-30. Our results indicate that F28F8.5 is an orthologue of MED28 and suggest that the potential to link cytoplasmic and nuclear events is conserved between MED28 vertebrate and nematode orthologues.

Subjects Cell Biology, Developmental Biology, Evolutionary Studies, Molecular Biology
Keywords Gene expression regulation, *Caenorhabditis elegans*, Development, Evolution, Mediator complex, MED28

INTRODUCTION

The Mediator complex is a multiprotein assembly that is capable of integrating cellular signals with the regulation of transcription through direct interaction with RNA Polymerase II (Pol II). The Mediator complex is found in all eukaryotic organisms.

Submitted 13 October 2016
Accepted 8 May 2017
Published 6 June 2017

Corresponding author
Zdeněk Kostrouch,
Zdenek.kostrouch@lf1.cuni.cz

Academic editor
Heather Etchevers

Additional Information and Declarations can be found on page 23

DOI **10.7717/peerj.3390**

The core Mediator complex is comprised of 21 protein subunits in yeast and a similar number (26) in mammals, all named MED followed by a unique numerical designation (*Poss, Ebmeier & Taatjes, 2013*; *Allen & Taatjes, 2015*). In addition to this core Mediator complex, four additional subunits comprising the CDK8 or kinase module can associate with the core (*Poss, Ebmeier & Taatjes, 2013*). The Mediator complex likely co-evolved with basal transcription factors with a level of conservation between different phyla that is relatively low (*Poss, Ebmeier & Taatjes, 2013*; *Allen & Taatjes, 2015*). While most Mediator subunits are present in similar molar ratios and comprise the core complex, some subunits were found to be present in variable amounts when complexes were isolated from tissue culture cells (*Kulak et al., 2014*). Quantification of proteomically analyzed Mediator subunits showed that distinct forms of the complex have variable transcriptional activity (*Paoletti et al., 2006*) and analysis of Mediator complex subunits in *Drosophila* indicated that some subunits are critical only for specific gene transcription from endogenous genes but not for transcription from synthetic promoters (*Kim et al., 2004*). This diversity of Mediator subunit function reflects distinct transcription factor interactions with Mediator components and with Pol II, greatly expanding its possible regulatory roles for Mediator. For example, some Mediator subunits are essential for the transcription of many different protein-coding genes, while other subunits are essential for only a subset of genes, translating cellular signaling pathways to the regulation of specific target gene sets (reviewed in *Grants, Goh & Taubert (2015)*).

One of the Mediator complex subunits, MED28, is only found in higher eukaryotes. MED28 was originally identified as a gene expressed in endothelial cells where it was named EG-1 (Endothelial-derived Gene-1) (*Liu et al., 2002*); it was later shown to be part of the Mediator complex and re-named MED28 (*Sato et al., 2004*; *Beyer et al., 2007*). In addition to its role in the Mediator complex, the MED28 subunit has several cytoplasmic-associated interactions. MED28 has been shown to associate with (1) the actin cytoskeleton and linked to the regulation of smooth muscle genes (*Wiederhold et al., 2004*), (2) several Src-family kinases and it is a target of their phosphorylation (*Lee et al., 2006*), and (3) the plasma membrane where it interacts with Grb2 and Merlin (also called Neurofibromin 2 or Schwannomin) (*Wiederhold et al., 2004*), membrane-cytoskeleton scaffolding proteins linking actin filaments to the cell membrane (*McClatchey & Giovannini, 2005*; *McClatchey & Fehon, 2009*). These many and diverse cytoplasmic interactions suggest that MED28 could function to transmit cytoskeletal signals to transcription in the nucleus (*Lee et al., 2006*).

Although conserved between insects and mammals, a bona fide MED28 homologue had yet to be identified in nematodes. The relatively low conservation of Mediator complex subunits between eukaryotic phyla (*Poss, Ebmeier & Taatjes, 2013*; *Allen & Taatjes, 2015*) makes the identification of orthologues in distant species difficult and some suggested orthologues may require re-classification. Our previous work showed that the protein previously identified as "MDT-28" (**Med**ia**t**or-28) in nematodes (*Bourbon, 2008*) is instead the nematode homologue of perilipin, a protein regulating lipid metabolism at the level of lipid droplets and is not related to MED28 (*Chughtai et al., 2015*). Thinking it was unlikely that a MED28 homologue would be absent in nematode

genomes, we searched for it using the conserved features of MED28 orthologues from various phyla. Herein we identify a previously uncharacterized protein, F28F8.5, as the closest MED28 homologue. We show that F28F8.5 localizes to both nuclear and cytoplasmic compartments in most, if not all, cells throughout development. Downregulation by RNAi, or disruption of *F28F8.5* by deletion, results in multiple developmental defects during embryonic and larval development. Our work indicates that the homologue of Mediator complex subunit 28 exists in nematodes and suggests that the potential to link cytoplasmic and nuclear events is conserved between vertebrate and nematode MED28 homologues.

MATERIALS AND METHODS

Sequence analysis

The UniProtKB (http://www.uniprot.org) and NCBI (https://www.ncbi.nlm.nih.gov) databases were searched with BLAST, PSI-BLAST (*Altschul et al., 1997*), HHblits (*Remmert et al., 2011*), and HHpred (*Söding, Biegert & Lupas, 2005*) programs. The protein sequences were identified with their UniProtKB identifiers and the nucleotide sequences with their NCBI ones. The sequences were aligned with T-coffee (*Notredame, Higgins & Heringa, 2000*; *Di Tommaso et al., 2011*) and PROMALS (*Pei & Grishin, 2007*; *Pei et al., 2007*; *Pei, Kim & Grishin, 2008*). The secondary structure predictions were performed with PSIPRED (*Jones, 1999*; *Cuff & Barton, 2000*; *McGuffin, Bryson & Jones, 2000*). Multiple sequence alignments were displayed and analyzed with Jalview (*Clamp et al., 2004*).

RNA isolation and cDNA synthesis

RNA and cDNA were prepared as described (*Zima et al., 2015*) with modifications. Cultured nematodes were collected in water and pelleted by centrifugation for 5 min at 200 × g and 4 °C. The excess of water was removed and the pellet was frozen at −80 °C. For the isolation of RNA, the pellet was quickly melted and dissolved in 300 µl of resuspension buffer (10 mM Tris–HCl; 10 mM EDTA, 5% 2-mercaptoethanol; 0.5% SDS; pH 7.5). After adding 8 µl of proteinase K (20 mg/ml), the sample was mixed and incubated 1 h at 55 °C. RNA was isolated by phenol–chloroform extraction and ethanol precipitation. The obtained RNA was incubated with RQ1 DNase (Promega, Fitchburg, WI, USA) and purified again by phenol–chloroform extraction and ethanol precipitation. Complementary DNA (cDNA) was prepared with SuperScript III (Invitrogen, Carlsbad, CA, USA) using random hexamers.

Strains, transgenic lines and genome editing

The *Caenorhabditis elegans* Bristol N2 strain was used whenever not specifically stated and maintained as described (*Brenner, 1974*).

KV3: (8418)—heterozygous animals carrying one edited disrupted allele of *F28F8.5* ($P_{F28F8.5}$ *(V:15573749)::gfp::let858(stop)::SEC::F28F8.5*—edited *F28F8.5* disrupted by *gfp* and self-excising cassette (SEC)) and one WT allele of *F28F8.5*. This line segregates mutant animals.

KV4: (8419)—edited *F28F8.5* carrying *gfp::F28F8.5* in its normal genomic position ($P_{F28F8.5}$*(V:15573749)::gfp::F28F8.5* on both alleles.

Preparation of $P_{F28F8.5(400\ bp)}$*::F28F8.5::gfp*

For preparation of transgenic lines encoding F28F8.5::GFP from extrachromosomal arrays under regulation of endogenous promoter, we used the PCR fusion-based technique (*Hobert, 2002*). Primers 7886 and 7888 were used for amplification of the genomic sequence of *F28F8.5* (consisting of approximately 400 bp of the predicted promoter region preceding the coding region of *F28F8.5*). The gene encoding GFP was amplified from the pPD95.75 vector with primers 6232 and 6233. The complete construct was amplified with primers 7887 and 6234. The resulting fusion construct contains the 3′ UTR from pPD95.75 (originally from the *unc-54* gene). The PCR mixture was injected into the gonads of young adult hermaphrodite animals together with marker plasmid pRF4. The sequences of all primers used in the paper are in Supplemental Information.

Genome editing

Lines with edited genomes were prepared from wild type N2 animals using the CRISPR/Cas9 system as described (*Dickinson et al., 2013*, *2015*; *Ward, 2015*; *Dickinson & Goldstein, 2016*). Using this strategy, the *F28F8.5* gene was edited by insertion of a construct including the coding sequence of GFP and a SEC containing the *sqt-1(d)* gene (a visible selection marker leading to a Rol phenotype), *hs::Cre* (heat shock inducible Cre recombinase) and hygR (hygromycin resistance) genes. The sgRNA sequence was targeted near the start of the coding sequence for the *F28F8.5* gene using a modified pJW1219 plasmid (Addgene, Cambridge, MA, USA) as the Cas9 vector (pMA007); it was prepared by PCR with primers 8403A and 8333 and used in a concentration of 50 ng/µl for microinjections. The plasmid pMA007 was co-injected with the rescue repair template plasmid based upon modified pDD282 vector (pMA006) in a concentration of 10 ng/µl and with three markers (see below). The repair template plasmid pMA006 was prepared in two steps. First the plasmid pMA005 was prepared from gDNA of *F28F8.5* (containing both repair arms) and amplified by PCR with primers 8404 and 8405 and cloned into pCU19 backbone. The plasmid pMA005 was subsequently modified—the FP-SEC segment was added and the CRISPR/Cas9 site was altered to protect against Cas9 attack. The linear PCR product of pMA005 was prepared using primers 8406 and 8407 with overlapping regions for Gibson assembly (New England BioLabs, Ipswich, MA, USA). The primer 8406 was prepared with alternate codons for protection against CRISPR/Cas9 site. Linear insert of FP-SEC was prepared by PCR from pDD282 plasmid (Addgene, Cambridge, MA, USA) with primers 8408 and 8409. Primers were prepared with overlapping parts for cloning into linear pMA005 plasmid by Gibson assembly and the final rescue plasmid pMA006 was prepared. Plasmids pGH8 (10 ng/µl), pCFJ104 (5 ng/µl), and pCFJ90 (2.5 ng/µl) (Addgene, Cambridge, MA, USA) were used as fluorescent co-injection markers. After microinjections the population of nematodes were grown for three days at 25 °C and hygromycin (Invitrogen) was added in a final

concentration of 250 μg/ml. After three days integrated nematodes were selected according to the rolling phenotype and loss of extrachromosomal arrays.

Using this strategy, we obtained a heterozygous line (KV3) with a disrupted *F28F8.5* gene with an inserted *gfp* regulated by the endogenous promoter of *F28F8.5* in one allele and one WT allele. This line segregated homozygous animals for $P_{F28F8.5}$:: *F28F8.5::gfp* (edited *F28F8.5* with SEC—$P_{F28F8.5}$ *(V:15573749)::gfp::let858(stop)*::SEC::*F28F8.5*) with disrupted *F28F8.5* on both alleles and expressing GFP under the regulation of the endogenous promoter. Animals of this line were clearly distinguishable by their developmental phenotypes, weak expression of GFP in the cytoplasm and the presence of *rol* marker. These animals were sterile and had severe developmental defects (see Results). The genotypes were confirmed by single worm PCR of representative animals after their microscopic analysis (with primers 8398 and 8414).

The excision of the SEC was achieved by a 4 h heat shock at 34 °C. The line KV4 was obtained: animals with both alleles carrying the edited *F28F8.5* gene in the form of *gfp::F28F8.5* in its normal genomic position (edited *F28F8.5* with *gfp* tagged to the N—terminus—$P_{F28F8.5}$*(V:15573749)::gfp::F28F8.5*).

The presence of the knock-in of *gfp* was confirmed by single nematode PCR with primers 7887 and 8454, 8398 and 8454. The PCR products were purified and sequenced with primers 8455 and 8456. PCR was done by REDTaq ReadyMix PCR reaction (Sigma-Aldrich, St. Louis, Missouri, USA) or by Phusion High-Fidelity DNA Polymerase (New England Biolabs, Ipswich, MA, USA). During the maintenance of the heterozygous line KV3, animals with one edited disrupted *F28F8.5* allele and one allele with edited *F28F8.5* after self-excision of SEC were also generated (recognizable by the Rol phenotype, expression of *gfp* in nuclei and lack of developmental phenotypes). Schemes for genome editing are accessible in Files S4–S7.

Downregulation of gene expression by RNA interference

For RNAi done by microinjections, *F28F8.5* cDNA was prepared from total cDNA using primers 7889 and 7890. The plasmid pPCRII(Topo) (Invitrogen, Carlsbad, CA, USA) containing *F28F8.5b* cDNA was linearized using restriction enzymes *Not*I/*Sac*I. The dsRNA was prepared by in vitro transcription using SP6/T7 Riboprobe® in vitro Transcription Systems (Promega, Madison, WI, USA) from opposing promoters synthesizing complementary single stranded RNA (ssRNA) for both strands of *F28F8.5* cDNA and its complementary strand. After in vitro transcription (~2 h) equal volumes of sense and antisense RNA were mixed, incubated at 75 °C for 10 min and slowly cooled to room temperature during 30 min. Control RNAi was prepared from the promoter region of *nhr-60* as previously described (*Šimečková et al., 2007*) and repeated with dsRNA prepared using the vector L4440. Vectors used for preparation of dsRNA were linearized and transcribed using T7 RNA polymerase. The dsRNA concentration was measured using a UV spectrophotometer and diluted to the concentration of ~2 μg/μl that was used for injections (*Tabara et al., 1999*; *Timmons, Court & Fire, 2001*; *Vohanka et al., 2010*).

Microinjections

Microinjections of plasmids, DNA amplicons or dsRNA into gonads of young adult hermaphrodites were done using an Olympus IX70 microscope equipped with a Narishige microinjection system (Olympus, Tokyo, Japan). The plasmids were injected into the gonads of young adult hermaphrodites as described (*Tabara et al., 1999*; *Timmons, Court & Fire, 2001*; *Vohanka et al., 2010*).

Microscopy

Fluorescence microscopy and Nomarski optics microscopy were done using an Olympus BX60 microscope equipped with DP30BW CD camera (Olympus, Tokyo, Japan). Animals were analyzed on microscopic glass slides with a thin layer of 2% agarose and immobilized by 1 mM levamisole (Sigma-Aldrich, St. Louis, MO, USA). Confocal microscopy of live homozygous animals with edited *F28F8.5* expressing *gfp::F28F8.5* was performed using an inverted Leica SP8 TCS SMD FLIM system equipped with a 63 × 1.2 NA water immersion objective, a pulsed white light laser (470–670 nm), AOBS and two internal hybrid single photon counting detectors, and operated by Leica Application Suite X program (Leica Microsystems, Wetzlar, Germany). The GFP fluorescence was excited at a wavelength of 488 nm and the emitted light was simultaneously recorded in two spectral ranges (Channel 1—495 nm to 525 nm, Channel 2—525 nm to 580 nm; the two channel setup was used to help resolve between spectrally different autofluorescence and GFP fluorescence signals).

Fluorescence-lifetime imaging microscopy

For FLIM acquisitions the single photon counting signal from the internal hybrid detectors, acquired during confocal acquisitions, was simultaneously processed by HydraHarp400 TCSPC electronics (PicoQuant, Berlin, Germany) and information about the arrival times of all photons was stored to a hard-drive in TTTR data format. TTTR is freely accessible at https://www.picoquant.com/images/uploads/page/files/14528/technote_tttr.pdf. Data structure, program description and user instructions are also freely accessible at https://github.com/PicoQuant/PicoQuant-Time-Tagged-File-Format-Demos/blob/master/PTU/Matlab/Read_PTU.m. The signal from both time synchronized channels was added up. The false color scale (1–3 ns) is based on the average photon arrival time, with blue color representing short lifetime and red color long lifetime fluorescence.

Single nematode PCR

Single animal PCR was used for verification of all transgenic lines. Following the microscopy examination, selected animals were removed from microscopic slides and transferred into caps of PCR tubes with 4 µl of solution of Proteinase K (20 mg/ml) diluted 1:333 in Barstead Buffer (resulting in Barstead Lysis Buffer which consists of 50 mM KCl, 10 mM Tris pH 8.3, 2.5 mM $MgCl_2$, 0.45% (v/v) NP40 (Nonidet P-40), 0.45% (v/v) Tween-20, 0.01% (w/v)). Proteinase K was diluted immediately before use as a 20 mg/ml stock solution which was kept on ice and diluted to final working solution

at a concentration of 60 μg/ml. The tube was sealed in bottom-up position and the sample transferred to the bottom of the tube by centrifugation. The tube was frozen for 10 min at −70 °C. Next, the tube was heated for 1 h at 65 °C and additional 15 min at 95 °C. The resulting sample was used immediately for amplification of DNA by PCR or stored at −80 °C before further analysis. Similarly, genomic DNA was prepared from selected nematode culture plates and used for further screening by PCR and sequencing.

The resulting precipitated DNA was dissolved in 10 μl of deionized water and used for amplification by PCR using primers outside the edited genomic regions. Specificity of amplification was confirmed by DNA sequencing.

Similarly, homozygous animals with edited *F28F8.5* (with *gfp* inserted in front of the *F28F8.5* START codon) were analyzed by single worm PCR with primers 7887 (sense primer) and 7890 or 8454 (antisense primers).

Quantitative RT-PCR

For quantitative RT-PCR, the technique described by *Ly, Reid & Snell (2015)* was used with modifications. For assessment of the level of expression of *F28F8.5* from homozygous animals with the edited disrupted gene, five adult homozygous mutant animals recognized by the phenotype and the same number of young WT hermaphrodites with minimum number of formed embryos were manually harvested and collected in separate Eppendorf tubes. Reverse transcription was done using the Maxima H Minus cDNA synthesis kit (Thermo Fischer, Waltham, MA, USA) as recommended by manufacturer. Universal probe library and primers designed with the help of ProbeFinder Assay Design Software were used and qPCR was run on LightCycler 2.0 purchased from Roche (Roche, s.r.o. Prague, Czech Republic). An average of three sample cDNAs and three control cDNAs were analyzed (twice in duplicates and one time as single experiments), all containing the same amount of RNA for RT for each experiment. The expression of *F28F8.5* was normalized to *ama-1* and the values obtained in homozygous mutant animals with disrupted *F28F8.5* gene were compared to values obtained in control WT N2 animals.

Binding studies

Binding studies were done as described (*Kostrouch et al., 2014*) with modifications. The coding region of *mdt-6* was amplified using primers 8292 and 8293 from cDNA prepared from mixed stages *C. elegans* cultures and cloned into pTNT vector (Promega, Madison, WI, USA, amplified with primers 8277 and 8278) using the Quick Ligation Kit (New England Biolabs, Ipswich, MA, USA) and expressed in the rabbit reticulocyte TNT-system (Promega, Madison, WI, USA). The in vitro transcribed protein was labeled using ^{35}S Methionine (Institute of Isotopes, Budapest, Hungary). F28F8.5 coding sequence (amplified using 8255 and 8256 primers with 15 bp overhangs for insertion into the vector) was cloned into pGEX-2T vector ((Amersham Pharmacia Biotech, Amsterdam, UK), amplified with primers 8253 and 8254) using the GeneArt Seamless PLUS Cloning and Assembly Kit (Thermo Fisher Scientific, Waltham, MA, USA), transformed into BL21 *Escherichia coli* cells and the production of protein was induced by

isopropyl β-D-1-thiogalactopyranoside (IPTG) (Sigma-Aldrich, St. Louis, MO, USA). The Mediator subunit MDT-30 was amplified from mixed stages *C. elegans* cDNA with sense primer 8302 and reverse primer 8527 (containing FLAG sequence), cloned into pET28a(+) vector ((Addgene, Cambridge, MA, USA), amplified with primers 8519 and 8520) using the Quick Ligation Kit (New England Biolabs), transformed into BL21 *E. coli* cells and induced by IPTG. The lysate from bacteria producing His_6-MDT-30-FLAG was used directly or purified on HiTrap Chelating HP column (GE Healthcare, Chicago, IL, USA). Proteins produced by the TNT system or bacterial lysates of bacteria transformed with FLAG labeled Mediator subunits were incubated with glutathione–agarose (Sigma-Aldrich, St. Louis, MO, USA) adsorbed with equal amounts of GST or GST-F28F8.5. Radioactively labeled proteins were detected using TRI-CARB 1600TR, Liquid Scintillation Analyzer (Packard, Meriden, CT, USA).

The resulting samples (labeled proteins bound to GST- or GST-F28F8.5) were separated by polyacrylamide gel electrophoresis. ^{35}S-MDT-6 was visualized by autoradiography and subsequently, the gel containing radioactively labeled protein was localized using superimposed autoradiograms, excised and the radioactivity determined in the scintillation detector. FLAG-labeled MDT-30 was determined by Western blot using an anti-FLAG antibody (monoclonal anti-FLAG, M2 (Sigma-Aldrich)) and quantified densitometrically by ImageJ computer program (https://imagej.nih.gov/ij/download.html) (*Schneider, Rasband & Eliceiri, 2012*).

RESULTS

Identification of the closest homologue of vertebrate Mediator complex subunit 28 in *C. elegans*

To identify the *C. elegans* homologue of MED28, we queried protein databases with curated SwissProt sequences from UniProtKB. They comprised several mammalian and insect proteins (e.g., human MED28_HUMAN and *D. melanogaster* MED28_DROME). The more sensitive profile-to-profile HHblitz and HHpred algorithms provided hits to a *C. elegans* annotated protein F28F8.5a and b with highly significant *E*-values. According to Wormbase (WS248), two protein isoforms are produced from the *F28F8.5* gene, isoform a with the length of 200 amino acids and isoform b that has a two amino acid insertion at position 20 of the N-terminal evolutionarily non-conserved region. The best results were obtained when pre-aligned vertebrate and insect MED28 homologues were used as query in three iterations ($E < 10^{-48}$ and the probability of true positive >99.99%). When the pre-aligned nematode sequences homologues to F28F8.5 were used to query profiles of human or *Drosophila* sequences in reciprocal searches, MED28 proteins were obtained with equally significant scores. BLAST and PSI-BLAST searches in their standard settings were not able to reveal a significant hit ($E < 10^{-3}$); the only nematode hit was a *Trichinella spiralis* protein (E5RZQ1). However, when the searches in protein databases were limited to sequences from *Ecdysozoa* with *Insecta* excluded (conservative inclusion threshold $E < 10^{-6}$) in the first two iterations and then continued in the complete database of sequences from all species in the subsequent

Figure 1 A multiple sequence alignment of selected metazoan homologues of MED28 compared with F28F8.5. Aligned with PROMALS (http://prodata.swmed.edu/promals/promals.php), variable C- and N-termini not shown, amino acid residue types colored according to Clustal scheme in Jalview, red bars indicate consensus positions of predicted α-helices. Sequences from top to bottom (organism, identifier): *Caenorhabditis elegans*, O18692; *Trichinella spiralis*, E5RZQ1; *Wuchereria bancrofti*, EJW84794.1; *Pristionchus pacificus*, translated contig of CN657719.1 FG102945.1 CN657262.1 CN656622.1; *Ancylostoma ceylanicum*, A0A016SKV7; *Globodera pallida*, translated CV578368.1; *Panagrolaimus davidi*, translated JZ658977.1; *Ixodes scapularis*, B7PAW5; *Drosophila melanogaster*, MED28_DROME; *Homo sapiens*, MED28_HUMAN. Readers with specific color preferences may download the compared sequences from (File S1) and create the Clustal scheme with different color specifications using the Jalview program (http://www.jalview.org/).

iterations, the final hits of F28F8.5 included human and *Drosophila* MED28. PSI-BLAST with *T. spiralis* query sequence in database limited to *Ecdysozoa* in the first two iterations provided both human and *Drosophila* MED28 and F28F8.5 in one run ($E < 10^{-8}$). We concluded from these searches that F28F8.5 is a homologue of MED28 and very likely its previously unrecognized orthologue.

All PSI-BLAST MED28 homologues possess variable N- and C-termini of 3–80 amino acids showing no conservation across Metazoa. This conservation is loose even just within *Drosophilae* or *Caenorhabditae* sequences. Only the central core of about 110 amino acids is preserved in metazoan evolution. Figure 1 shows a sequence alignment of this conserved core of selected MED28 homologues. All sequences are predicted to fold into three helices forming a putative coiled coil fold (UniProt annotation). Submitting the alignment shown in Fig. 1 to HHpred for 3D structure recognition reveals a structural fold of yeast MED21 (PDB identifier 1ykh_B). It is indeed a three-helix coiled coil forming a heterodimer with MED7. It can be expected that MED28 forms a very similar fold interacting with a yet to be determined subunit of the MED complex.

F28F8.5 is a nuclear as well as a cytoplasmic protein

Information available in WormBase suggests that the *F28F8.5* gene can be expressed as both an individual and multigene transcript, located as the last gene in a four gene operon that is both SL-1 and SL-2 trans-spliced. To determine the intracellular localization of F28F8.5, we edited the *F28F8.5* gene using CRISPR/Cas9 technology. We inserted the gene coding for GFP directly in front of the first codon. The arrangement used in our

experiment (based on *Dickinson et al. (2013*, *2015)*, *Ward (2015)* and *Dickinson & Goldstein (2016)*) employed a SEC that was added after *gfp*. This strategy initially created a disrupted *F28F8.5* gene and putative null allele that can be detected by expression of GFP alone regulated by the endogenous promoter elements of *F28F8.5*. We found that only heterozygous animals could be propagated due to the sterility of homozygotes tagged in this manner. Assuming this tag is not deleterious to the expression of other genes in the operon, this result suggests that *F28F8.5* is an essential gene.

After removal of the SEC from this edited *F28F8.5* gene induced by heat shock (visualized by continuous expression of GFP::F28F8.5 fusion protein and loss of the Rol phenotypic marker), the endogenous locus had an N-terminus GFP-tagged *F28F8.5* gene that we maintained as homozygous animals, demonstrating this edited allele is fully functional. Note that both known protein isoforms of F28F8.5 (a and b) would be tagged on their N-terminus with GFP by this method.

The GFP::F28F8.5 pattern was ubiquitous, both nuclear and cytoplasmic from embryos to adults (Fig. 2). Prominent nuclear localization was found in oocytes, zygotes, larvae, and adults. Cells with clear nuclear accumulation of GFP::F28F8.5 included epidermal, intestinal, pharyngeal, uterine and vulval muscle cells (Fig. 2). The gonad expressed *gfp::F28F8.5* and mitotic as well as meiotic nuclei accumulated GFP::F28F8.5 protein (Fig. 2).

Selected animals were analyzed by confocal microscopy for determination of subcellular distribution of GFP::F28F8.5. Scanning through several focal planes revealed signal in the GFP excitation/emission range in nuclei as well as in the cytoplasm of embryos, all larval stages and adults (Fig. 3). Structures resembling gut granules were also strongly positive in the GFP recording mode. In order to distinguish between GFP-specific fluorescence and autofluorescence, we applied FLIM with an expectation that autofluorescence (such as that from gut granules) is likely to produce a signal with a short fluorescence lifetime opposed to GFP-specific fluorescence. Structures such as gut granules were clearly detected (Fig. 3, panels O, Q, S, T and U, blue color) while fluorescence with a longer lifetime expected for GFP::F28F8.5 was detected in the germline, in oocytes and embryos and in most somatic nuclei of larvae as well as adult animals (Fig. 3, panels O, Q, S, T and U, red and yellow colors).

We also generated transgenic lines encoding F28F8.5::GFP from extrachromosomal arrays consisting of an endogenous internal *F28F8.5* promoter regulating a fusion gene with *gfp* attached to F28F8.5 on its C-terminal end. As with the N-terminally tagged F28F8.5, F28F8.5::GFP showed both nuclear and cytoplasmic localization. As expected for an extrachromosomal transgene, the expression of *F28F8.5::gfp* was not detected in the germline. This reporter was expressed in embryos starting at the twofold stage and continued throughout development (Fig. S1). We did notice that *F28F8.5::gfp* was expressed in the excretory canal cell (Figs. S1M, S1N, S1P and S1Q), a pattern not observed with the endogenously edited GFP-tagged gene.

F28F8.5 regulates development

To achieve loss-of-function, RNAi was used to downregulate *F28F8.5* expression. Analysis of 2,567 progeny of 17 young adult hermaphrodites inhibited for F28F8.5 function by

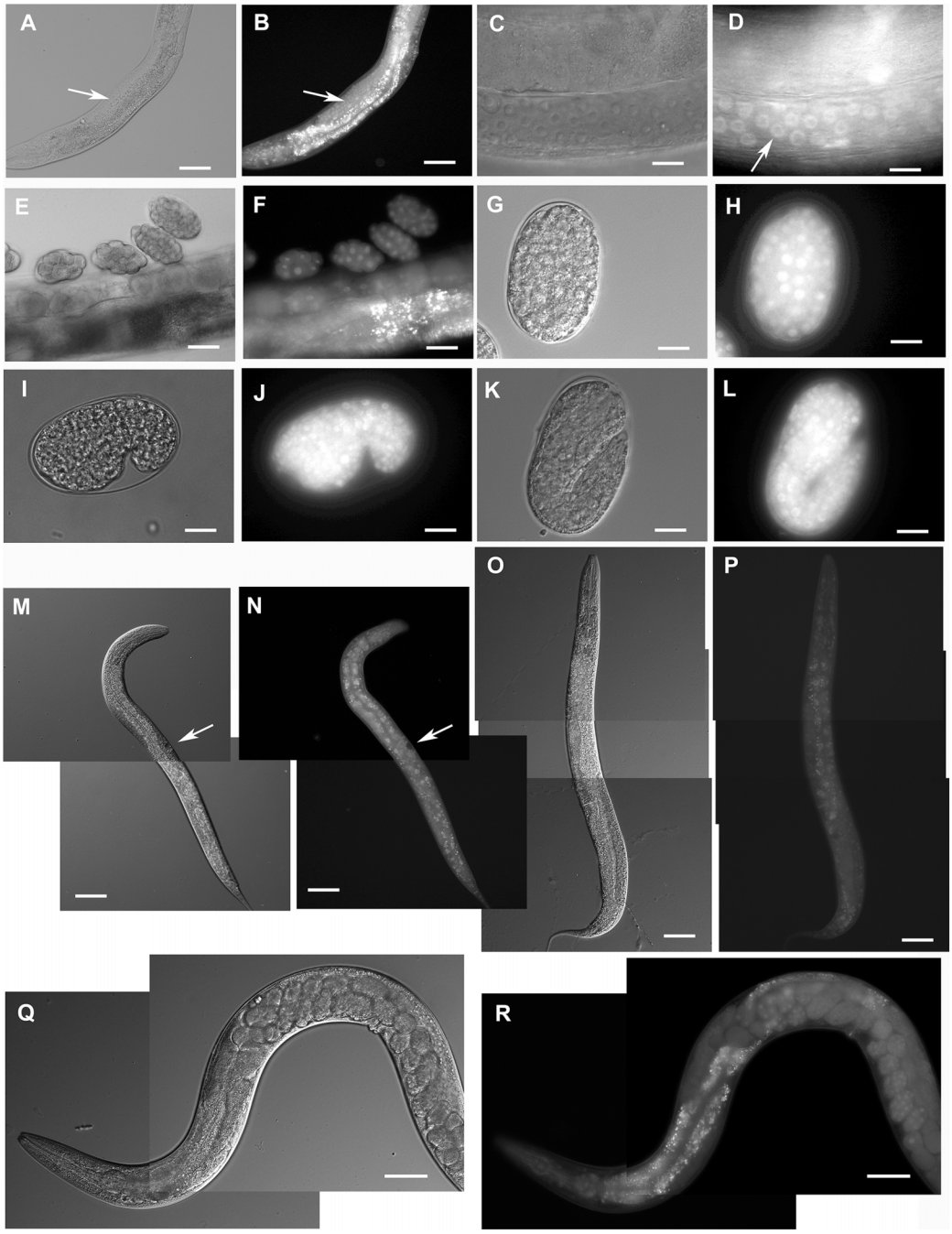

Figure 2 Expression pattern of GFP::F28F8.5 in homozygous animals with edited *F28F8.5* gene. GFP tagged to F28F8.5 at its N-terminus using CRISPR/Cas9 technology visualized the expression of F28F8.5 in the gonads (Panels B and D, arrows) in mitotic nuclei and continues throughout the embryonic development (Panels F, H, J, and L). The wide and likely ubiquitous expression of GFP::F28F8.5 continues during larval stages (larvae L3 and L4 are shown in panels M, N and O, P, respectively) as well as in adults (panels Q and R). Expression of the edited gene in the nuclei of the developing vulva is indicated by the arrows in panels M and N. Panels A, C, E, G, I, K, M, O, and Q show larvae in Nomarski optics and panels B, D, F, H, J, L, N, P, and R in GFP fluorescence. Bars represent 50 μm.

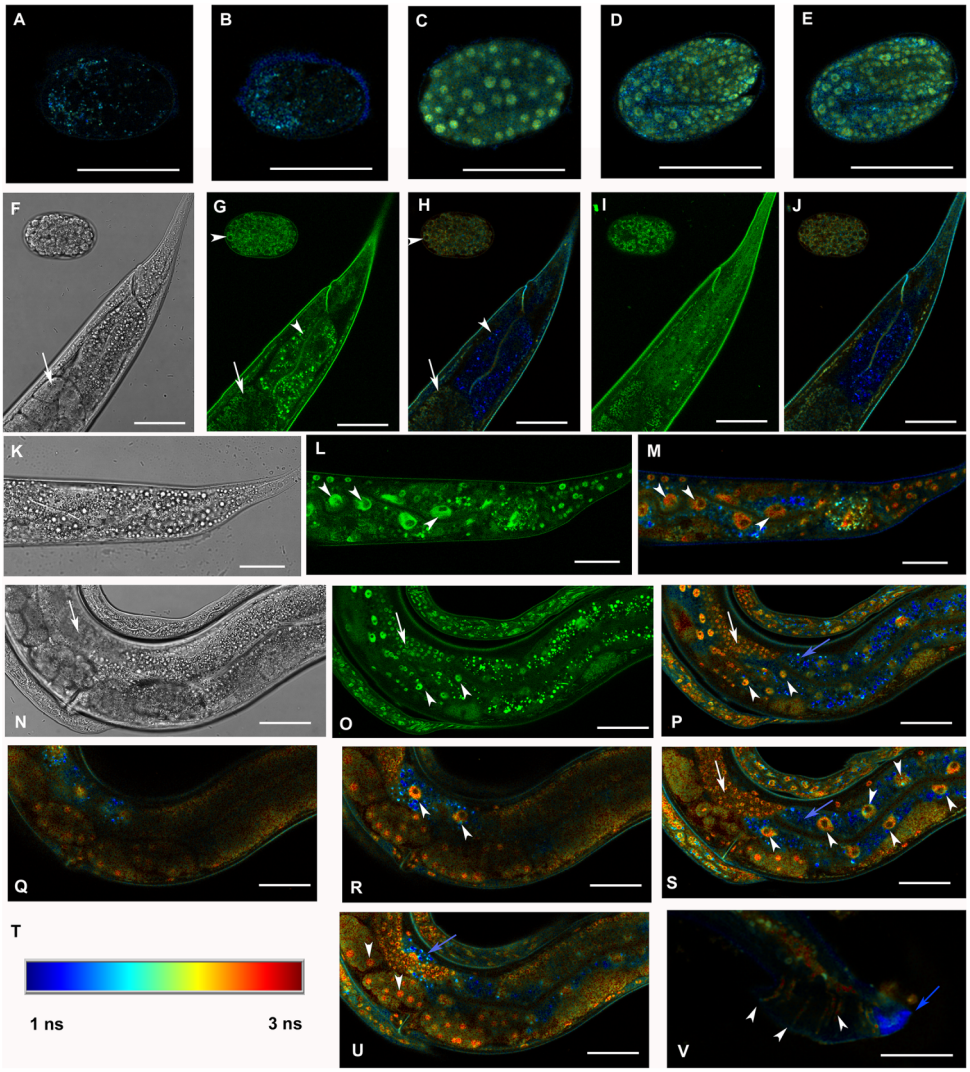

Figure 3 Analysis of GFP::F28F8.5 expression in homozygous animals with edited *F28F8.5* gene by confocal microscopy and fluorescence lifetime imaging microscopy (FLIM). All confocal images of GFP fluorescence are recorded in Channel 1 (495–525 nm). FLIM images (panels A to E, H, J, L, M, O to S, U, and V) are calculated from merged recordings in Channel 1 and Channel 2 (525–585 nm). Panels F, K, and N are images in Nomarski optics at the same optical focus as in corresponding confocal images of GFP fluorescence (panels G, I, L, O). Panels A and B show control images of WT embryos in bean and comma stages, respectively. No specific signal is detected in control embryos by FLIM. Panel C shows an embryo in bean stage expressing GFP::F28F8.5 from the edited gene. Two focal planes of an embryo expressing GFP::F28F8.5 in twofold stage are shown in panels D and E. FLIM detects GFP::F28F8.5 in most or all nuclei of developing embryos. Panels F to J show the distal part of a young adult control hermaphrodite animal and a control embryo in late bean stage. FLIM images in panels H and J show mostly short lifetime fluorescence in the cytoplasm of embryonic cells as well as cells and subcellular structures in the adult control animal (visualized by blue color). Arrowheads pointing at the embryo in panels G and H indicate weak autofluorescence in the cytoplasm of embryonic cells. Arrows in panels F, G and H indicate the turn of gonad and arrowheads indicate nuclei of an enterocyte which is devoid of almost all fluorescence (panels G and H). Panels K to S and U and V show animals with edited *F28F8.5* (*gfp::F28F8.5*). Panel M shows the distal part of an adult hermaphrodite animal expressing GFP::F28F8.5 from the edited gene at recording settings identical with that used in the control sample shown in panels A, B, H, and J. FLIM analysis shows a long lifetime fluorescence in nuclei and in the cytoplasm of most cells that contrasts with the low level of fluorescence seen in the control sample. Arrowheads indicate

Figure 3 ... **continued**
nuclei of enterocytes in panels L and M. Panels N to V show images of an adult animal and two L1 larvae with edited *F28F8.5*. Panels P to S, and U show selected focal planes in FLIM. Panel T shows the calibration table for FLIM in the range of 1–3 ns used in all panels presenting FLIM analysis. Blue areas shown in FLIM pictures represent short lifetime fluorescence presumably corresponding to autofluorescence (blue arrows in panels O, S, and U). Arrowheads in panels O, P, R, and S indicate nuclei of enterocytes and in panel U nuclei of early embryos with long lifetime fluorescence characteristic for GFP. Panel V shows the distal part of a male expressing GFP:F28F8.5 in male specific structures, in nuclei as well as in rays (marked by arrowheads) indicating that GFP::F28F8.5 is expressed not only in cell nuclei but also in the cytoplasmic structures. Bars represent 30 μm in panels A to E and 50 μm in panels F to S and U and V.

microinjection of dsRNA into the syncytial gonad revealed that F28F8.5 is essential for proper development (Fig. 4). From the total progeny, 1,127 animals were affected (44%) exhibiting embryonic and larval arrest and a range of less severe phenotypes, including defective molting, protruding vulvae that often burst, male tail ray defects (Fig. 4), and uncoordinated (Unc) movement. In contrast with this, control young adult N2 hermaphrodites injected with control dsRNA showed embryonic arrest in less than 2% of progeny (seven hermaphrodites injected, total progeny observed 1,066, embryonic arrest found in 19 embryos).

Complete loss of F28F8.5 that occurred in homozygous animals with both edited disrupted alleles of the *F28F8.5* gene (that are found among the progeny of heterozygous animals carrying one edited disrupted allele and one WT allele) resulted in defective development that was most pronounced in late larval stages. The phenotypes included a dumpy phenotype (Dpy) (Fig. 5C), irregular gut, severely defective growth of the gonad with signs of defect in directional growth (Figs. 5E and 5M) and Pvul phenotype (Figs. 5K and 5L). Most animals had darker gut cells than controls of the same age. The gonad did not develop fully in most animals (Figs. 5C–5L) and often contained empty spaces that were prevalent in some animals, leading to the formation of larvae with optically thin, empty-like tissue in the position of the gonad. The gonads contained foci of irregular tissue with an uncharacteristic appearance. Tissue defects were also visible in extragonadal locations, especially in the place of excretory canals. Body defects were also observed in the position of the uterus that was not properly formed and the spermatheca that was not identifiable in a large proportion of animals.

Estimation of the level of *F28F8.5* expression in homozygous mutant animals (originating from maternal load or from SEC self-excision (*Dickinson et al., 2015*)) from three experiments indicated that mutants with disrupted F28F8.5 had the level of expression about 17 times lower compared to the levels found in WT controls (File S8).

Heterozygous hermaphrodites carrying one edited disrupted allele of *F28F8.5* and one WT allele were grossly normal and produced viable embryos. Unlike in homozygous animals carrying the excised SEC allele, the GFP fluorescence was mostly cytoplasmic and most nuclei were not showing accumulation of GFP. In some embryos, however, the nuclei accumulated GFP indicating probable spontaneous SEC self-excision (Fig. 6).

Analysis of progeny of the heterozygous strain KV3 revealed differences compared to the expected Mendelian segregation of phenotypes. Animals with one edited disrupted

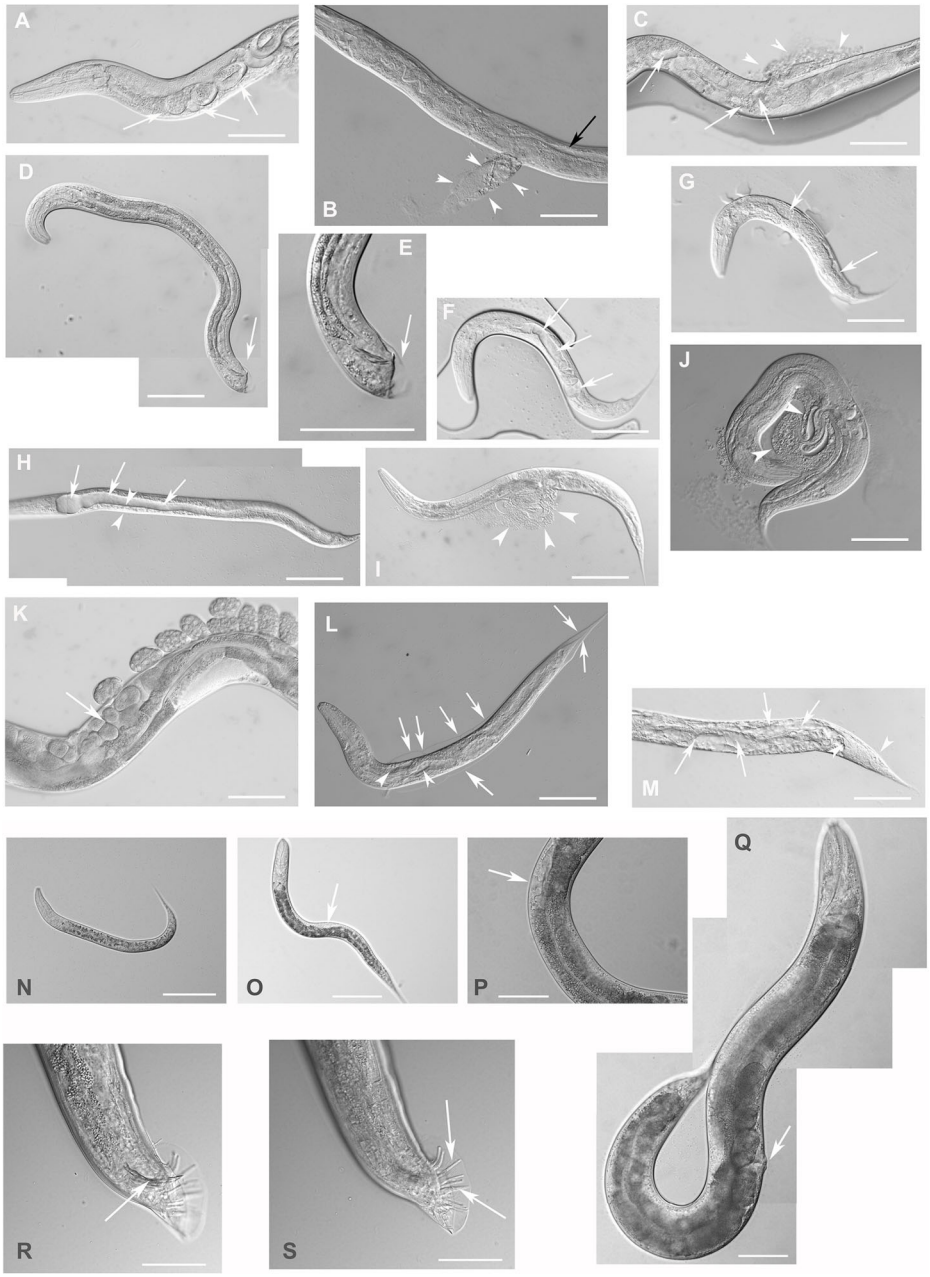

Figure 4 Downregulation of *F28F8.5* by RNAi induces developmental defects. Animals developed from parents injected with dsRNA specific for *F28F8.5* show retention of normal and malformed embryos (panels A and K, respectively), vacuoles (panels A and C, arrows), herniation and burst through the vulva (panels B, C, I, and J, arrowheads) and defective development of the gonad (panels J and M). Panel D shows a male nematode with defects of male specific structures—missing rays and fan and an abnormal distal part of the body (arrow). Panel E shows the magnified distal part of the male nematode in panel D and the defective male specific structures (arrow). Panels F and H show L3 larvae that were found atrophic, with thin enterocytes (arrowheads) and a dilated gut lumen (arrows). The dumpy phenotype with masses of tissue and vacuoles (panel G, arrows) were also common in the progeny of microinjected parents. Other phenotypes seen included molting defects indicated by arrows in panel L and cellular defects (indicated by arrowheads in panels L and M). Animals treated by control RNAi were morphologically normal and representative images are shown in panels N to Q. Panel N shows a L2

Figure 4 ... **continued**
larva, panel O shows a young L3 larva with developing germline (arrow). Panel P shows a young L4 Larva with developing vulva marked by an arrow. Panel Q shows a grossly normal adult hermaphrodite animal with few developing embryos and vulva (arrow). Panel R and S show the distal part of the body of a male animal with normal appearance of male specific structures. Arrow marks spicules (in panel R) and normal sensory rays (in panel S). All images are in Nomarski optics. Bars represent 50 μm.

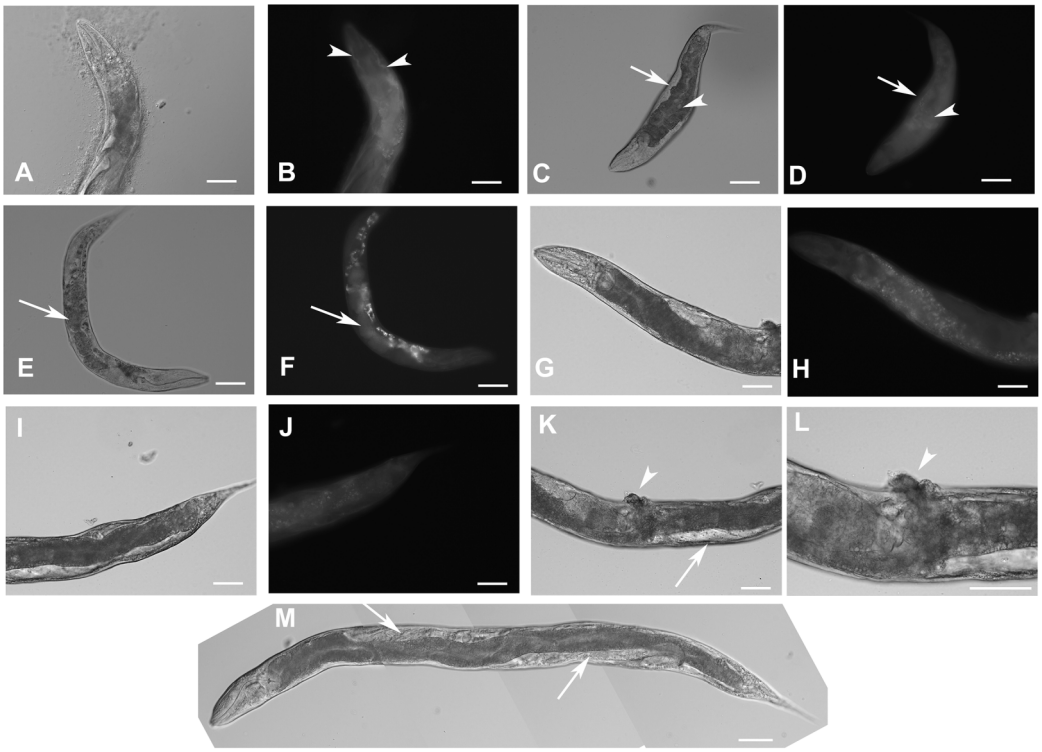

Figure 5 Disruption of *F28F8.5* by CRISPR/Cas9 technique. Animals with disrupted *F28F8.5* on both alleles express GFP under the regulation of *F28F8.5* promoter. Panels A to J show paired images of animals in Nomarski optics and in GFP fluorescence. Panels A and B show an adult hermaphrodite animal with diffuse fluorescence in cells in the head area including anterior arms of the excretory cell (arrowheads). Panels C and D show a malformed larva probably in L3 stage with a Dpy phenotype and diffuse fluorescence in a malformed gonad (arrows) and the intestine (arrowheads). Panels E and F show an adult hermaphrodite animal with diffuse fluorescence in gut, pharyngeal cells and severely malformed gonad containing irregular structures (arrows). Panels G, H, I, and J show an adult animal with a malformed gonad, Pvul phenotype, dense gut and diffuse GFP fluorescence throughout the body. Panels K and L show the central part of the body of a hermaphrodite with the Pvul phenotype (arrowhead) and malformation of gonad (arrow). Panel M is composed of three consecutive images showing an adult hermaphrodite animal with severely malformed gonad (arrows), and missing uterus and spermathecae. The fluorescence images show that unlike GFP::F28F8.5, GFP alone localizes diffusely in the cytoplasm and is not found in nuclei. Bars represent 50 μm.

F28F8.5 allele and one edited *F28F8.5* allele with excised SEC were detected. They were recognizable by the Rol phenotype, expression of GFP in nuclei and lack of developmental phenotypes. This genotype was supported by PCR amplification of genomic regions from single nematodes and obtained pattern of amplified DNA fragments. These lines were not stable and were not preserved.

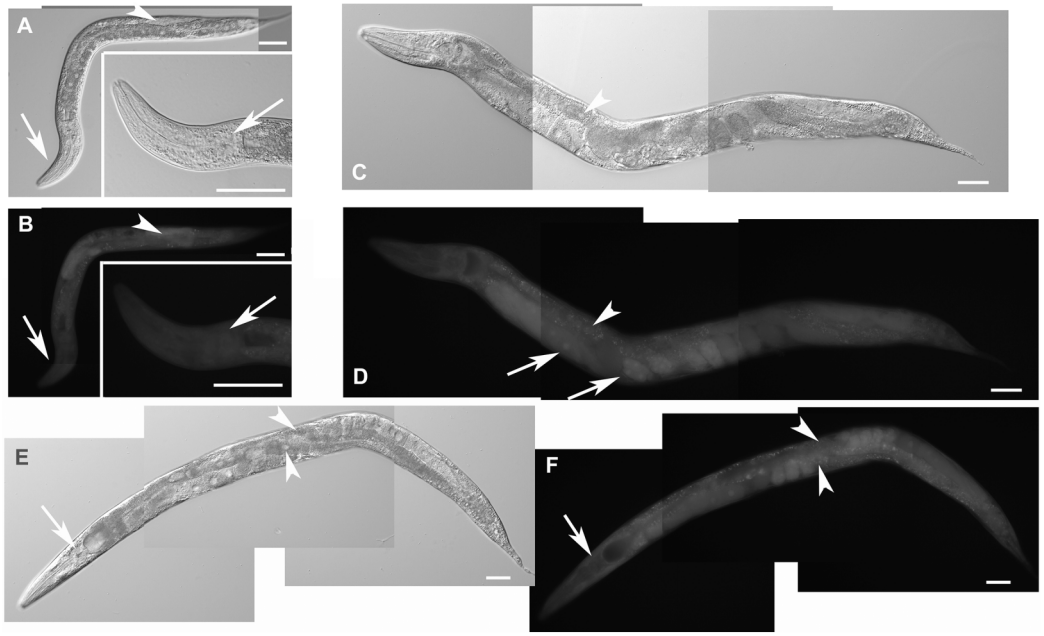

Figure 6 Heterozygous animals with one edited disrupted allele of *F28F8.5* and one WT allele. Heterozygous hermaphrodites carrying one edited allele of *F28F8.5* and one WT had grossly normal appearance and could be recognized by *rol* phenotype, presence of embryos, weak mostly cytoplasmic GFP fluorescence and absence of nuclear localization of GFP fluorescence. Panels A (Nomarski optics) and B (GFP fluorescence) show an L3 larva with weak fluorescence (panel B, arrowhead points at the gonad and arrows point at the head and pharynx). Inlets show head area at higher magnification (rotated 90° clockwise). Panels C and D show an adult hermaphrodite animal (C in Nomarski optics and D in GFP fluorescence) with weak cytoplasmic fluorescence in most cells. The arrowhead in panel D points at the nucleus of an enterocyte in focal plane that is devoid of GFP fluorescence. Arrows indicate two embryos with GFP fluorescence accumulated in nuclei which is most likely the result of spontaneous SEC self-excision. Panels E and F show an adult hermaphrodite in Nomarski optics (panel E) and GFP fluorescence (panel F). Arrows indicate the head area with diffuse intracellular fluorescence visible in panel F. Arrowheads point at two nuclei of enterocytes in focal plane that are also devoid of fluorescence. In contrast to the animal shown in panels C and D, the animal shown in the panel E and F contains embryos that have mostly diffuse cytoplasmic expression of GFP. Bars represent 50 μm.

F28F8.5 interacts with Mediator complex subunits

To determine if F28F8.5 could be part of the Mediator complex in *C. elegans*, we explored its ability to interact with previously identified Mediator subunits. We expressed ^{35}S-labeled MDT-6, part of the "head" module where MED28 is located, in rabbit reticulocyte lysate and assayed its binding to bacterially expressed GST-F28F8.5 or to GST only. As shown in Figs. 7A and 7B, a strong interaction (~7.7-fold enrichment) was detected between MDT-6 to F28F8.5 that exceeded that seen with GST alone. We also assayed for interaction between GST-F28F8.5 and MDT-30, but we were unable to obtain a satisfactory ^{35}S-Methionine labeled protein in the rabbit reticulocyte system. Therefore, we expressed MDT-30 containing a FLAG sequence inserted at the C-terminus and a His_6 sequence positioned at the N-terminus. After expression in bacteria and purification on a nickel column, we found that the MDT-30-FLAG bound F28F8.5 preferentially (~2.5-fold enrichment) in comparison to GST alone, as revealed by Western blot using an anti-FLAG antibody (Figs. 7C and 7D).

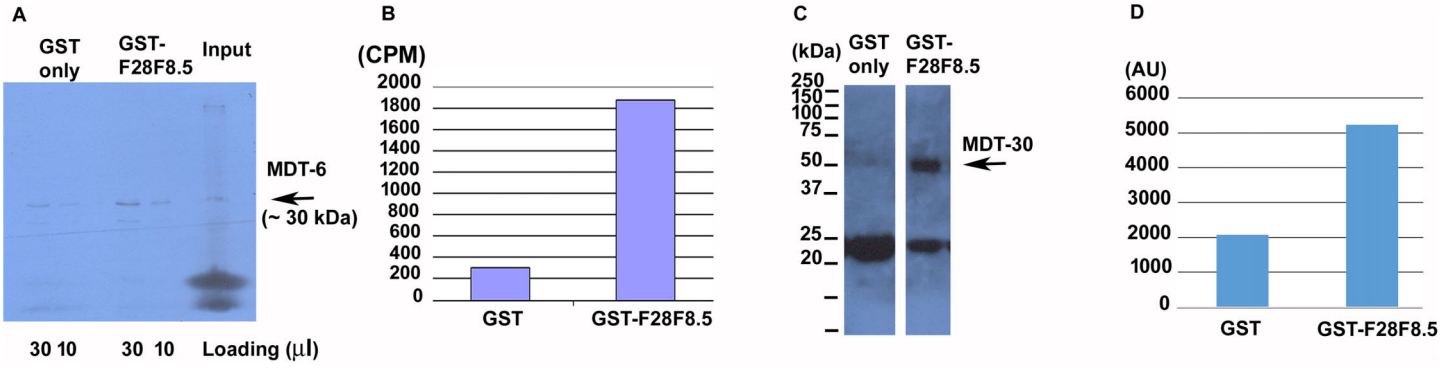

Figure 7 Binding of F28F8.5 to MDT-6 and MDT-30 in vitro. GST-F28F8.5 or GST alone were expressed in bacteria and purified using glutathione–agarose beads that were incubated with ^{35}S-Methionine-MDT-6 produced using rabbit reticulocyte lysate (A and B) or His_6-MDT-30-FLAG expressed in bacteria and purified using a nickel column (C and D). Panels A and C show fractions bound to glutathione–agarose beads resolved by polyacrylamide gel electrophoresis and visualized by autoradiography (panel A). For quantification, dried gel areas corresponding to proteins detected by radioactivity were excised and the radioactively labeled MDT-6 was determined using scintillation counter (panel B). Panels C and D show the interaction of FLAG-MDT-30 with GST-F28F8.5 or GST alone. FLAG-MDT-30 pulled down by GST or GST-F28F8.5 was determined by Western blot using an anti-FLAG antibody (panel C) and by densitometry (panel D). Both assayed Mediator subunits, MDT-6 and MDT-30 bind GST-F28F8.5 preferentially in comparison to GST only.

DISCUSSION

In this work, we identified an uncharacterized predicted protein F28F8.5 as the likely nematode homologue of MED28. This is supported by our findings that F28F8.5 interacts with nematode homologues of MED6 and MED30 (MDT-6, and MDT-30), the close sequence similarity of F28F8.5 to MED28 detected informatically in nematode genomes, a conserved dual nuclear and cytoplasmic expression pattern, and its involvement in a wide range of developmental processes. Thus we suggest F28F8.5 be identified as MDT-28, with the original gene for MDT-28 now recognized as the nematode homologue of perilipin, now named PLIN-1 (*Chughtai et al., 2015*).

The Mediator complex as a multiprotein structure is able to interact with a large number of additional proteins and integrate regulatory signals from several cell-signaling cascades (*Allen & Taatjes, 2015*). The Mediator complex possesses a high degree of structural flexibility and variable subunit composition (reviewed in *Poss, Ebmeier & Taatjes (2013)*). In yeast, a set of core subunits is important for a wide range of gene transcription (e.g., Med17 and Med22 (*Thompson & Young, 1995*; *Holstege et al., 1998*)), while others are non-essential in terms that single mutants can be maintained at laboratory conditions (Med1, Med2, Med3, Med5, Med9, Med15, Med16, Med18, Med19, Med20, Med31, and CDK module subunits Med12 (srb8), Med13 (srb9), srb10 (CDK8), and srb11 (CycC) (*Dettmann et al., 2010*)). Med31 and Srb9/Med13 Mediator subunits have different roles in gene selective transcription in *Saccharomyces cervisiae* and in *Candida albicans* (*Uwamahoro et al., 2012*). Mass spectrometry analyses indicate that many Mediator subunits are present in stoichiometric quantities but some subunits are over- or under-represented in budding and fission yeast and human HeLa cells (*Kulak et al., 2014*). Isolation of mammalian Mediator complexes lacking one or more of the 26 core subunits was reported for Med1 (TRAP220) (*Malik et al., 2004*), Med1 (Med220)

and Med26 (a.k.a. Med70 or CRSP70, or ARC70) (*Taatjes & Tjian, 2004*) (reviewed in *Allen & Taatjes (2015)*, the unified nomenclature can be found in (*Bourbon et al., 2004*) and for Med70 in *Rachez & Freedman (2001)*). While in cells with a stem cell like character, a broad spectrum of Mediator subunits was detected during; differentiation the expression of some Mediator subunits was markedly decreased (MED14, MED18, MED12, CDK8, MED26 in myotubes versus myoblasts) (*Deato et al., 2008*). In hepatocytes MED1, MED6, MED7, MED12, MED14, MED16, MED18, MED23, and CDK8 are decreased or even undetectable upon differentiation from hepatoblasts to hepatocytes (*D'Alessio et al., 2011*). Quantitative mass spectrometry analyses of Mediator complexes isolated by immunoprecipitation using four different Mediator subunits expressed as FLAG-tagged proteins in HeLa cells (Med10, Med26, Med28, Med29) identified most subunits of the Mediator complex in similar quantities with the exception of MED30, which was found in elevated ratios by Med28 pull-down experiments compared to other tested subunits. Med26 and Med29 precipitated more abundantly in their own pull-downs. Med31 was immunoprecipitated more efficiently in complexes with Med10 and Med25 was the least abundant subunit in all examined pull-downs (*Paoletti et al., 2006*). In-keeping with this, the abundance of individual Mediator subunits identified by quantitative proteomics indicate that some subunits are in similar abundance while others are under-represented or more numerous in yeast as well as in HeLa cells (*Kulak et al., 2014*). This suggests that Mediator complexes with specialized functions are likely to exist. A similar situation may be observed on ribosomes. Although the structure of ribosomal subunits is very firm and is given by the secondary structure of ribosomal RNAs and the presence of ribosomal proteins (*Ban et al., 2000*; *Schluenzen et al., 2000*; *Wimberly et al., 2000*), ribosome function during translation of mRNAs can be effectively regulated by viral proteins (*Diaz et al., 1993*, *1996*) which reveals the existence of a regulable "ribosomal code." The regulation of ribosome biogenesis and translation through the p53 pathway and methylation of ribosomal RNA by fibrillarin is leading to cancer specific ribosomes (*Marcel et al., 2013*). Cells infected with the viral oncogene v-erbA, the viral form of thyroid hormone receptor alpha, produce ribosomes with decreased levels of RPL11 which are translating more effectively Hsp70, a protein critical for tumorigenesis in avian erythroblastosis (*Nguyen-Lefebvre et al., 2014*). In comparison to ribosomal subunits, the Mediator complex possesses some analogies and differences.

The unit that is forming the structural backbone of Mediator is MED14 which is critical for both basal and activated transcription (*Cevher et al., 2014*). Mediator complexes bound to specific transcription factors (SREB Mediator, VP16-Mediator, TR-Mediator, VDR-Mediator, p53-Mediator) and the unliganded Mediator assume all distinct sterical conformations with fundamentally altered exposed protein surfaces (*Poss, Ebmeier & Taatjes, 2013*) that can be expected to form a multipotent basis for additional protein-protein interactions. This is possible because the fundamental features of the Mediator subunits are their intrinsically disordered regions that are to a certain degree positionally conserved between species, while others evolved in a phylum or species-specific way (*Nagulapalli et al., 2016*). In yeast, Med3 and Med15 form amyloid-like protein aggregates under H_2O_2 stress conditions. The amyloid formation can be

induced by overexpression of Med3 or glutamine-rich domain of Med15. This subsequently leads to the loss of Med15 module from Mediator and a change in the stress response (*Zhu et al., 2015*). The Mediator complexes contact a wide range of transcription factors using a fuzzy protein interface (*Brzovic et al., 2011*; *Warfield et al., 2014*). It can be therefore anticipated that additional proteins with a similar protein–protein interaction potential have the capability to interact with Mediator subunits if they are translocated into the nucleus.

Although individual Mediator complex subunits were shown to be associated with specific functions (reviewed in *Grants, Goh & Taubert (2015)*), the function of the nematode orthologue of MED28 could not be studied since it was not yet identified. MED28 has a special position in-between Mediator subunit proteins for its dual regulatory role, one as a Mediator subunit (*Sato et al., 2004*; *Beyer et al., 2007*) and the second, which is cytoplasmic, at the level of the cytoskeleton (*Wiederhold et al., 2004*; *Lee et al., 2006*; *Lu et al., 2006*; *Huang et al., 2012*). It can be anticipated that the interaction of primarily cytoplasmic proteins with MED28 if translocated to the nucleus may be able to bring cytoplasmic regulatory interactions towards the regulation of gene expression. In-between cytoplasmic proteins regulating gene expression, probably the most studied is beta-catenin, an adaptor of interaction between the cytoskeleton and cell adhesion molecules which critically regulates gene expression in the Wnt pathway. This connection is known in *C. elegans* to great detail (reviewed in *Grants, Goh & Taubert (2015)*). Interestingly, the phenotypes that we observed in F28F8.5 knock-down and loss of function experiments overlap with the EGFR regulatory cascade in *C. elegans*, especially the developmental defects of the vulva and of male specific structures, most obviously, male rays (*Grants, Goh & Taubert, 2015*; *Grants et al., 2016*). Our observation of the expression of *F28F8.5* in male rays and the defective development of male specific structures after *F28F8.5* RNAi support the cytoplasmic role of F28F8.5, that is in mammals mediated by Grb2 (*Wiederhold et al., 2004*). This cytoplasmic function of F28F8.5 is supported by the known involvement of the nematode homologue of Grb2, SEM-5, in the regulation of development of male rays. F28F8.5 protein contains a predicted SH2 binding site for Grb2 in the loop positioned in-between the two helices of F28F8.5, similarly as MED28 (identified using the site prediction tool Motif Scan http://scansite.mit.edu/motifscan_seq.phtml) (*Wiederhold et al., 2004*). Although, it has to be stressed that there are no close structures available for a high-probability prediction of the structure of F28F8.5. The burst through vulva phenotype is also likely to be connected to LET-60/Ras signaling (*Ecsedi, Rausch & Grosshans, 2015*) that also supports the conservation of the dual, nuclear and cytoplasmic functions, of MED28 homologues throughout the evolution of Metazoa.

We propose that MED28 is a candidate Mediator complex subunit linking cytoplasmic structural signals towards the core of transcription regulation. The connection between cytoplasmic events and regulation of gene expression can be seen frequently. Numerous transcription factors are regulated by their spatial restriction, binding or incorporation into cytoplasmic structures and organelles. Many proteins that have primarily cytoplasmic structural functions were shown to possess transcription regulating activity (e.g., proteins

interacting with steroid receptors (*George, Schiltz & Hager, 2009*), FOX transcription factors (*Gan et al., 2005*; *Wang et al., 2015*), and BIR-1/Survivin (*Kostrouch et al., 2014*)). In-between interactions of MDT-28 that we identified, the interaction with MDT-30 may suggest an additional link towards connection of structural signals with the regulation of gene expression. MED30 was shown to be pulled down by MED28 quantitatively with higher efficiency compared to other subunits, possibly suggesting that these two subunits may be present in some subpopulations of Mediator complexes that could lack other Mediator subunits. MED30 is similarly as MED28 a likely more recent Mediator subunit specific to Metazoa and absent in yeast and it is intriguing to speculate that the more recently evolved Mediator subunits are linked with the evolution of structurally differentiated cells and tissues. It can be anticipated that impairment of cellular structure sensing could be involved in cancer biology. In-keeping with this, MED30 was recently identified as an upregulated gene in stomach cancer connected with cancer proliferative properties (*Lee et al., 2015*) and in development of cardiomyopathy in mice carrying a missense mutation in the first exon (*Krebs et al., 2011*). MED28 was also connected with cancer behavior and migration of cancer cells (*Huang et al., 2012*, *2017*). Wormbase also lists phenotypes similar to F28F8.5 knock-down by RNAi for *mdt-30*, namely a Dpy, burst through vulva and locomotion defect but not a germline defect (Wormbase WS, accessed on March 11, 2017). The gene *mdt-30* is organized in an operon together with F44B9.8 which is an ortholog of human RFC5 (replication factor C subunit 5) and its inhibition by RNAi leads to embryonic defects. Similarly as F28F8.5, *mdt-30* is likely to be expressed independently from the operon since it is trans-spliced with both SL1 and SL2 splice leaders (Wormbase WS, accessed on March 11, 2017).

Our results demonstrated phenotypic differences comparing knock down versus knockout of F28F8.5 activity. For example, downregulation of *F28F8.5* by RNAi resulted in embryonic lethality and larval arrest whereas null mutants with a disrupted *F28F8.5* gene found in the progeny of heterozygous animals with one edited disrupted allele and one WT allele or one edited disrupted allele and one edited allele coding for GFP::F28F8.5 were able to reach adulthood. Morevoer, most phenotypes that we observed in our RNAi experiments have previously been reported in Wormbase (WS254) based on high throughput screens (*Kamath & Ahringer, 2003*; *Simmer et al., 2003*; *Frand, Russel & Ruvkun, 2005*; *Sönnichsen et al., 2005*). One explanation of the differences between knockdowns versus knockouts is that heterozygous animals with one functional allele of *F28F8.5* supply their embryos with maternal transcripts, while the embryos in the progeny of parents with *F28F8.5* downregulated by RNAi are devoid of this maternal load; maternal rescue of loss-of-function mutations is frequently observed in *C. elegans* early development. This model further predicts that the amount of *F28F8.5* product inherited maternally is not sufficient for normal development of the gonad and other post-embryonic developmental events such as male tail development. Alternatively, our F28F8.5 disruptions could be affecting other genes in the operon, although none have been reported to result in high level embryonic lethality when eliminated individually. The three other genes within this operon are *atx-3*, the orthologue of human ataxin-3,

F28F8.9, a non-characteristic predicted protein and F28F8.7, an orthologue of human ELMSAN1 (ELM2 and Myb/SANT domain containing 1) and TRERF1 (transcriptional regulating factor 1). RNAi experiments have been reported for *atx-3* and F28F8.9, of which only inhibition of *atx-3* produced embryonic arrest in 10–25% of embryos. This suggests that even if our gene disruption is affecting other genes in the operon (as reported in *Bosher et al. (1999)*), the severe larval changes reported here are most likely the consequence of inhibition of *F28F8.5*. In addition, *F28F8.5* is also expressed independently from its own promoter based on our translational fusions and reported SL1 splice leader (*Mounsey, Bauer & Hope, 2002*; *Matus et al., 2010*). Further studies will be required to sort out the potentially complex interactions among these genes in development.

The broad expression pattern and indispensability of F28F8.5 we find during embryonic development is similar to findings reported for Med28 in other systems ((*Li et al., 2015*); Mouse Genome Database (http://www.mousephenotype.org/data/genes/MGI:1914249) (*Eppig et al., 2015*); Human Protein Atlas (http://www.proteinatlas.org) (*Uhlén et al., 2015*)). F28F8.5 was also shown to have tissue-specific functions, as in the anchor cell where it is important for the regulation of anchor cell translocation across the basement membrane during the formation of the developing vulva (*Matus et al., 2010*).

Our experiments with transgenes fused to GFP also show the differences between the expression of N- or C-terminally labeled F28F8.5. The expression of fusion transgenes is not entirely without functional and developmental consequences. N-terminally labeled F28F8.5 is likely to be able to maintain the nuclear functions of F28F8.5. It is also able to support, at least partially the cytoplasmic functions of F28F8.5 in male rays, since they are formed but are not entirely normal and defects in some animals were observed. It seems likely that GFP-labeled subunits in viable lines may help localize the place of action of labeled proteins as well as their function in *C. elegans*. We did not observe elevated cytoplasmic expression of GFP::F28F8.5 in the anchor cell described by *Matus et al. (2010)*. This is probably dependent on the position of GFP in the fusion protein which was on the C-terminus, in the case of the study by *Matus et al. (2010)* as well as in the case of the data reported by Wormbase (both based on a clone originally prepared by Ian Hope). It has been suggested that proteins containing GFP at their C-terminus are more frequently properly intracellularly localized compared to proteins containing GFP at their N-terminus (*Palmer & Freeman, 2004*). GFP positioned at the N-terminus might also fold differently and fail to produce fluorescence in oxidizing compartments (*Aronson, Costantini & Snapp, 2011*).

The direct link between effector proteins and the regulation of transcription can be traced to Eubacteria and Archaea. Lrp/AsnC proteins, metabolic effectors in Archaea and related Lrs14 proteins are serving as multipotent (Lrp) and specific (Asn) regulators of gene expression. Lrs14 has a clear negative autoregulatory potential illustrating the ancient origin of the transcriptional function of effector proteins (*Bell & Jackson, 2000*; *Thaw et al., 2006*; *Orell et al., 2013*). Similarities between the core transcriptional machinery of Eukaryotes and Archaea can be clearly found (*Hirata & Murakami, 2009*).

While the archaeal transcriptional complex seems to be sufficiently dependent on two basal transcriptional regulators, TBP and TFB, Pol II dependent transcription in higher eukaryotes requires five or six general transcription factors (reviewed in *Burton et al. (2016)*) and the modular assembly of the Mediator complex at the promoters of regulated genes. This modular complex is capable of linking the informatic network necessary for cells differentiated to multiple cell types (or in other words multiple structural cell states) with gene expression. MED28 homologues are thus likely to be able to bring cytoplasmic proteins to the core of gene transcription. This may explain why MED28 evolved in multicellular eukaryotes containing structurally differentiated cells.

In conclusion, MED28 homologues in vertebrates, insects, and nematodes share similarities indicating their conserved roles in cytoplasmic and nuclear events. It can be hypothesized that many proteins that are primarily building blocks of cellular structures and structure-associated proteins are likely to be part of regulatory loops that regulate gene expression. Similarly, as is the case of evolution of operons in Rhabditida that are formed during evolution if they are biologically tolerated for the sake of other regulatory or energetic gains (*Qian & Zhang, 2008*; *Blumenthal, 2012*), regulation by structural proteins may also be evolving for a limited number of structural proteins leaving other structure-forming proteins available for evolution of other functions. The homologues of MED28 in mammals, insects and nematodes therefore may be a link between cellular structural states and regulation of gene expression.

ABBREVIATIONS

F28F8.5[1]	gene coding for protein F28F8.5
F28F8.5a	splice form a
F28F8.5a	protein form a
F28F8.5b	splice form b
F28F8.5b	protein form b
gDNA	genomic DNA
$\boldsymbol{P_{F28F8.5}}$***(V:15573749)::gfp::F28F8.5***	edited *F28F8.5* with *gfp* tagged to the N-terminus in the position *V:15573749* (allele named edited *gfp::F28F8.5*)
$\boldsymbol{P_{F28F8.5}}$ ***(V:15573749)::gfp::let858(stop)::SEC::F28F8.5***	edited *F28F8.5* disrupted by *gfp* and SEC (allele named edited disrupted *F28F8.5*)
$\boldsymbol{P_{F28F8.5(400\ bp)}}$***::F28F8.5::gfp***	*F28F8.5* tagged with *gfp* on its C-terminus regulated by its predicted internal promoter with the size of 400 bp upstream of the ATG
GFP::F28F8.5	protein F28F8.5 tagged on its N-terminus with GFP
F28F8.5::GFP	protein F28F8.5 tagged on its C-terminus with GFP

[1] *F28F8.5* is now renamed with WormBase approval to *mdt-28*.

MED28	vertebrate Mediator complex subunit 28 gene
MED28	vertebrate Mediator complex subunit 28 protein
Med28	Mediator complex subunit 28 in a general sense; this nomenclature is also used in *Drosophila* and mouse gene nomenclature

ACKNOWLEDGEMENTS

The authors thank WormBase and NCBI for accessibility of data and bioinformatic support and Caenorhabditis Genetics Center CGC for the N2 wild type strain. The authors thank Dr. Heather Etchevers, Dr. Stefan Taubert and the two anonymous reviewers for their very helpful comments, suggestions and corrections.

ADDITIONAL INFORMATION AND DECLARATIONS

Funding

This work was supported by the European Regional Development Fund "BIOCEV—Biotechnology and Biomedicine Centre of the Academy of Sciences and Charles University in Vestec" (CZ.1.05/1.1.00/02.0109) (The Start-Up Grant to the group Structure and Function of Cells in Their Normal State and in Pathology—Integrative Biology and Pathology (5.1.10)) and the LQ1604 National Sustainability Program II (Project BIOCEV-FAR) and the project Biocev (CZ.1.05/1.1.00/02.0109) from the Ministry of Education, Youth and Sports of Czech Republic; the grant PRVOUK-P27 and PROGRES Q26/LF1 from Charles University in Prague; the grant SVV 260377/2017, SVV 260257/2016, SVV 260149/2015 and SVV 260023/2014 from Charles University in Prague. This work was supported by the project OPPK No. CZ.2.16/3.1.00/24024, awarded by European Fund for Regional Development (Prague & EU—We invest for your future). MWK is supported by the Intramural Research Program of the National Institute of Diabetes and Digestive and Kidney Diseases (NIDDK) of the National Institutes of Health, USA. This work was supported in part by a monetary gift from MediCentrum Praha, Czech Republic. The imaging was done at the Imaging Methods Core Facility at BIOCEV, supported by the Czech-BioImaging large RI project (LM2015062 funded by MEYS CR). ZK and MK contributed with personal funds to this work. The funders (except authors) had no role in study design, data collection and analysis, decision to publish, or preparation of the manuscript.

Grant Disclosures

The following grant information was disclosed by the authors:
European Regional Development Fund "BIOCEV—Biotechnology and Biomedicine Centre of the Academy of Sciences and Charles University in Vestec": CZ.1.05/1.1.00/02.0109.
The Start-Up Grant: 5.1.10.
Ministry of Education, Youth and Sports of Czech Republic: BIOCEV-FAR, CZ.1.05/1.1.00/02.0109.

Charles University in Prague: PRVOUK-P27, PROGRES Q26/LF1, SVV 260377/2017, SVV 260257/2016, SVV 260149/2015 and SVV 260023/2014.
European Fund for Regional Development: CZ.2.16/3.1.00/24024.
Intramural Research Program of the National Institute of Diabetes and Digestive and Kidney Diseases (NIDDK) of the National Institutes of Health, USA.
MediCentrum Praha, Czech Republic.
Czech-BioImaging large RI project (MEYS CR): LM2015062.

Competing Interests

Marta Kostrouchová is an Academic Editor for PeerJ. No other competing interests declared.

Author Contributions

- Markéta Kostrouchová conceived and designed the experiments, performed the experiments, analyzed the data, wrote the paper, prepared figures and/or tables, reviewed drafts of the paper.
- David Kostrouch conceived and designed the experiments, performed the experiments, analyzed the data, wrote the paper, prepared figures and/or tables, reviewed drafts of the paper.
- Ahmed A. Chughtai conceived and designed the experiments, performed the experiments, analyzed the data, wrote the paper, prepared figures and/or tables, reviewed drafts of the paper.
- Filip Kaššák conceived and designed the experiments, performed the experiments, analyzed the data, wrote the paper, prepared figures and/or tables, reviewed drafts of the paper.
- Jan P. Novotný conceived and designed the experiments, performed the experiments, analyzed the data, wrote the paper, prepared figures and/or tables, reviewed drafts of the paper.
- Veronika Kostrouchová performed the experiments, analyzed the data, wrote the paper, prepared figures and/or tables, reviewed drafts of the paper.
- Aleš Benda conceived and designed the experiments, performed the experiments, analyzed the data, wrote the paper, prepared figures and/or tables, reviewed drafts of the paper.
- Michael W. Krause conceived and designed the experiments, performed the experiments, analyzed the data, wrote the paper, prepared figures and/or tables, reviewed drafts of the paper.
- Vladimír Saudek conceived and designed the experiments, performed the experiments, analyzed the data, wrote the paper, prepared figures and/or tables, reviewed drafts of the paper.
- Marta Kostrouchová conceived and designed the experiments, performed the experiments, analyzed the data, contributed reagents/materials/analysis tools, wrote the paper, prepared figures and/or tables, reviewed drafts of the paper, contributed with personal funds.

- Zdeněk Kostrouch conceived and designed the experiments, performed the experiments, analyzed the data, contributed reagents/materials/analysis tools, wrote the paper, prepared figures and/or tables, reviewed drafts of the paper, contributed with personal funds.

Data Availability

The following information was supplied regarding data availability:

The raw data has been supplied as Supplemental Dataset Files.

Supplemental Information

Supplemental information for this article can be found online at http://dx.doi.org/10.7717/peerj.3390#supplemental-information.

REFERENCES

Allen BL, Taatjes DJ. 2015. The Mediator complex: a central integrator of transcription. *Nature Reviews Molecular Cell Biology* **16(3)**:155–166 DOI 10.1038/nrm3951.

Altschul SF, Madden TL, Schäffer AA, Zhang J, Zhang Z, Miller W, Lipman DJ. 1997. Gapped BLAST and PSI-BLAST: a new generation of protein database search programs. *Nucleic Acids Research* **25(17)**:3389–3402 DOI 10.1093/nar/25.17.3389.

Aronson DE, Costantini LM, Snapp EL. 2011. Superfolder GFP is fluorescent in oxidizing environments when targeted via the Sec translocon. *Traffic* **12(5)**:543–548 DOI 10.1111/j.1600-0854.2011.01168.x.

Ban N, Nissen P, Hansen J, Moore PB, Steitz TA. 2000. The complete atomic structure of the large ribosomal subunit at 2.4 Å resolution. *Science* **289(5481)**:905–920 DOI 10.1126/science.289.5481.905.

Bell SD, Jackson SP. 2000. Mechanism of autoregulation by an archaeal transcriptional repressor. *Journal of Biological Chemistry* **275**:31624–31629 DOI 10.1074/jbc.M005422200.

Beyer KS, Beauchamp RL, Lee MF, Gusella JF, Naar AM, Ramesh V. 2007. Mediator subunit MED28 (Magicin) is a repressor of smooth muscle cell differentiation. *Journal of Biological Chemistry* **282(44)**:32152–32157 DOI 10.1074/jbc.m706592200.

Blumenthal T. 2012. Trans-splicing and operons in *C. elegans*. In: Jane Mendel E, ed. *The C. elegans Research Community*. WormBook. *Available at http://www.wormbook.org*.

Bosher JM, Dufourcq P, Sookhareea S, Labouesse M. 1999. RNA interference can target pre-mRNA: consequences for gene expression in a *Caenorhabditis elegans* operon. *Genetics* **153(3)**:1245–1256.

Bourbon H-M. 2008. Comparative genomics supports a deep evolutionary origin for the large, four-module transcriptional Mediator complex. *Nucleic Acids Research* **36(12)**:3993–4008 DOI 10.1093/nar/gkn349.

Bourbon H-M, Aguilera A, Ansari AZ, Asturias FJ, Berk AJ, Bjorklund S, Blackwell TK, Borggrefe T, Carey M, Carlson M, Conaway JW, Conaway RC, Emmons SW, Fondell JD, Freedman LP, Fukasawa T, Gustafsson CM, Han M, He X, Herman PK, Hinnebusch AG, Holmberg S, Holstege FC, Jaehning JA, Kim Y-J, Kuras L, Leutz A, Lis JT, Meisterernest M, Naar AM, Nasmyth K, Parvin JD, Ptashne M, Reinberg D, Ronne H, Sadowski I, Sakurai H, Sipiczki M, Sternberg PW, Stillman DJ, Strich R, Struhl K, Svejstrup JQ, Tuck S, Winston F, Roeder RG, Kornberg RD. 2004. A unified nomenclature for protein subunits of Mediator complexes linking transcriptional regulators to RNA polymerase II. *Molecular Cell* **14**:553–557 DOI 10.1016/j.molcel.2004.05.011.

Brenner S. 1974. The genetics of *Caenorhabditis elegans*. *Genetics* **77(1)**:71–94.

Brzovic PS, Heikaus CC, Kisselev L, Vernon R, Herbig E, Pacheco D, Warfield L, Littlefield P, Baker D, Klevit RE, Hahn S. 2011. The acidic transcription activator Gcn4 binds the mediator subunit Gal11/Med15 using a simple protein interface forming a fuzzy complex. *Molecular Cell* **44(6)**:942–953 DOI 10.1016/j.molcel.2011.11.008.

Burton ZF, Opron K, Wei G, Geiger JH. 2016. A model for genesis of transcription systems. *Transcription* **7**:1–13 DOI 10.1080/21541264.2015.1128518.

Cevher MA, Shi Y, Li D, Chait BT, Malik S, Roeder RG. 2014. Reconstitution of active human core Mediator complex reveals a critical role of the MED14 subunit. *Nature Structural & Molecular Biology* **21(12)**:1028–1034 DOI 10.1038/nsmb.2914.

Chughtai AA, Kaššák F, Kostrouchová M, Novotný JP, Krause MW, Saudek V, Kostrouch Z, Kostrouchová M. 2015. Perilipin-related protein regulates lipid metabolism in *C. elegans*. *PeerJ* **3**:e1213 DOI 10.7717/peerj.1213.

Clamp M, Cuff J, Searle SM, Barton GJ. 2004. The Jalview Java alignment editor. *Bioinformatics* **20(3)**:426–427 DOI 10.1093/bioinformatics/btg430.

Cuff JA, Barton GJ. 2000. Application of multiple sequence alignment profiles to improve protein secondary structure prediction. *Proteins* **40(3)**:502–511 DOI 10.1002/1097-0134(20000815)40:3<502::aid-prot170>3.0.co;2-q.

D'Alessio JA, Ng R, Willenbring H, Tjian R. 2011. Core promoter recognition complex changes accompany liver development. *Proceedings of the National Academy of Sciences of the United States of America* **108(10)**:3906–3911 DOI 10.1073/pnas.1100640108.

Deato MDE, Marr MT, Sottero T, Inouye C, Hu P, Tjian R. 2008. MyoD targets TAF3/TRF3 to activate myogenin transcription. *Molecular Cell* **32(1)**:96–105 DOI 10.1016/j.molcel.2008.09.009.

Dettmann A, Jäschke Y, Triebel I, Bogs J, Schröder I, Schüller H-J. 2010. Mediator subunits and histone methyltransferase Set2 contribute to Ino2-dependent transcriptional activation of phospholipid biosynthesis in the yeast *Saccharomyces cerevisiae*. *Molecular Genetics and Genomics* **283(3)**:211–221 DOI 10.1007/s00438-009-0508-9.

Di Tommaso P, Moretti S, Xenarios I, Orobitg M, Montanyola A, Chang J-M, Taly J-F, Notredame C. 2011. T-Coffee: a web server for the multiple sequence alignment of protein and RNA sequences using structural information and homology extension. *Nucleic Acids Research* **39(Suppl_2)**:W13–W17 DOI 10.1093/nar/gkr245.

Diaz JJ, Dodon MD, Schaerer-Uthurralt N, Simonin D, Kindbeiter K, Gazzolo L, Madjar J-J. 1996. Post-transcriptional transactivation of human retroviral envelope glycoprotein expression by herpes simplex virus Us11 protein. *Nature* **379**:273–277 DOI 10.1038/379273a0.

Diaz JJ, Simonin D, Massé T, Deviller P, Kindbeiter K, Denoroy L, Madjar J-J. 1993. The herpes simplex virus type 1 US11 gene product is a phosphorylated protein found to be non-specifically associated with both ribosomal subunits. *Journal of General Virology* **74(Pt 3)**:397–406 DOI 10.1099/0022-1317-74-3-397.

Dickinson DJ, Goldstein B. 2016. CRISPR-based methods for *Caenorhabditis elegans* genome engineering. *Genetics* **202(3)**:885–901 DOI 10.1534/genetics.115.182162.

Dickinson DJ, Pani AM, Heppert JK, Higgins CD, Goldstein B. 2015. Streamlined genome engineering with a self-excising drug selection cassette. *Genetics* **200(4)**:1035–1049 DOI 10.1534/genetics.115.178335.

Dickinson DJ, Ward JD, Reiner DJ, Goldstein B. 2013. Engineering the *Caenorhabditis elegans* genome using Cas9-triggered homologous recombination. *Nature Methods* **10**:1028–1034 DOI 10.1038/nmeth.2641.

Ecsedi M, Rausch M, Grosshans H. 2015. The let-7 microRNA directs vulval development through a single target. *Developmental Cell* **32(3)**:335–344 DOI 10.1016/j.devcel.2014.12.018.

Eppig JT, Blake JA, Bult CJ, Kadin JA, Richardson JE, Mouse Genome Database Group. 2015. The mouse genome database (MGD): facilitating mouse as a model for human biology and disease. *Nucleic Acids Research* **43(D1)**:D726–D736 DOI 10.1093/nar/gku967.

Frand AR, Russel S, Ruvkun G. 2005. Functional genomic analysis of *C. elegans* molting. *PLoS Biology* **3(10)**:e312 DOI 10.1371/journal.pbio.0030312.

Gan L, Zheng W, Chabot JG, Unterman TG, Quirion R. 2005. Nuclear/cytoplasmic shuttling of the transcription factor FoxO1 is regulated by neurotrophic factors. *Journal of Neurochemistry* **93(5)**:1209–1219 DOI 10.1111/j.1471-4159.2005.03108.x.

George AA, Schiltz RL, Hager GL. 2009. Dynamic access of the glucocorticoid receptor to response elements in chromatin. *International Journal of Biochemistry & Cell Biology* **41(1)**:214–224 DOI 10.1016/j.biocel.2008.09.019.

Grants JM, Goh GYS, Taubert S. 2015. The Mediator complex of *Caenorhabditis elegans*: insights into the developmental and physiological roles of a conserved transcriptional coregulator. *Nucleic Acids Research* **43(4)**:2442–2453 DOI 10.1093/nar/gkv037.

Grants JM, Ying LTL, Yoda A, You CC, Okano H, Sawa H, Taubert S. 2016. The mediator kinase module restrains epidermal growth factor receptor signaling and represses vulval cell fate specification in *Caenorhabditis elegans*. *Genetics* **202(2)**:583–599 DOI 10.1534/genetics.115.180265.

Hirata A, Murakami KS. 2009. Archaeal RNA polymerase. *Current Opinion in Structural Biology* **19(6)**:724–731 DOI 10.1016/j.sbi.2009.10.006.

Hobert O. 2002. PCR fusion-based approach to create reporter gene constructs for expression analysis in transgenic *C. elegans*. *Biotechniques* **32**:728–730.

Holstege FCP, Jennings EG, Wyrick JJ, Lee TI, Hengartner CJ, Green MR, Golub TR, Lander ES, Young RA. 1998. Dissecting the regulatory circuitry of a eukaryotic genome. *Cell* **95(5)**:717–728 DOI 10.1016/s0092-8674(00)81641-4.

Huang C-Y, Chou Y-H, Hsieh N-T, Chen H-H, Lee M-F. 2012. MED28 regulates MEK1-dependent cellular migration in human breast cancer cells. *Journal of Cellular Physiology* **227(12)**:3820–3827 DOI 10.1002/jcp.24093.

Huang C-Y, Hsieh N-T, Li C-I, Weng Y-T, Liu H-S, Lee M-F. 2017. MED28 regulates epithelial-mesenchymal transition through NFκB in human breast cancer cells. *Journal of Cellular Physiology* **232(6)**:1337–1345 DOI 10.1002/jcp.25610.

Jones DT. 1999. Protein secondary structure prediction based on position-specific scoring matrices. *Journal of Molecular Biology* **292(2)**:195–202 DOI 10.1006/jmbi.1999.3091.

Kamath RS, Ahringer J. 2003. Genome-wide RNAi screening in *Caenorhabditis elegans*. *Methods* **30(4)**:313–321 DOI 10.1016/s1046-2023(03)00050-1.

Kim TW, Kwon YJ, Kim JM, Song YH, Kim SN, Kim YJ. 2004. MED16 and MED23 of mediator are coactivators of lipopolysaccharide- and heat-shock-induced transcriptional activators. *Proceedings of the National Academy of Sciences of the United States of America* **101(33)**:12153–12158 DOI 10.1073/pnas.0401985101.

Kostrouch D, Kostrouchová M, Yilma P, Chughtai AA, Novotný JP, Novák P, Kostrouchová V, Kostrouchová M, Kostrouch Z. 2014. SKIP and BIR-1/Survivin have potential to integrate proteome status with gene expression. *Journal of Proteomics* **110**:93–106 DOI 10.1016/j.jprot.2014.07.023.

Krebs P, Fan W, Chen Y-H, Tobita K, Downes MR, Wood MR, Sun L, Li X, Xia Y, Ding N, Spaeth JM, Moresco EMY, Boyer TG, Lo CW, Yen J, Evans RM, Beutler B. 2011. Lethal

mitochondrial cardiomyopathy in a hypomorphic *Med30* mouse mutant is ameliorated by ketogenic diet. *Proceedings of the National Academy of Sciences of the United States of America* **108(49)**:19678–19682 DOI 10.1073/pnas.1117835108.

Kulak NA, Pichler G, Paron I, Nagaraj N, Mann M. 2014. Minimal, encapsulated proteomic-sample processing applied to copy-number estimation in eukaryotic cells. *Nature Methods* **11(3)**:319–324 DOI 10.1038/nmeth.2834.

Lee M-F, Beauchamp RL, Beyer KS, Gusella JF, Ramesh V. 2006. Magicin associates with the Src-family kinases and is phosphorylated upon CD3 stimulation. *Biochemical and Biophysical Research Communications* **348(3)**:826–831 DOI 10.1016/j.bbrc.2006.07.126.

Lee YJ, Han M-E, Baek S-J, Kim S-Y, Oh S-O. 2015. MED30 regulates the proliferation and motility of gastric cancer cells. *PLoS ONE* **10(6)**:e0130826 DOI 10.1371/journal.pone.0130826.

Li L, Walsh RM, Wagh V, James MF, Beauchamp RL, Chang Y-S, Gusella JF, Hochedlinger K, Ramesh V. 2015. Mediator subunit Med28 is essential for mouse peri-implantation development and pluripotency. *PLoS ONE* **10(10)**:e0140192 DOI 10.1371/journal.pone.0140192.

Liu C, Zhang L, Shao Z-M, Beatty P, Sartippour M, Lane TF, Barsky SH, Livingston E, Nguyen M. 2002. Identification of a novel endothelial-derived gene EG-1. *Biochemical and Biophysical Research Communications* **290(1)**:602–612 DOI 10.1006/bbrc.2001.6119.

Lu M, Zhang L, Sartippour MR, Norris AJ, Brooks MN. 2006. EG-1 interacts with c-Src and activates its signaling pathway. *International Journal of Oncology* **29(4)**:1013–1018 DOI 10.3892/ijo.29.4.1013.

Ly K, Reid SJ, Snell RG. 2015. Rapid RNA analysis of individual *Caenorhabditis elegans*. *MethodsX* **2**:59–63 DOI 10.1016/j.mex.2015.02.002.

Malik S, Guermah M, Yuan CX, Wu W, Yamamura S, Roeder RG. 2004. Structural and functional organization of TRAP220, the TRAP/mediator subunit that is targeted by nuclear receptors. *Molecular and Cellular Biology* **24(18)**:8244–8254 DOI 10.1128/MCB.24.18.8244-8254.2004.

Marcel V, Ghayad SE, Belin S, Therizols G, Morel AP, Solano-Gonzàlez E, Vendrell JA, Hacot S, Mertani HC, Albaret MA, Bourdon JC, Jordan L, Thompson A, Tafer Y, Cong R, Bouvet P, Saurin J-C, Catez F, Prats A-C, Puisieux A, Diaz J-J. 2013. p53 acts as a safeguard of translational control by regulating fibrillarin and rRNA methylation in cancer. *Cancer Cell* **24(3)**:318–330 DOI 10.1016/j.ccr.2013.08.013.

Matus DQ, Li XY, Durbin S, Agarwal D, Chi Q, Weiss SJ, Sherwood DR. 2010. In vivo identification of regulators of cell invasion across basement membranes. *Science Signaling* **3(120)**:ra35 DOI 10.1126/scisignal.2000654.

McClatchey AI, Fehon RG. 2009. Merlin and the ERM proteins—regulators of receptor distribution and signaling at the cell cortex. *Trends in Cell Biology* **19(5)**:198–206 DOI 10.1016/j.tcb.2009.02.006.

McClatchey AI, Giovannini M. 2005. Membrane organization and tumorigenesis—the NF2 tumor suppressor, Merlin. *Genes & Development* **19(19)**:2265–2277.

McGuffin LJ, Bryson K, Jones DT. 2000. The PSIPRED protein structure prediction server. *Bioinformatics* **16(4)**:404–405 DOI 10.1093/bioinformatics/16.4.404.

Mounsey A, Bauer P, Hope IA. 2002. Evidence suggesting that a fifth of annotated *Caenorhabditis elegans* genes may be pseudogenes. *Genome Research* **12(5)**:770–775 DOI 10.1101/gr208802.

Nagulapalli M, Maji S, Dwivedi N, Dahiya P, Thakur JK. 2016. Evolution of disorder in Mediator complex and its functional relevance. *Nucleic Acids Research* **44(4)**:1591–1612 DOI 10.1093/nar/gkv1135.

Nguyen-Lefebvre AT, Leprun G, Morin V, Viñuelas J, Couté Y, Madjar J-J, Gandrillon O, Gonin-Giraud S. 2014. V-erbA generates ribosomes devoid of RPL11 and regulates translational activity in avian erythroid progenitors. *Oncogene* **33(12)**:1581–1589 DOI 10.1038/onc.2013.93.

Notredame C, Higgins DG, Heringa J. 2000. T-coffee: a novel method for fast and accurate multiple sequence alignment. *Journal of Molecular Biology* **302(1)**:205–217 DOI 10.1006/jmbi.2000.4042.

Orell A, Peeters E, Vassen V, Jachlewski S, Schalles S, Siebers B, Albers SV. 2013. Lrs14 transcriptional regulators influence biofilm formation and cell motility of Crenarchaea. *ISME Journal* **7(10)**:1886–1898 DOI 10.1038/ismej.2013.68.

Palmer E, Freeman T. 2004. Investigation into the use of C- and N-terminal GFP fusion proteins for subcellular localization studies using reverse transfection microarrays. *Comparative and Functional Genomics* **5(4)**:342–353 DOI 10.1002/cfg.405.

Paoletti AC, Parmely TJ, Tomomori-Sato C, Sato S, Zhu D, Conaway RC, Conaway JW, Florens L, Washburn MP. 2006. Quantitative proteomic analysis of distinct mammalian Mediator complexes using normalized spectral abundance factors. *Proceedings of the National Academy of Sciences of the United States of America* **103(50)**:18928–18933 DOI 10.1073/pnas.0606379103.

Pei J, Grishin NV. 2007. PROMALS: towards accurate multiple sequence alignments of distantly related proteins. *Bioinformatics* **23(7)**:802–808 DOI 10.1093/bioinformatics/btm017.

Pei J, Kim B-H, Grishin NV. 2008. PROMALS3D: a tool for multiple protein sequence and structure alignments. *Nucleic Acids Research* **36(7)**:2295–2300 DOI 10.1093/nar/gkn072.

Pei J, Kim B-H, Tang M, Grishin NV. 2007. PROMALS web server for accurate multiple protein sequence alignments. *Nucleic Acids Research* **35(Suppl_2)**:W649–W652 DOI 10.1093/nar/gkm227.

Poss ZC, Ebmeier CC, Taatjes DJ. 2013. The Mediator complex and transcription regulation. *Critical Reviews in Biochemistry and Molecular Biology* **48(6)**:575–608 DOI 10.3109/10409238.2013.840259.

Qian W, Zhang J. 2008. Evolutionary dynamics of nematode operons: easy come, slow go. *Genome Research* **18(3)**:412–421 DOI 10.1101/gr.7112608.

Rachez C, Freedman LP. 2001. Mediator complexes and transcription. *Current Opinion in Cell Biology* **13(3)**:274–280 DOI 10.1016/s0955-0674(00)00209-x.

Remmert M, Biegert A, Hauser A, Soding J. 2011. HHblits: lightning-fast iterative protein sequence searching by HMM-HMM alignment. *Nature Methods* **9(2)**:173–175 DOI 10.1038/nmeth.1818.

Sato S, Tomomori-Sato C, Parmely TJ, Florens L, Zybailov B, Swanson SK, Banks CA, Jin J, Cai Y, Washburn MP, Conaway JW, Conaway RC. 2004. A set of consensus mammalian mediator subunits identified by multidimensional protein identification technology. *Molecular Cell* **14(5)**:685–691 DOI 10.1016/j.molcel.2004.05.006.

Schluenzen F, Tocilj A, Zarivach R, Harms J, Gluehmann M, Janell D, Bashan A, Bartels H, Agmon I, Franceschi F, Yonath A. 2000. Structure of functionally activated small ribosomal subunit at 3.3 angstroms resolution. *Cell* **102**:615–623 DOI 10.2210/pdb1fka/pdb.

Schneider CA, Rasband WS, Eliceiri KW. 2012. NIH Image to ImageJ: 25 years of image analysis. *Nature Methods* **9(7)**:671–675 DOI 10.1038/nmeth.2089.

Šimečková K, Brožová E, Vohánka J, Pohludka M, Kostrouch Z, Krause MW, Rall JE, Kostrouchová M. 2007. Supplementary nuclear receptor NHR-60 is required for normal embryonic and early larval development of *Caenorhabditis elegans*. *Folia Biologica* **53**:85–96.

Simmer F, Moorman C, van der Linden AM, Kuijk E, van den Berghe PVE, Kamath RS, Fraser AG, Ahringer J, Plasterk RHA. 2003. Genome-wide RNAi of *C. elegans* using the hypersensitive rrf-3 strain reveals novel gene functions. *PLoS Biology* **1(1)**:e12 DOI 10.1371/journal.pbio.0000012.

Söding J, Biegert A, Lupas AN. 2005. The HHpred interactive server for protein homology detection and structure prediction. *Nucleic Acids Research* **33(Suppl_2)**:W244–W248 DOI 10.1093/nar/gki408.

Sönnichsen B, Koski LB, Walsh A, Marschall P, Neumann B, Brehm M, Alleaume AM, Artelt J, Bettencourt P, Cassin E, Hewitson M, Holz C, Khan M, Lazik S, Martin C, Nitzsche B, Ruer M, Stamford J, Winzi M, Heinkel R, Röder M, Finell J, Häntsch H, Jones SJ, Jones M, Piano F, Gunsalus KC, Oegema K, Gönczy P, Coulson A, Hyman AA, Echeverri CJ. 2005. Full-genome RNAi profiling of early embryogenesis in *Caenorhabditis elegans*. *Nature* **434(7032)**:462–469 DOI 10.1038/nature03353.

Taatjes DJ, Tjian R. 2004. Structure and function of CRSP/Med2; a promoter-selective transcriptional coactivator complex. *Molecular Cell* **14(5)**:675–683 DOI 10.1016/j.molcel.2004.05.014.

Tabara H, Sarkissian M, Kelly WG, Fleenor J, Grishok A, Timmons L, Fire A, Mello CC. 1999. The rde-1 gene, RNA interference, and transposon silencing in *C. elegans*. *Cell* **99(2)**:123–132 DOI 10.1016/s0092-8674(00)81644-x.

Thaw P, Sedelnikova SE, Muranova T, Wiese S, Ayora S, Alonso JC, Brinkman AB, Akerboom J, van der Oost J, Rafferty JB. 2006. Structural insight into gene transcriptional regulation and effector binding by the Lrp/AsnC family. *Nucleic Acids Research* **34(5)**:1439–1449 DOI 10.1093/nar/gkl009.

Thompson CM, Young RA. 1995. General requirement for RNA polymerase II holoenzymes in vivo. *Proceedings of the National Academy of Sciences of the United States of America* **92(10)**:4587–4590 DOI 10.1073/pnas.92.10.4587.

Timmons L, Court DL, Fire A. 2001. Ingestion of bacterially expressed dsRNAs can produce specific and potent genetic interference in *Caenorhabditis elegans*. *Gene* **263(1–2)**:103–112 DOI 10.1016/s0378-1119(00)00579-5.

Uhlén M, Fagerberg L, Hallstrom BM, Lindskog C, Oksvold P, Mardinoglu A, Sivertsson A, Kampf C, Sjöstedt E, Asplund A, Olsson I, Edlund K, Lundberg E, Navani S, Szigyarto CA, Odeberg J, Djureinovic D, Takanen JO, Hober S, Alm T, Edqvist P-H, Berling H, Tegel H, Mulder J, Rockberg J, Nilsson P, Schwenk JM, Hamsten M, von Feilitzen K, Forsberg M, Persson L, Johansson F, Zwahlen M, von Heijne G, Nielsen J, Pontén F. 2015. Tissue-based map of the human proteome. *Science* **347(6220)**:1260419 DOI 10.1126/science.1260419.

Uwamahoro N, Qu Y, Jelicic B, Lo TL, Beaurepaire C, Bantun F, Quenault T, Boag PR, Ramm G, Callaghan J, Beilharz TH, Nantel A, Peleg AY, Traven A. 2012. The functions of Mediator in *Candida albicans* support a role in shaping species-specific gene expression. *PLoS Genetics* **8(4)**:e1002613 DOI 10.1371/journal.pgen.1002613.

Vohanka J, Šimečková K, Machalová E, Behenský F, Krause MW, Kostrouch Z, Kostrouchová M. 2010. Diversification of fasting regulated transcription in a cluster of duplicated nuclear hormone receptors in *C. elegans*. *Gene Expression Patterns* **10(6)**:227–236 DOI 10.1016/j.gep.2010.05.001.

Wang W, Li X, Lee M, Jun S, Aziz KE, Feng L, Tran MK, Li N, McCrea PD, Park JI, Chen J. 2015. FOXKs promote Wnt/beta-catenin signaling by translocating DVL into the nucleus. *Developmental Cell* **32**:707–718 DOI 10.1016/j.devcel.2015.01.031.

Ward JD. 2015. Rapid and precise engineering of the *Caenorhabditis elegans* genome with lethal mutation co-conversion and inactivation of NHEJ repair. *Genetics* **199(2)**:363–377 DOI 10.1534/genetics.114.172361.

Warfield L, Tuttle LM, Pacheco D, Klevit RE, Hahn S. 2014. A sequence-specific transcription activator motif and powerful synthetic variants that bind Mediator using a fuzzy protein interface. *Proceedings of the National Academy of Sciences of the United States of America* **111(34)**:E3506–E3513 DOI 10.1073/pnas.1412088111.

Wiederhold T, Lee M-F, James M, Neujahr R, Smith N, Murthy A, Hartwig J, Gusella JF, Ramesh V. 2004. Magicin, a novel cytoskeletal protein associates with the NF2 tumor suppressor merlin and Grb2. *Oncogene* **23(54)**:8815–8825 DOI 10.1038/sj.onc.1208110.

Wimberly BT, Brodersen DE, Clemons WM Jr, Morgan-Warren RJ, Carter AP, Vonrhein C, Hartsch T, Ramakrishnan V. 2000. Structure of the 30S ribosomal subunit. *Nature* **407(6802)**:327–339 DOI 10.1038/35030006.

Zhu X, Chen L, Carlsten JOP, Liu Q, Yang J, Liu B, Gustafsson CM. 2015. Mediator tail subunits can form amyloid-like aggregates in vivo and affect stress response in yeast. *Nucleic Acids Research* **43(15)**:7306–7314 DOI 10.1093/nar/gkv629.

Zima V, Šebková K, Šimečková K, Dvořák T, Saudek V, Kostrouchová M. 2015. Prorenin receptor homologue VHA-20 is critical for intestinal pH regulation, ion and water management and larval development in *C. elegans*. *Folia Biologica* **61**:168–177.

Trichoplax adhaerens reveals a network of nuclear receptors sensitive to 9-*cis*-retinoic acid at the base of metazoan evolution

Jan Philipp Novotný[1,2], Ahmed Ali Chughtai[1], Markéta Kostrouchová[1,3], Veronika Kostrouchová[1], David Kostrouch[1], Filip Kaššák[1], Radek Kaňa[4], Bernd Schierwater[5,6], Marta Kostrouchová[1] and Zdenek Kostrouch[1]

[1] Biocev, First Faculty of Medicine, Charles University, Vestec, Czech Republic
[2] Department of Medicine V., University of Heidelberg, Heidelberg, Germany
[3] Department of Pathology, Third Faculty of Medicine, Charles University, Prague, Czech Republic
[4] Institute of Microbiology, Laboratory of Photosynthesis, Czech Academy of Sciences, Třeboň, Czech Republic
[5] Institute for Animal Ecology and Cell Biology, University of Veterinary Medicine, Hannover, Germany
[6] Department of Ecology and Evolutionary Biology, Yale University, New Haven, CT, United States of America

ABSTRACT

Trichoplax adhaerens, the only known species of Placozoa is likely to be closely related to an early metazoan that preceded branching of Cnidaria and Bilateria. This animal species is surprisingly well adapted to free life in the World Ocean inhabiting tidal costal zones of oceans and seas with warm to moderate temperatures and shallow waters. The genome of *T. adhaerens* (sp. Grell) includes four nuclear receptors, namely orthologue of RXR (NR2B), HNF4 (NR2A), COUP-TF (NR2F) and ERR (NR3B) that show a high degree of similarity with human orthologues. In the case of RXR, the sequence identity to human RXR alpha reaches 81% in the DNA binding domain and 70% in the ligand binding domain. We show that *T. adhaerens* RXR (TaRXR) binds 9-*cis* retinoic acid (9-*cis*-RA) with high affinity, as well as high specificity and that exposure of *T. adhaerens* to 9-*cis*-RA regulates the expression of the putative *T. adhaerens* orthologue of vertebrate L-malate-NADP$^+$ oxidoreductase (EC 1.1.1.40) which in vertebrates is regulated by a heterodimer of RXR and thyroid hormone receptor. Treatment by 9-*cis*-RA alters the relative expression profile of *T. adhaerens* nuclear receptors, suggesting the existence of natural ligands. Keeping with this, algal food composition has a profound effect on *T. adhaerens* growth and appearance. We show that nanomolar concentrations of 9-*cis*-RA interfere with *T. adhaerens* growth response to specific algal food and causes growth arrest. Our results uncover an endocrine-like network of nuclear receptors sensitive to 9-*cis*-RA in *T. adhaerens* and support the existence of a ligand-sensitive network of nuclear receptors at the base of metazoan evolution.

Subjects Evolutionary Studies, Genomics, Molecular Biology, Diabetes and Endocrinology
Keywords *Trichoplax adhaerens*, RXR, 9-*cis* retinoic acid, Food, ERR, HNF4, COUP, Nuclear receptor

Submitted 21 April 2017
Accepted 18 August 2017
Published 29 September 2017

Corresponding author
Zdenek Kostrouch,
Zdenek.kostrouch@lf1.cuni.cz

Academic editor
Christopher Cooper

Additional Information and Declarations can be found on page 23

DOI **10.7717/peerj.3789**

INTRODUCTION

Life on Earth began 4.1 to 3.5 billion years ago (*Bell et al., 2015*) with the appearance of the first unicellular organisms that subsequently evolved, in part, to multicellular lifeforms forming the kingdom Metazoa that have specialized tissues for digestion, regulation of homeostasis, locomotion, perception, analysis of the environment and reproduction.

In contrast to unicellular organisms, metazoans are in need of regulatory mechanisms that provide the means of coordination between various tissues in a tight arrangement with cellular homeostasis. This coordination on the level of humoral signaling includes regulation by nuclear receptors (NRs), which respond to small, mostly hydrophobic molecules, including hormones produced by specific tissues, metabolites or even molecules present in the environment and transfer these signals to the nucleus, thus leading to a dynamically changing but adaptive gene expression (*Escriva, Bertrand & Laudet, 2004*).

NRs therefore play an important role in maintaining intra- and inter-cellular functions in multicellular organisms. Their overall structure is common in most nuclear receptors and consists of an A/B (N-terminal) domain, the DNA binding domain (DBD), a hinge region, the ligand binding domain (LBD) and the C-terminal domain (*Kumar & Thompson, 1999*; *Robinson-Rechavi, Escriva Garcia & Laudet, 2003*). The DBD and LBD of NRs exhibit an especially high degree of conservation and the changes that were acquired during evolution allow classification of the NR protein family into six subfamilies (*Laudet, 1997*; *Escriva et al., 1998*). NRs that evolved within these subfamilies show functional connections that include specialization of regulatory functions in time or cell type restriction, fortification of ancestral functions or their specific inhibition by newly evolved NRs (*Escriva, Bertrand & Laudet, 2004*; *Kostrouchova & Kostrouch, 2015*).

With the overall structure maintained across metazoan species, nuclear receptors show significant heterogeneity regarding their quantity and function, many of which have not yet been explored in e.g., *Caenorhabditis elegans* with over 280 nuclear receptors (reviewed in *Kostrouchova & Kostrouch, 2015*).

The evolutionary changes accumulated in diversified NRs allow functional subspecialization at the level of specific sequence binding within gene promoters (response elements), protein-protein interactions with functionally linked receptor interactors and adoption of new ligands as specific hormonal regulators. The evolution of hormonal ligands acquired by different species during evolution is well documented and indicates the potential of NRs to adopt new ligands as regulators (*Escriva, Delaunay & Laudet, 2000*; *Markov & Laudet, 2011*). Indeed, it is now thought that NRs evolved as environmental sensors that were able to sense a wide variety of compounds with low affinity and specificity, some of which later-on acquired higher affinity binding towards certain ligands that are products of metabolic pathways (*Holzer, Markov & Laudet, 2017*). This can be exemplified by the high affinity and specificity binding of certain receptors, such as the mineralocorticoid or androgen receptors, while the family of PPARs shows a rather promiscuous binding to a variety of different substances (*Issemann & Green, 1990*). Keeping in mind the metabolic origin of NR ligands, it is not completely surprising to see different ligands binding to

orthologues across species, such as Triac and T3 in the case of TR (*Paris et al., 2008*), thus changing in the course of evolution and adapting to new environments.

This is accompanied by the essential questions, to what degree the plasticity of ligand selection is a fundamental property of NRs and what the origin of specific ligand binding by NRs might be. It has been suggested that the original NR, which is the ancestral NR possessing gene regulatory capacity, may have been an unliganded molecular regulator (*Escriva et al., 1997*). However, it is now believed that the ancestral NR is most closely related to the NR2 subfamily, as members of this family can be found in basal metazoans and are sensors of fatty acids (*Holzer, Markov & Laudet, 2017*). More recently, it was proposed that the ligand binding and ligand-dependent regulatory potential of NRs is an inherent feature of the evolution of NRs (*Bridgham et al., 2010*). Due to their nature of fine tuning cellular responses in response to environmental changes without necessarily showing high affinity binding to a set of ligands, cross-species comparison of nuclear receptor networks might shed light on the details of the NR network function (*Holzer, Markov & Laudet, 2017*).

A search for NRs that may be closely related to an ancient ancestor of the NR family led to the discovery of an RXR orthologue in Cnidaria (*Kostrouch et al., 1998*). Surprisingly, this receptor showed not only extremely high degree of sequence identity with vertebrate RXRs, far surpassing the degree of conservation observed in insects but also by its ability to bind the same ligand as vertebrate RXRs, *9-cis*-retinoic acid (*9-cis*-RA), with an affinity close to that reported for vertebrate RXRs. Similarly, as vertebrate RXRs, the jellyfish RXR showed a specific binding preference for *9-cis*-RA over all-*trans*-retinoic acid (AT-RA) and was able to heterodimerize with vertebrate thyroid hormone receptor alpha. Recent genome sequencing projects confirmed the existence of highly conserved RXR across several metazoan species including insects (*Locusta migratoria* (*Nowickyj et al., 2008*)), that are evolutionarily older than species with a more diversified RXR orthologue such as Usp found in *Drosophila* (reviewed in *Gutierrez-Mazariegos, Schubert & Laudet, 2014*).

To date, the nuclear receptor network has mainly been studied in complex organisms already in possession of an extensive endocrine network. Albeit dissection of nuclear receptor networks in these organisms can outline functions and associated regulatory cascades, basal tasks might be obscured by the gain of further, more specialized functions. Genome analysis of the basal metazoan *Trichoplax adhaerens* by whole genome sequencing revealed four highly conserved nuclear receptors, namely orthologues of HNF4 (NR2A), RXR (NR2B), ERR (NR3B) and COUP-TF (NR2F) (*Baker, 2008*; *Srivastava et al., 2008*) and thus allows assessment of the most basal workings of nuclear receptors. Surprisingly, the degree of conservation of the predicted placozoan NRs with known vertebrate NRs is not only very high at the level of the predicted secondary structure, as can be expected for true NRs, but also at the level of the primary amino acid sequence. Especially the similarity of the placozoan RXR (TaRXR) to its vertebrate orthologues is high, as it is in the case of the cubomedusan RXR. *T. adhaerens,* which shows characteristics of a basal metazoan with only a few cell types (*Smith et al., 2014*) and a relatively simple 4 member NR complement, offers a unique model that may shed light on the evolution of gene regulation by NRs.

In this presented work, we attempted to study the placozoan RXR orthologue functionally. Our results show that *T. adhaerens* RXR binds 9-*cis*-RA with an affinity comparable to that of vertebrate and jellyfish RXRs and that *T. adhaerens* responds to nanomolar concentrations of 9-*cis*-RA with a transcriptional upregulation of the putative orthologue of a malic enzyme that is regulated by a heterodimer formed by liganded thyroid hormone receptor and RXR in vertebrates. We also show that 9-*cis*- RA affects the relative expression of the four NRs present in *T. adhaerens* genome suggesting that these NRs may form a regulatory network capable of responding to possible ligands present in these animals or their environment. In line with this, growth, multiplication and appearance of *T. adhaerens* are strongly affected by food composition, especially by red pigment containing algae suggesting that specific food components or their metabolites may be ligands involved in the ancestral regulatory network of NRs. In support of this, 3.3 nM 9-*cis*-RA interferes with *T. adhaerens* growth response to the feeding by *Porphyridium cruentum* and causes balloon-like phenotypes and death of animals while animals fed by *Chlorella sp*. are partially protected against the treatment by 3.3 nM 9-*cis*-RA, do not develop balloon-like phenotypes but are also arrested in their growth and propagation indicating that 9-*cis*-RA interferes with *T. adhaerens* growth and development.

METHODS

Bioinformatics and cloning of RXR

The predicted RXR gene models on jgi (http://jgi.doe.gov/) (*Nordberg et al., 2014*) were screened for the characteristic molecular signature of the DNA binding domain (C-X2-C-Xl3-C-X2-C-X15-C-X5-C-X9-C-X2-C-X4-C-X4-M) (*Kostrouch, Kostrouchova & Rall, 1995*) and the appropriate predicted gene model (protein ID 53515) was selected for further use.

The alignment of different RXRs was performed by Clustal Omega (http://www.ebi.ac.uk/Tools/msa/clustalo/) (*Sievers et al., 2011*) and adjusted/exported as an image file using Jalview (http://www.jalview.org). Protein domain characterization was performed with SMART (*Schultz et al., 1998*; *Letunic, Doerks & Bork, 2015*). Analysis of HNF4, ERR and COUP-TF was done similarly. Phylogenetic analysis was performed on RXR ClustalO alignment using PhyMLv3.1 (*Guindon et al., 2010*) implemented in SeaView v4.6.1 with a 100 bootstrap analysis and SPR distance computation. The tree was then visualized using FigTree v1.4.3.

T. adhaerens total RNA was obtained from 50-100 pooled individual animals and extracted using TRIZOL® reagent (Invitrogen, Carlsbad, CA, USA) according to the protocol supplied by the manufacturer.

Subsequently, cDNA was prepared with random hexamers and SuperScript III (Invitrogen™) according to the manufacturer's protocol. Several RXR transcripts were then amplified by PCR with primers covering the starting sequence ((GCG-GATCC)ATGGAGGACAGATCGTTTAAAAAA), starting at 32 bp 5′ of ATG (TCTACCAATGTTTATCGCATCGGTTA) and starting at 97 bp 5′ of ATG (TTAAGGCT-TAACTGATGATGTTGTGAATG) with a common reverse primer covering the last 24 bp of the predicted gene sequence ((CGGAATTC)TTAAGAACTGCCTGTTTCCAGCAT).

Each PCR product was then ligated into pCR®2.1-TOPO® or pCR®4-TOPO® vector with the classic TA Cloning Kit and TOPO TA Cloning Kit (Invitrogen™), respectively. The ligated products were then transformed using One Shot® TOP10 Chemically Competent *E. coli* and cultured on LB Agar plates containing 100 μg/ml ampicillin. Plasmid DNA was extracted from obtained colonies and screened for mutations by sequencing using vector specific M13 forward and reverse primers. Only non-mutated sequences were used in subsequent experiments. The RXR fragments were then restricted and inserted into pGEX-2T vector system for bacterial expression (Addgene, Cambridge, MA, USA). Proper insertion was verified by sequencing.

Protein expression

Bl21 pLysS bacteria were transformed with previously described RXR mRNA inserted into pGEX-2T vector. Stocks of transformed bacteria were stored in 8% glycerol according to the Novagen pET System Manual (11th edition) (https://www.google.cz/search?q=Novagen+pET+System+Manual+&ie=utf-8&oe=utf-8&client=firefox-b&gfe_rd=cr&ei=T9z1WMHJDsni8AfpmoGoCQ). For protein expression, bacteria were scraped from stock and incubated in Liquid Broth (LB) with ampicillin (100 μg/ml) and chloramphenicol (34 μg/ml) overnight. The culture was then used to inoculate 100 ml of LB + antibiotics and grown to OD600 = 0.6–0.8 at 37 °C, then induced with 100 μl 1M IPTG (isopropyl-D-thiogalactopyranoside) (Sigma-Aldrich, St. Louis, MO, USA) and moved to 25 °C (RT) for 5 h. The culture was then spun at 9,000 xg for 15 min and the supernatant discarded. The bacterial pellet was resuspended in 10 ml GST binding buffer (25 mM Tris pH 7.5, 150 mM NaCl, 1 mM EDTA) + protease inhibitor (S8820 Sigma Fast, Sigma-Aldrich, St. Louis, MO, USA or cOmplete™, EDTA-free Protease Inhibitor Cocktail, Roche, Basel, Switzerland). Bacteria were then lysed by 6 × 20 s ultrasonication on ice (50 watts, 30 kHz, highest setting—100%) (Ultrasonic Processor UP50H, Hielscher Ultrasonics GmbH, Teltow, Germany) and subsequently incubated with 15–20 mg glutathione agarose beads (Sigma-Aldrich®) prepared according to manufacturer's instructions. Incubation took place at 4 °C for about 10 h after which the beads were washed according to instructions, resuspended in regeneration buffer (50mM Tris–HCl pH7.4, 1mM EDTA, 120 mM KCl, 5 mM DTT, 8% glycerol (v/v)) or 50mM TRIS–HCl pH 7.4 + 9% (v/v) glycerol for subsequent thrombin (bovine plasma, Sigma-Aldrich®) cleavage, if performed, and then adjusted for regeneration buffer conditions. GST-TaRXR was eluted from glutathione agarose beads using 10 mM reduced glutathione (Sigma-Aldrich, StLouis, Mo, USA) in 50 mM Tris–HCl buffer pH 8.0. The size of the GST-TaRXR fusion protein was checked by polyacrylamide gel electrophoresis. Thrombin cleavage was performed at RT for 4 h and the quality of the purified protein was assessed by polyacrylamide gel electrophoresis.

Radioactive *9-cis RA* binding assay

Radioactive ^{3}H-labelled 9-*cis-RA* and ^{3}H-labelled AT-RA were purchased from PerkinElmer (Waltham, MA, USA). Binding was performed in 100 μl binding buffer (50mM Tris–HCl pH7.4, 1mM EDTA, 120 mM KCl, 5 mM DTT, 8% glycerol (v/v), 0.3%

to 0.5% (w/v) CHAPS (3-[(3-Cholamidopropyl)dimethylammonio]-1-propanesulfonate hydrate, Sigma-Aldrich)) for 2 h on wet ice in a dark environment. The protein used for binding was either GST-RXR fusion protein on beads with about 375 ng/assay and thrombin-cleaved RXR. For estimation of specific binding, 200x excess of either 9-*cis*- RA or AT-RA (Sigma-Aldrich) was used. In case of GST-RXR fusion protein, 50 µl of the supernatant was removed after 30 s at 1300 g and washed 3x with 1000 µl wash buffer (50 mM Tris–HCl pH7.4, 1 mM EDTA, 120 mM KCl, 5 mM DTT, 8% (v/v) glycerol, 0.5% (w/v) CHAPS) removing 900 µl after each wash. For cleaved RXR protein 10 µl hydroxyapatite slurry (AG-1 XB Resin, Bio-Rad, Hercules, CA, USA) suspended in binding buffer (12.7 mg/100 µl) were added to the assay and mixed twice, collecting the apatite slurry by centrifugation (15 s at 600 g). 95 µl of the supernatant was removed and the slurry washed twice with 1 ml of wash buffer, removing 900 µl after each wash. Work with retinoids was done under indirect illumination with a 60 W, 120 V yellow light bulb (BugLite, General Electric Co, Nela Parc, Cleveland Oh, USA) as described (*Cahnmann, 1995*). The radioactivity of the GST-fusion protein and cleaved protein was measured using Packard Tri-Carb 1600TR Liquid Scintillation Analyzer (Packard, A Canberra Company, Canberra Industries, Meriden, CT, USA) and Ultima Gold Scintillation Fluid (PerkinElmer, Waltham, MA, USA). The fraction of bound ^{3}H-labelled 9-cis-RA and ^{3}H-labelled all-*trans*-RA was determined as a ratio of the bound radioactivity of precipitated GST-TaRXR/total radioactivity used at the particular condition (determined as the sum of bound radioactivity and the total radioactivity of collected wash fluids) in the absence of non-radioactive competitors or 200 fold excess of 9-cis-RA and all-trans-RA in the case of ^{3}H-labelled 9-*cis*-RA and 40 fold excess of non-radioactive competitors in the case of ^{3}H-labelled all-*trans*-RA (to compensate for the higher affinity of 9-*cis*-RA compared to all-*trans*-RA in binding to TaRXR).

Culture of *T. adhaerens* and algae

Trichoplax adhaerens was cultured in Petri dishes containing filtered artificial seawater (Instant Ocean, Spectrum Brands, Blacksburg, VA, USA) with a salinity of approx. 38–40 ppt. *Rhodomonas salina* (strain CCAP 978/27), *Chlorella sp.*, *Porphyridium cruentum* (UTEX B637) and other non-classified algae, as well as aquarium milieu established in the laboratory by mixing salt water obtained from a local aquarium shop were used to maintain the stock. The cultures were kept at approx. 23 °C and an automated illumination for 12 h/day was used with a conventional light bulb on a daylight background from late spring to mid-summer in the laboratory located at 50.07031N, 14.42934E with laboratory windows oriented eastward. The natural illumination included almost direct morning light from 8 AM to 10.30 AM, indirect sunlight for most of the daytime and sunlight reflected from a building across the street from 1 PM to 6 PM. Algae were maintained as described (*Kana et al., 2012*; *Kana et al., 2014*). The experiments were performed predominantly during sunny weather.

Treatment of *T. adhaerens* with retinoic acids

Incubation of the animals was done overnight in the absence of light. Each batch within an experiment was derived from similar cultures and fed with similar amounts and

composition of algae. All experiments were started in a dark room with indirect yellow light illumination (similarly as in the case of the ligand binding studies) and further incubations were done in the dark for 24 h. In experiments aimed at the visualization of 9-*cis*-RA effect on *T. adhaerens* response to feeding conditions, parallel cultures were set and fed with *P. cruentum*. Large animals of approximately the same size were individually transferred to new control and experimental cultures and fed with *P. cruentum* algal cells. After 6 h of incubation under natural indirect illumination, all animals in both control and experimental cultures were photographed (max. magnification on Olympus SZX7 with Olympus E-410 camera) and the final volume of cultures was adjusted to 50 ml (determined by the weight of cultures in 110 mm glass Petri dishes). Next, the room was darkened and further manipulations were done under indirect illumination with yellow light. Five μl of vehicle (1% DMSO in ethanol) or vehicle containing 9-*cis*-RA was added into 50 ml of final volume to the final concentration of 9-*cis*-RA 3.3 nM. Similarly, parallel sub-cultures were prepared from slowly growing cultures fed by microorganisms covering glass slides in an equilibrated 25 l laboratory aquarium and fed by *Chlorella sp*. Cultures were incubated in the dark for 24 h and all animals were counted under microscope and photographed again. The cultures were then left under natural illumination and cultured for an additional two or three weeks. Animals fed by *P. cruentum* were measured again at 72, 90 and 450 h and those fed by *Chlorella sp*. at 72, 90 and 378 h.

Quantitative PCR

Droplet digital PCR was performed on a QX100 Droplet Digital PCR System (Bio-Rad Laboratories, Hercules, CA, USA). For this, *T. adhaerens* was cultured according to culture conditions described and 4-10 animals removed per 100 μl TRIZol reagent (Invitrogen, Carlsbad, CA, USA). Total RNA was measured by a UV spectrophotometer and used as a reference for normalization.

Reverse transcription was performed with SuperScript III Reverse Transcriptase (ThermoFisher, Waltham, MA, USA) according to manufacturer's instructions. The cDNA (corresponding to 100–500 ng of RNA) was then mixed with ddPCR Supermix (Bio-Rad, Hercules, CA, USA) according to the manufacturer's instructions and analyzed. PCR primers were designed using the UPL online ProbeFinder (Roche) software and were as follows:

TaRXR—left:tctgcaagttggtatgaagca, right: agttggtgtgctattctttacgc

TaHNF4 ref|XM_002115774.1|:

left: ggaatgatttgattttacctcgac, right: tacgacaagcgatacgagca

TaCOUP-TF (ref|XM_002109770.1|):

left: attttgaatgctgcccaatg, right: ttactggttgtggagtatggaaac

TaSoxB1 (ref|XM_002111308.1|):

left: tgtcagatgcggataaacga, right: ggatgttccttcatgtgtaatgc

TaTrox-2 (ref|XM_002118165.1|):

left: gcctatagtcgatcctgccata, right: ttggtgatgatggttgtcca

TaPaxB1 (gb|DQ022561.1):

left: tcaaacgggttctgttagcc, right: ggtgttgccaccttaggc

TaERR (nuclear receptor 3, gb|KC261632.1):
left: ttacgcatgtgatatggttatgg, right: agcgtgcctatttatttcgtct

Results were subsequently analyzed using the Bio-Rad ddPCR software. Manual correction of the cut off was performed when automated analysis was not possible. To visualize changes in nuclear receptor expression in the absence of a reliable housekeeping gene as a reference, we considered the absolute quantity of each nuclear receptor as a percentage of the overall nuclear receptor expression and subsequently visualized the change of receptor expression by subtraction of the percentage of the control experiment. Absolute copy numbers of the proposed malic enzyme orthologue in *T. adhaerens* have been normalized to overall RNA quantity for expressional analysis.

Experiments with quantification by qRT-PCR were performed on a Roche LightCycler II with OneTaq polymerase and the same probes as for ddPCR.

For the estimation of the relative expression of NRs in small (<0.5 mm) versus big animals (>1 mm), 20 to 30 animals from the same culture were used for each paired experiment.

Identification of *T. adhaerens* orthologue of L-malate-NADP$^+$ oxidoreductase (EC 1.1.1.40)

P48163 (MAOX_HUMAN) protein sequence was used as the query sequence and searched against *T. adhaerens* database with BLASTP on http://blast.ncbi.nlm.nih.gov/Blast.cgi using standard algorithm parameters. The best hit was a hypothetical protein TRIADDRAFT_50795 with a sequence identity of 57% and a query coverage of 93% and was assumed to be *T. adhaerens* closest orthologue of vertebrate L-malate-NADP$^+$ oxidoreductase.

Microscopy and image analysis

Observation of *T. adhaerens* was done with an Olympus SZX10 microscope equipped with DF Plan 2x objective and Olympus DP 73 camera operated by CellSens Dimension computer program (kindly provided by Olympus, Prague, Czech Republic) or Olympus CKX41 or SZX7 with Olympus E-410 camera and QuickPhoto Micro 3.1 program.

Circularity was calculated by establishing the area (A) and perimeter (p) of *T. adhaerens* using ImageJ (https://imagej.nih.gov/ij/) and then calculated with the isoperimetric quotient $Q = \frac{4\pi A}{p^2}$, (A, Area; p, perimeter). GraphPad Prism 5 (or higher) was used for graphical representation and calculations of the confidence intervals with $p = 0.05$.

RESULTS

T. adhaerens retinoid X receptor shows high cross-species sequence identity

By using the ab initio model of the JGI *Trichoplax* database as a reference, we screened the *Trichoplax* JGI database for RXR orthologues with a complete DBD and LBD sequence and were able to obtain, as well as verify a full length RXR transcript previously not annotated as the 'best model'. Blastp analysis showed a high sequence similarity to human, as well as mouse RXR with 66% overall sequence identity to human RXR alpha.

SMART analysis of the proposed TaRXR sequence showed a zinc finger DNA binding domain (amino acid residues 16–87) and a ligand binding domain (amino acid residues 155–342) with E values $<10^{-40}$. Blast analysis of the zinc finger DNA binding and ligand binding domains revealed a sequence identity of 81% and 70% to human RXR alpha, respectively. Both domains contained the predicted molecular pattern characteristic for each domain. The heptad repeat LLLRLPAL proposed for dimerization activity (*Forman & Samuels, 1990b*; *Forman & Samuels, 1990a*; *Kiefer, 2006*) as well as the LBD signature for 9-*cis*-RA binding Q-x(33)-L-x(3)-F-x(2)-R-x(9)-L-x(44)-R-x(63)-H (*Egea, Klaholz & Moras, 2000*) were present (Fig. 1). From 11 amino acid residues shown to be critical for 9-*cis*-RA binding (A271, A272, Q 275, L 309, F 313, R 316, L 326, A 327, R 371, C 432, H 435), nine are conserved, while the remaining two amino acids are substituted (A327S, and C432T (C432A in *Tripedalia cystophora*)). Due to the high sequence identity, we propose a 9-*cis*-retinoic acid binding capability of the hypothesized TaRXR sequence, as well as DNA binding capability. Phylogenetic analysis using PhyML algorithm indicates that TaRXR is likely to precede branching of RXRs in cubomedusae and scyphomedusae and clusters with RXRs in bilateria Fig. S1).

The remaining three NRs identified in the *T. adhaerens* genome show also very high overall sequence identity with vertebrate orthologues. Alignments of *T. adhaerens* HNF4, COUP-TF and ERR with orthologues from selected species can be found in File S2.

TaRXR shows preferential binding affinity to *9-cis* retinoic acid over all-*trans*-retinoic acid

In order to analyze the binding properties of TaRXR, we expressed TaRXR as a GST-fusion protein (GST-TaRXR) in bacteria which was then purified as a GST-fusion protein and used directly for binding studies or cleaved by thrombin and eluted as TaRXR. The binding of ^{3}H-labelled 9-*cis*-RA or ^{3}H-labelled all-*trans*-RA was determined by measuring total bound radioactivity and the radioactivity displaceable by 200 fold excess of nonradioactive competitors. Consistent with the high conservation of the LBD, the experiments showed that TaRXR prepared as thrombin cleaved TaRXR or GST-TaRXR binds 9-*cis*-RA with high affinity and specificity (Figs. 2A and 2B). The 9-*cis*-RA binding assay showed high affinity binding to GST-TaRXR with a saturation plateau from 5 nM to 10 nM (Fig. 2C). In contrast, all-*trans*-retinoic acid did not show high affinity binding to TaRXR of GST-TaRXR.

9-cis-retinoic acid induces malic enzyme gene expression at nanomolar concentrations

Next, we searched whether 9-*cis*-RA has observable biological effects on *T. adharens* at nanomolar concentrations. We hypothesized that TaRXR is likely to be involved in the regulation of metabolic events. In vertebrates, RXR is a dimerization partner of TR and together these two NRs are regulating a wide range of metabolic pathways. We, therefore, searched for an orthologue of vertebrate L-malate-NADP^{+} oxidoreductase (EC 1.1.1.40) in *T. adhaerens* genome since this enzyme is an established reporter of the state of thyroid hormone dependent regulation (see 'Discussion').

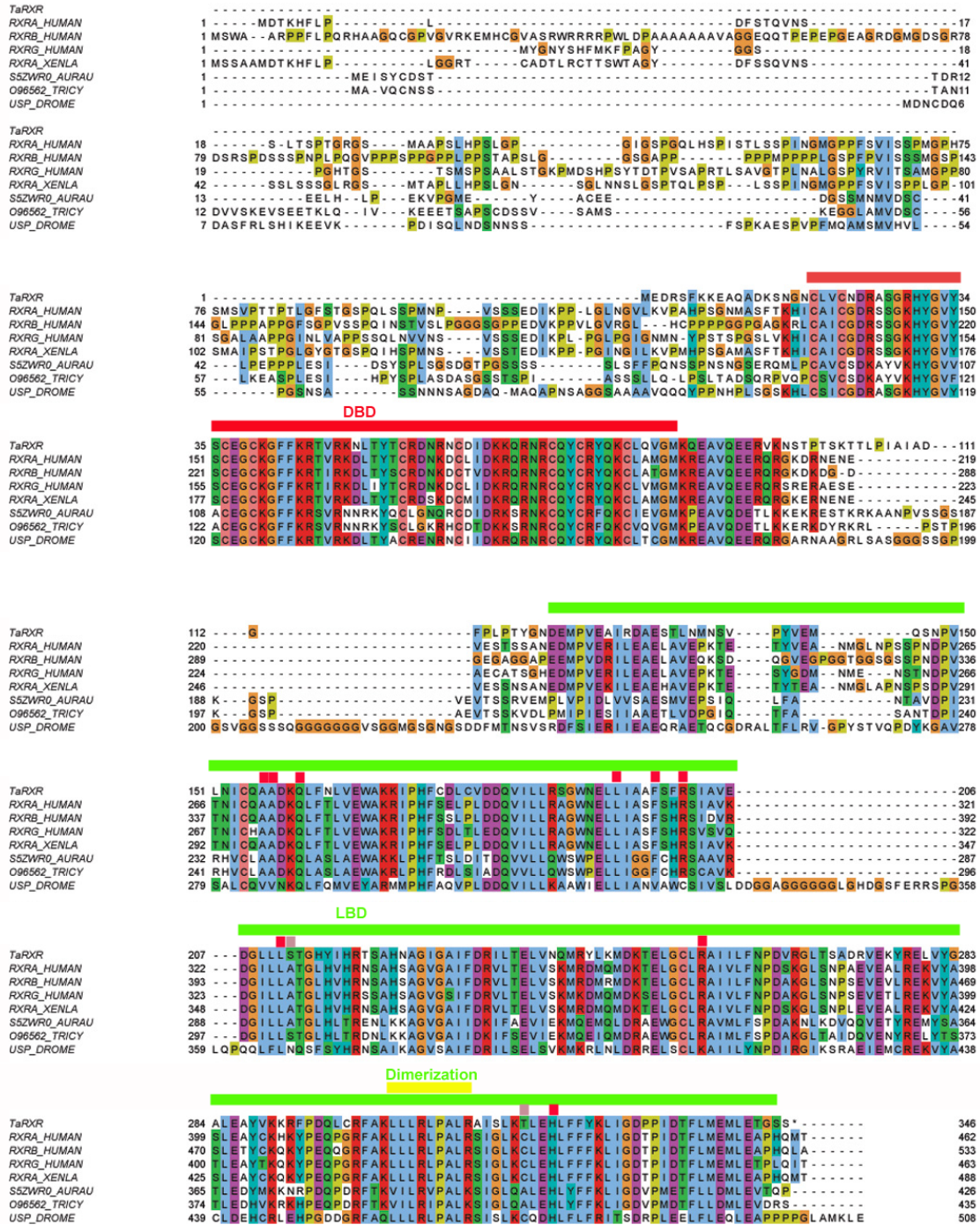

Figure 1 Multiple sequence alignment of selected metazoan homologues of RXR compared with TaRXR. Aligned with ClustalO, amino acid residue types colored according to Clustal scheme in Jalview, * indicates DBD footprint residues, # LBD footprint residues. Black box shows the DBD, red box represents the LBD. Sequences from top to bottom (organism, identifier): *Trichoplax adhaerens*, TaRXR ID 53515; *Homo sapiens*, sp|P19793|RXRA_HUMAN; *Homo sapiens*, sp|P28702|RXRB_HUMAN; *Homo sapiens*, sp|P48443|RXRG_HUMAN; *Xenopus laevis*, RXR alpha, sp|P51128|RXRA_XENLA; *Aurelia aurita*, RXR, tr|S5ZWR0|S5ZWR0_AURAU Retinoid X receptor; *Tripedalia cystophora*, RXR, tr|O96562|O96562_TRICY Retinoic acid X receptor; *Drosophila melanogaster*, USP, sp|P20153|USP_DROME. DNA binding domain (DBD, red line), Ligand binding domain (LBD, green line), dimerization domain (yellow line) and amino acid residues critical for 9-*cis*-RA binding (conserved—red rectangles, not conserved—pink rectangles) are indicated. Readers with specific color preferences may download the compared sequences (File S1) and create the Clustal scheme with different color specifications using the Jalview program (http://www.jalview.org/).

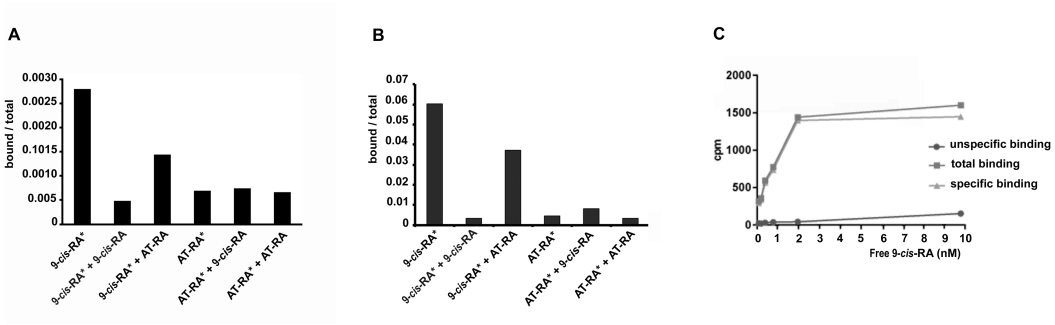

Figure 2 Binding of retinoic acids to TaRXR. (A) Single point analysis of binding preference of *T. adhaerens* RXR (thrombin cleaved) to ^{3}H-labelled 9-*cis*-RA over all-*trans*-RA. Radioactive 9-*cis*-RA (9-*cis*-RA*) binds at a concentration of 4 nM to 200 nanograms of *T. adhaerens* RXR. 200-fold excess of unlabeled *9-cis*-RA displaces more than 80% of labeled *9-cis*-RA from binding to *T. adhaerens* RXR (9-*cis*-RA* + 9-*cis*-RA) while the same molar excess of all-*trans*-RA (9-*cis*-RA*+ AT-RA) which is likely to contain approximately 1% spontaneously isomerized 9-*cis*- RA, competes away less than 50 % of bound ^{3}H-labeled 9-*cis*-RA. Radioactive ^{3}H-labeld all-*trans*-RA (AT-RA*) at identical conditions binds only slightly more than the observed non-specific binding. This interaction is not displaced by the excess of non-labeled 9-*cis*-RA (AT-RA* + 9-*cis*-RA) nor non-labeled all-*trans*-RA (AT-RA* + AT-RA). Results are expressed as a ratio of the radioactivity bound to TaRXR/total radioactivity used for the binding at the given condition. (B) Analysis of binding properties of *T. adhaerens* RXR (in the form of GST-TaRXR) to ^{3}H-labelled 9-*cis*-RA and ^{3}H-labelled all-*trans*-RA. The experiment differs from the experiment shown in A in 5-fold greater amount of radioactive all-*trans*-RA (and therefore only 40-fold excess of non-radioactive competitors). The experiment shows identical binding properties of GST-TaRXR as those observed with thrombin cleaved TaRXR. (C) Kinetic analysis of binding of ^{3}H-labeled 9-*cis*-RA to *T. adhaerens* RXR prepared as GST-fusion protein (GST-TaRXR). The plateau is reached at around 3 to 5×10^{-9} M.

The sequence of the *T. adhaerens* likely orthologue of vertebrate L-malate-NADP^{+} oxidoreductase was retrieved from the *Trichoplax* genomic database together with its presumed promoter based on the predicted sequence (File S3).

Droplet digital PCR showed an increased transcription of the predicted L-malate-NADP^{+} oxidoreductase gene after incubation of *T. adhaerens* with 9-*cis*-RA, but not with all-*trans*-RA (Fig. 3). In repeated experiments, we observed that the level of induction was higher at 9-*cis*-RA concentrations in the range of 1 to 10 nM, than above 10 nM. We also noticed that the level of the induction slightly varied based on the actual *T. adhaerens* cultures and the algal food composition of the *T. adhaerens* cultures.

Changes in the culture environment alter the expression pattern of the nuclear receptor complement in *T. adhaerens*

From the experience we gained by culturing *T. adhaerens*, as well as from the previous experiments we knew that the culture conditions could dramatically influence phenotype. Having the possible developmental functions of the ancestral NRs in mind, we raised the question whether the expression patterns of the NRs reflect changes in phenotype.

Firstly, we assayed the relative expression of RXR against all three other NRs in small versus big animals (<0.5 mm or >1 mm). The relative proportion of & expression compared to the remaining NRs was found to be higher in big animals (33%) than in small animals (24%). The treatment by 3.3 nM 9-*cis*-RA led to a dramatic increase of the relative

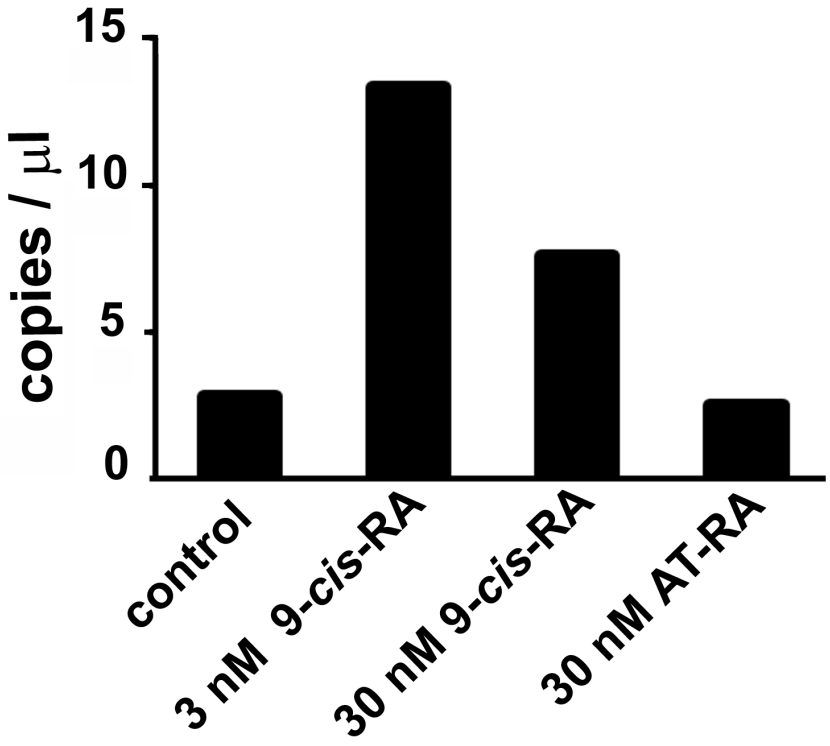

Figure 3 The effect of 9-*cis*-RA on the expression of the *T. adhaerens* closest putative homologue and likely orthologue of L-malate-NADP$^+$ oxidoreductase (EC1.1.1.40). Ten to fifteen animals were cultured in the dark overnight with indicated ligands or in medium containing only the solvent used for ligand solutions. Total RNA and cDNA were prepared using identical conditions and diluted to the same working concentration suitable for ddPCR. In repeated experiments, incubation with 3 nM 9-*cis*-RA induced expression of the putative *T. adhaerens* L-malate-NADP$^+$ oxidoreductase more than four times. Incubation with 30 nM 9-*cis*-RA induced enzyme expression also, but to a lesser extent and 30 nM all-*trans*-RA (AT-RA) did not upregulate the expression of the predicted L-malate-NADP$^+$ oxidoreductase.

expression of RXR in comparison to the rest of the NR complement (51%), indicating that phenotypic changes are connected with differential expression of NRs and that 9-*cis*- RA affects the expression of RXR.

In order to see the effect of 9-*cis*-RA on all NRs, we sampled and extracted RNA from cultures containing the same number of big and small animals treated with different concentrations of 9-*cis*-RA. The experimental cultures were started from the same original cultures and during incubation were fed with *Chlorella sp.* only since this algal food showed to have the least effect on *T. adhaerens* cultures. All four *T. adhaerens* NRs were quantified by either qRT-PCR or ddPCR.

Analysis of NR expression pattern in animals incubated with different concentrations of 9-*cis*-RA, revealed a relative increase in RXR expression at low nanomolar concentrations (<10 nM) in repeated experiments. In contrast, further increase of 9-*cis*-RA resulted in smaller changes compared to the expression pattern of NRs in control animals or even reverted the values observed in low nanomolar conditions (Fig. 4).

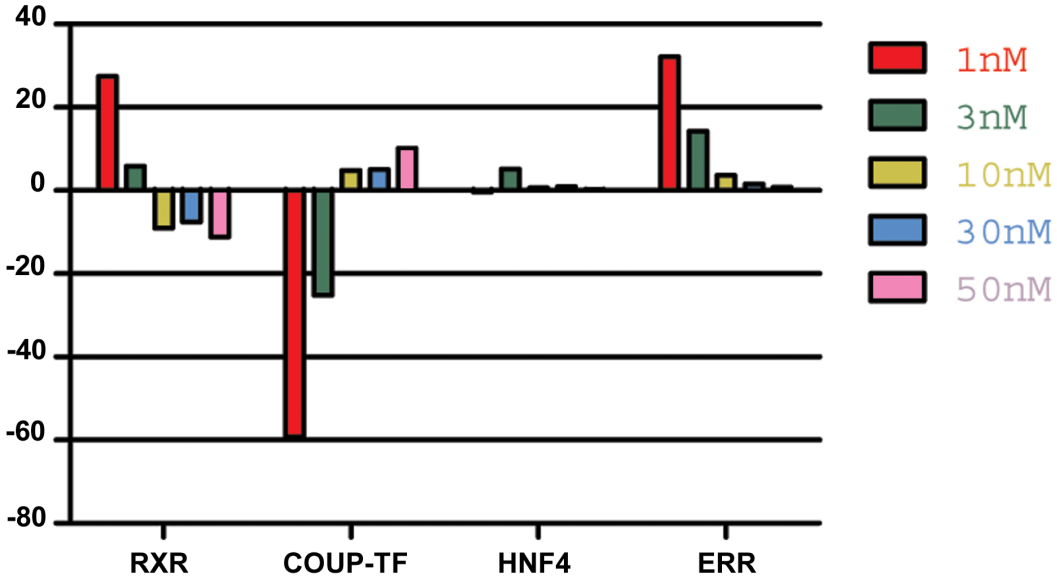

Figure 4 The effect of *9-cis*-RA on the expression of *T adhaerens* NRs. A representative experiment of the expression of *T. adhaerens* NRs in animals exposed to various concentrations of 9-*cis*-RA expressed as a ratio of obtained values compared to the control using ddPCR. One and 3 nM 9-*cis*-RA upregulate RXR and ERR, but downregulate COUP-TF. The expression of *T. adhaerens* HNF4 is not affected by 9-*cis*-RA. The effect of the exposure to 9-*cis*-RA is stronger in the case of 1 nM 9-*cis*-RA compared to 3 nM 9-*cis*-RA. The exposure to 30 nM, as well as 50 nM concentrations of 9-*cis*-RA reverse the effect of 9-*cis*-RA on the expression of RXR and COUP-TF, but do not influence the expression of ERR. The level of expression of HNF4 is not changed by exposure of *T. adhaerens* to various concentrations of 9-*cis*-RA. The data suggest that a network sensitive to nanomolar concentrations of 9-*cis*-RA at the expressional level is formed by RXR, COUP-TF and ERR. All four NRs have conserved P-box (regions responsible for binding to response elements (RE) in gene promoters) and are likely to bind overlapping REs and to form a functional network.

Food composition dramatically changes the phenotype and the reproduction rate of *T. adhaerens*

T. adhaerens retrieved from laboratory aquariums used for the stock cultures were relatively similar in appearance and included small round animals containing approximately 50 cells and grew to animals with an approximate diameter of 0.2 mm and rarely were bigger. Their rate of multiplication when transferred to Petri dishes was doubling in one month or even one week, depending on whether the glass was covered by microbial and algal films established during culturing in aquariums. We attempted to use several defined algae as artificial food. They included *Pyrrenomonas helgolandii*, *Picocystis salinarium*, *Tetraselmis subcoriformis*, *Rhodomonas salina*, *Phaeodactylum tricornutum*, *Porphyridium cruentum* and *Chlorella sp*. Individual subcultures of *T. adhaerens* differed in the rate of propagation and appearance as well as colors that were varying from greenish to brown and reddish taints depending on the food that was used as singular species food or mixtures (Fig. 5). Also, contaminants from the original algal food, which prevailed in some cultures, had an influence on *T. adhaerens* growth and behavior. In controlled experiments, it became clear that some food components or their metabolites are influencing growth and appearance of *T. adherens* more than food availability. When *T. adhaerens* were fed with

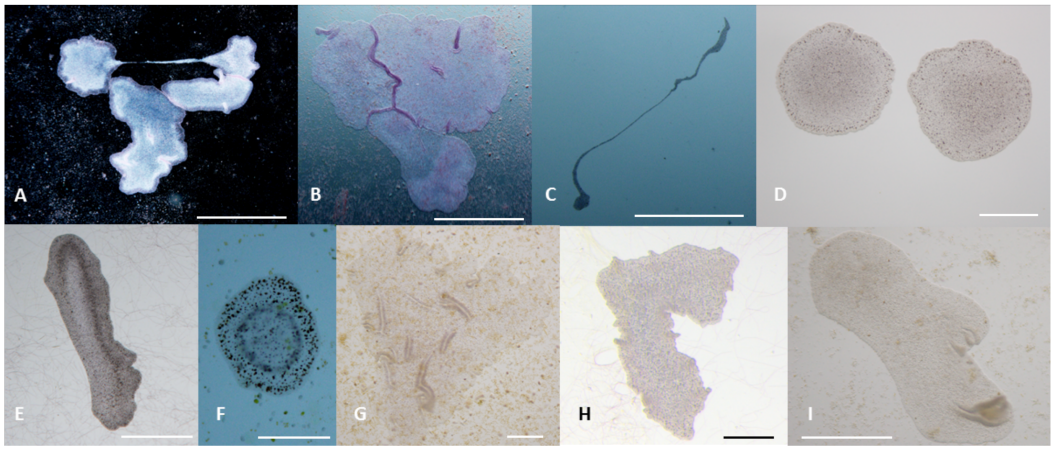

Figure 5 Phenotypes of *T. adhaerens* change at various feeding conditions. *T. adhaerens* acquires various body shapes in individual cultures dependent on food availability and composition. At conditions maintained in stable and biologically equilibrated stock aquariums, *T. adhaerens* is usually small and pale with diameter varying from 50 μm to 400 μm while cultures with added algae contain large flat animals with diameter reaching up to 1 mm (A and B). In some cultures, animals grow as long stretching structures, reaching a length exceeding one or even several centimeters (C). The algal food makes the animals greenish, reddish, rusty or brown with variable proportion of prominent dark cells. Animal shapes also vary from flat and round with smooth circumference, to curved or ruffled circumference or animals with long projections. Bars represent 1 mm in (A, B, I), 1 cm in C, 250 μm in (D), 500 μm in (E and H), 200 μm in (F) , and 100 μm in (G).

equal amounts of algal cells (although they differed in size and expected digestibility), the addition of algae containing red pigments—Cryptophytes (*Pyrrenomonas helgolandii* and *Rhodomonas salina*) or Rhodophyta (*Porphyridium cruentum*)—had a strong positive effect on *T. adhaerens* growth (Fig. 6), especially in combination with the green algae *Chlorella sp.* (Fig. 6).

Furthermore, the addition of *Porphyridium cruentum* to *Chlorella sp.* resulted in a significant change in circularity, while feeding *T. adhaerens* with 'triple food' containing *Chlorella*, *Rhodomonas* and *Porphyridium* showed the most pronounced effect. Culturing *T. adhaerens* on either of the single foods showed similar isoperimetric values (Fig. 7).

9-*cis*-RA interferes with *T. adhaerens* growth response to specific algal food

In order to see the effect of 9-*cis*-RA on *T. adhaerens* in cultures, we exposed cultures kept in a naturally established laboratory microenvironment or fed by specific algal foods to 3, 5 and 10 nM 9-*cis*-RA. The slowly growing cultures kept in naturally established laboratory microenvironment did not show any gross morphological changes even in 10 nM 9-*cis*-RA during the period of one week. Contrary to that, cultures fed with mixed algal food incubated in the presence of 3 and 5 nM 9-*cis*-RA ceased propagation and most animals developed a balloon-like phenotype, and later darkened and decomposed.

For controlled experiments, cultures fed by *P. cruentum* or *Chlorella sp*. were incubated in the presence of vehicle (DMSO/ethanol) or vehicle containing 9-*cis*-RA at 3.3 nM final concentration. After 24 h of incubation in the dark, control cultures fed by *P. cruentum*

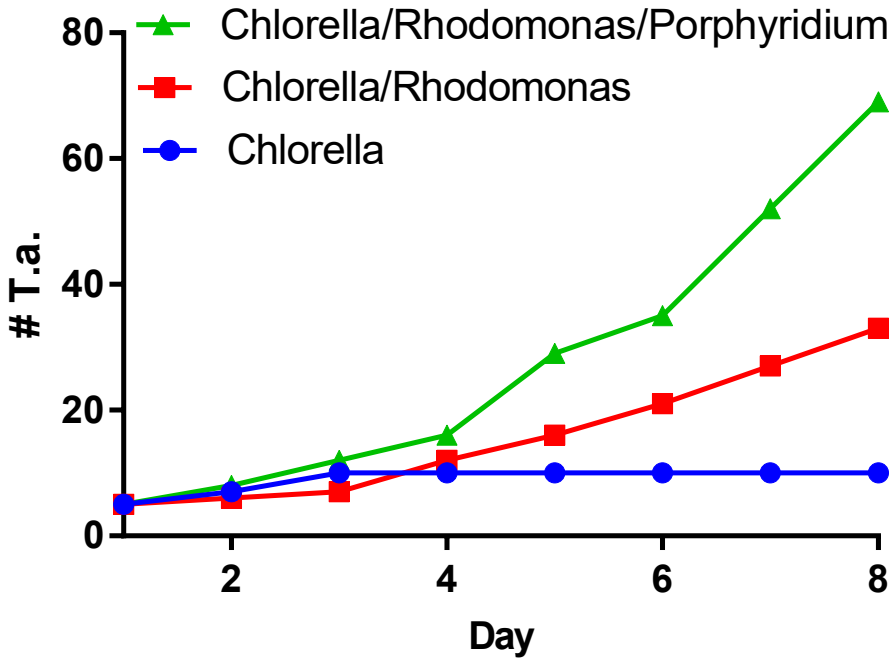

Figure 6 Propagation of *T. adhaerens* depends on algal food composition. Three cultures of five large animals in each were established and fed with the same number of algal cells consisting of *Chlorella sp.*, *Chlorella sp.* and *Rhodomonas salina* and *Chlorella sp.*, *Rhodomonas salina* and *Porphyridium cruentum*. While the culture fed with *Chlorella sp.* only doubled in the number of animals within a period of one week, cultures with red pigment containing algae multiplied more than five times and 10 times within the same time period.

propagated normally while animals fed by *P. cruentum* and incubated with 9-*cis*-RA decreased their area and perimeter (Fig. 8A). At 72 h of incubation, all animals fed by *P. cruentum* and treated by 3.3 nM 9-*cis*-RA developed the balloon-like phenotype and none of them survived 90 h of exposure to 9-*cis*-RA (Fig. 8B and Fig. S2). Animals transferred from stationary cultures grown in a naturally established laboratory microenvironment and subsequently fed by *Chlorella sp*. suffered initial loses at 24 h of incubation despite that their appearance seemed to be normal and well adopted to the new culture condition at time 0 (regarding feeding with algal food and immediately prior to addition of vehicle or 9-*cis*-RA to the culture and 6 h after the transfer from the parent cultures). Animals that survived the transfer and adopted to feeding by *Chlorella sp*., were not inhibited by exposure to 3.3 nM 9-*cis*-RA for 24 h (Fig. 8C) and even showed a slight statistically not significant increase in their area and perimeter. Nevertheless, the isoperimetric values of animals incubated for 24 h with 9-cis-RA showed a significant increase indicating a decrease of growth or exhaustion of peripheral area, that is likely to contain stem cells that further differentiate into the specialized cell types (*Jakob et al., 2004*). In contrary to animals fed by *P. cruentum,* exposure to 9-*cis*-RA was not associated with the development of the balloon-like phenotype and animals survived more than 250 h (Fig. S3). In contrast to control animals which started to proliferate after 100 h, animals exposed to 9-*cis*-RA did not proliferate between 90 and 280 h of subsequent culture (Fig. 8D) suggesting that

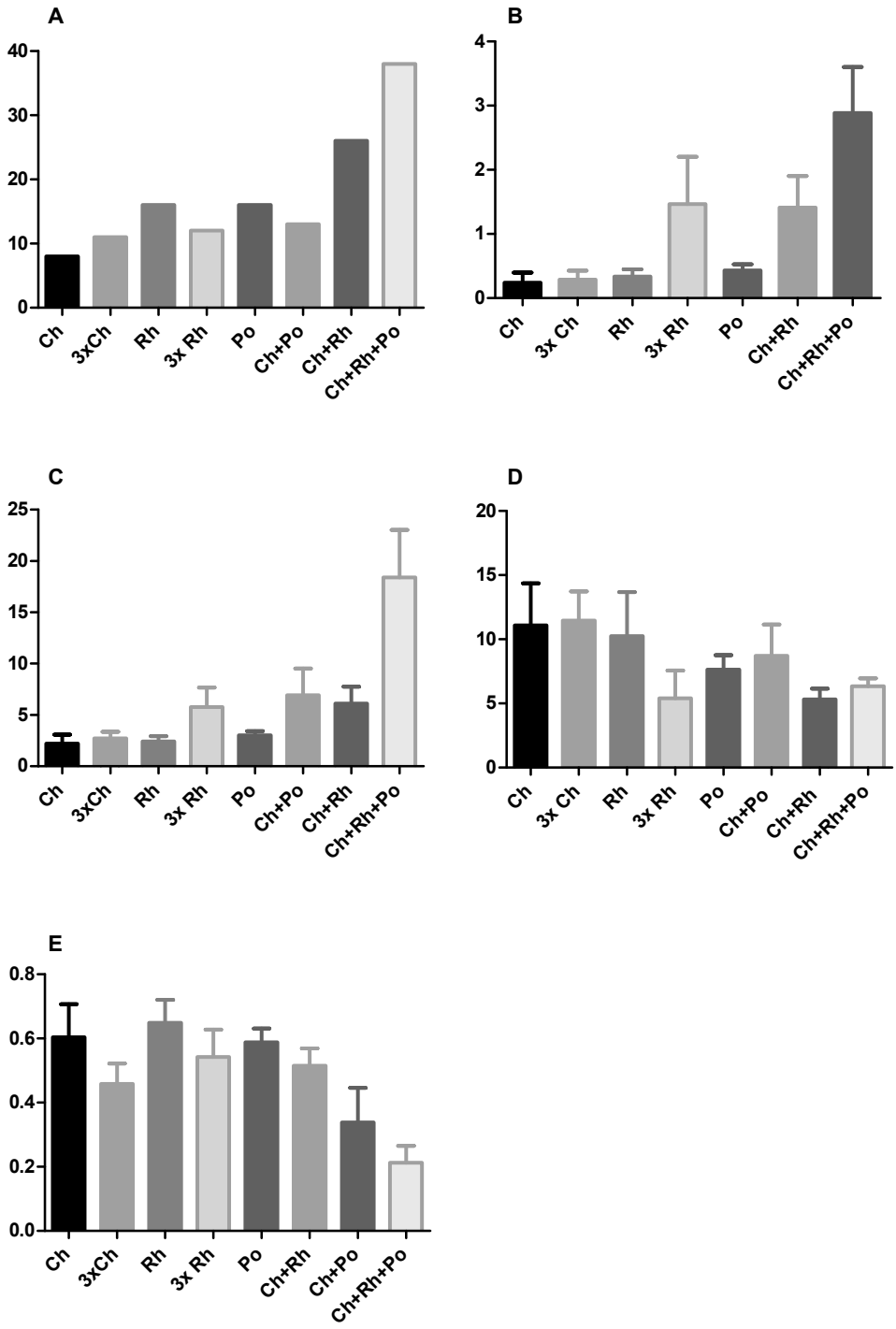

Figure 7 The effect of algal food composition on *T. adhaerens* growth and appearance. *T. adhaerens* was cultured similarly as shown in Fig. 6 and all animals were photographed and analyzed using ImageJ program for their number (A), mean area (B), mean perimeter (C), mean perimeter/area ratio (D) and mean isometric quotient (E) (continued on next page…)

Figure 7 (…continued)
after one week. Ch—stands for feeding with *Chlorella sp.*, Rh—*Rhodomonas salina*, Po—*Porphyridium cruentum*, and their combinations. 3Rh stands for a culture with three times higher concentration of *Rhodomonas salina* and 3Ch for three times higher concentration of *Chlorella sp.* (A) shows that addition of *Rhodomonas salina* (Ch + Rh) greatly increases the number of animals observed after one week of culture. This effect is even more pronounced in cultures containing all three algae, while three times bigger concentration of only one type of algae (Ch and Rh) has little or no effect. This is even more pronounced when the area and perimeter are determined (B and C). Determination of the isoperimetric quotient in individual cultures indicates that cultures with *Rhodomonas salina* have a significantly smaller ratio, suggesting higher proliferative rate of structures at the animal circumference (E). Bars represent 95% confidence interval. Raw data are provided as Files S5 and S6.

9-*cis*-RA interferes with animal response to specific food and processes necessary for animal growth and propagation. The growth arrest of *T. adhaerens* caused by 9-*cis*-RA was reverted by addition of *Porphyridium cruentum* indicating that a specific food constituent rather than food availability interferes with 9-*cis*-RA regulatory potential (Fig. S4).

DISCUSSION

T. adhaerens is probably the closest living species to basal metazoans with only four NRs

Trichoplax adhaerens is an especially interesting species from an evolutionary perspective. It shows the most primitive metazoan planar body arrangement known with a simple dorsal-ventral polarity, the establishment of which is one of the most ancient events in evolution of animal symmetries (*Smith et al., 1995*; *Stein & Stevens, 2014*). The Placozoa are disposed with only a few (probably six) morphologically recognizable cell types (*Jakob et al., 2004*; *Smith et al., 2014*).

In strong contrast to this, the *T. adhaerens* genome shows larger blocks of conserved synteny relative to the human genome than flies or nematodes (*Srivastava et al., 2008*). Genome analyses indicate that Placozoa are basal relative to Bilateria as well as all other diploblastic phyla (*Schierwater et al., 2009*), but all kinds of different views are also discussed (reviewed in *Schierwater et al., 2016*).

In concordance with this, its genome contains four (*Srivastava et al., 2008*) rather than 17 NRs, which can be found in the cnidarian *Nematostella vectensis* (*Reitzel & Tarrant, 2009*). Even though it has been proposed that Placozoa lost representatives of NR6 (SF1/GCNF), TR2/TR4 of the NR2 subfamily and invertebrate specific nuclear receptors (INR, clade of invertebrate-only nuclear receptors with no standard nomenclature) NR1/NR4 (*Bridgham et al., 2010*). The reasoning in this direction depends on the assumed phylogenic position of the phylum Placozoa.

The four NRs found in the genome of *T. adhaerens* are relatively highly related to their vertebrate counterparts, RXR (NR2B), HNF4 (NR2A), COUP-TF (NR2F) and ERR (NR3B) (*Srivastava et al., 2008*). Among them, *T. adhaerens* RXR and HNF4 show the highest degree of identity in protein sequence and the relatedness of *T. adhaerens* RXR (TaRXR) to human RXR is similar to that of *Tripedalia cystophora* RXR (jRXR) (*Kostrouch et al., 1998*), which has also been shown to bind 9-*cis*-RA at nanomolar concentrations. These results suggest that TaRXR is structurally and also functionally very closely related

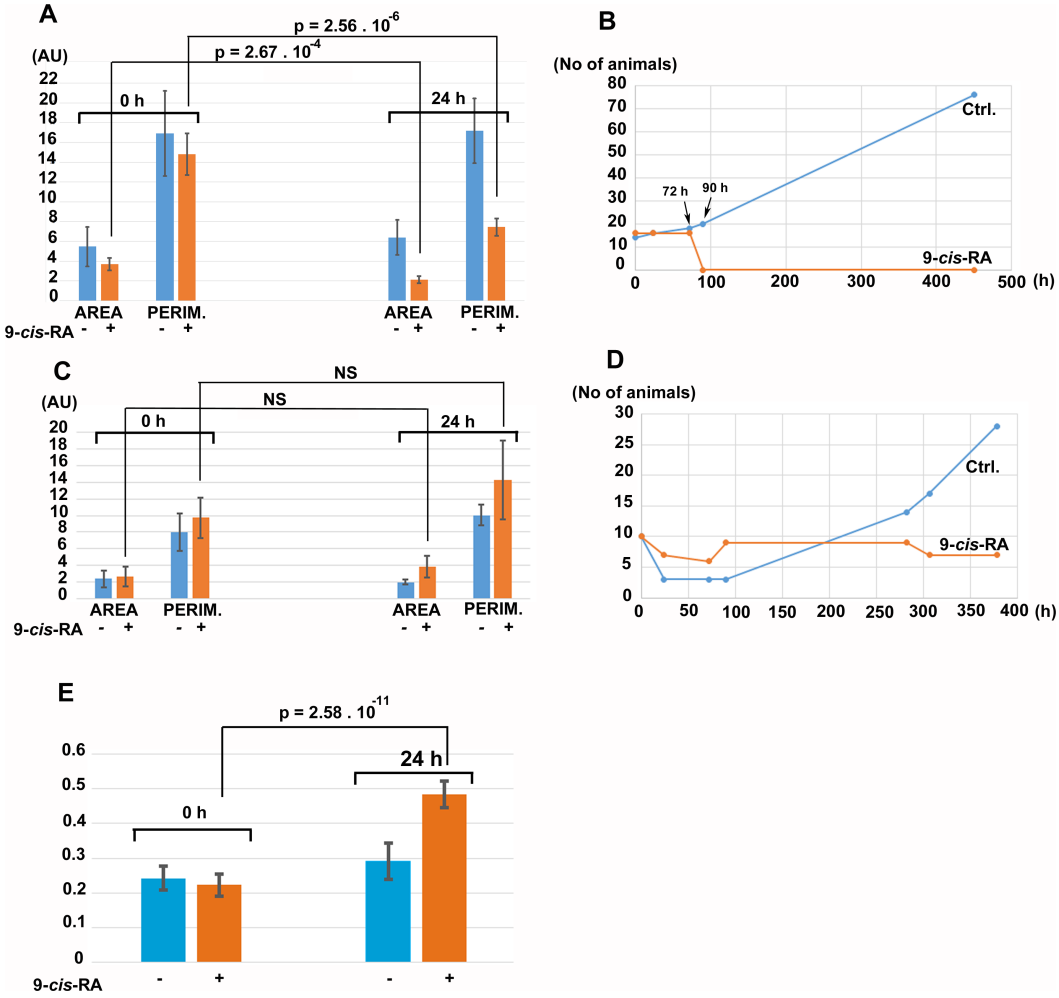

Figure 8 **The effect of 9-*cis*-RA on growth of *T. adhaerens* fed by *Porphyridium cruentum* or *Chlorella sp.*** (A) shows the comparison of the total area and total perimeter of control *T. adhaerens* and *T. adhaerens* treated by 9-*cis*-RA for 24 h expressed as arbitrary units derived from pixel measurements obtained at 24 h and compared to values obtained immediately prior to incubation. The data indicates that animals incubated in 3.3 nM 9-*cis*-RA decreased their area and perimeter to approximately 50% in comparison to control animals. (B) shows the development of cultures over a three-week period. The animals treated by 9-*cis*-RA developed a balloon-like phenotype at 72 h of incubation and died at 90 h of incubation. (C and D) show the data obtained with *T. adhaerens* originating from cultures fed by naturally established biofilms in laboraotory aquariums, fed by *Chlorella sp.* and treated similarly as shown in (A and B). (E) shows the analysis of circularity of animals presented in (A) and documents that animals treated by 9-*cis*-RA increased their circularity already at 24 h of exposure suggesting arrest of growth of animal peripheral tissues.

to its vertebrate counterparts, most probably representing the most basal liganded NR of all Metazoa known today.

T. adhaerens RXR binds preferentially 9-*cis*-RA

By using a radioactively labelled ligand, we could demonstrate that the RXR orthologue in *T. adhaerens* binds 9-*cis*-RA with very high affinity and shows a strong binding preference

to 9-*cis*-RA over all-*trans*-RA similarly, as is the case in vertebrate RXRs (*Allenby et al., 1993*) and the cnidarian TcRXR (*Kostrouch et al., 1998*).

9-*cis*-RA affects the expression of a *T. adhaerens* orthologue of a conserved metabolically active enzyme, L-malate-NADP$^+$ oxidoreductase

A biological role of 9-*cis*-RA binding with high affinity to the placozoan RXR receptor is supported by our *in vivo* experiments. In the search for genes that may be under the regulation of TaRXR, we identified a putative orthologue of vertebrate L-malate-NADP$^+$ oxidoreductase (EC 1.1.1.40) and analyzed the effect of 9-*cis*-RA or all-*trans*-RA on its expression. In agreement with our binding experiments, we observed induction of this enzyme's expression at low nanomolar concentrations of 9-cis-RA (1 to 10 nM). Interestingly, higher concentrations of 9-*cis*-RA (30 nM) had a smaller effect on expression and all-*trans*-RA had no effect up to 30 nM concentrations. A plausible explanation for this could be that 9-*cis*-RA also acts as a ligand for other *T. adhaerens* NRs which may have an opposite effect on the expression of L-malate-NADP$^+$ oxidoreductase. Furthermore, 9-*cis*-RA could act as a supranatural ligand and the continuous occupation of TaRXR by this high affinity ligand may interfere with the normal function of the receptor within the transcription initiation machinery.

In mammals, regulation of malic enzyme expression is mediated by a thyroid hormone receptor (TR)—RXR heterodimer (*Dozin, Cahnmann & Nikodem, 1985*; *Dozin, Magnuson & Nikodem, 1985*; *Petty et al., 1989*; *Petty et al., 1990*). By showing a 9-*cis*-RA dependent change in the expression of the likely placozoan malic enzyme orthologue *in vivo*, we provide indirect evidence of a conserved RXR mediated regulation of gene expression. Although the expression of L-malate-NADP$^+$ oxidoreductase in mammals is usually used as a factor reflecting regulation by thyroid hormone (*Dozin, Magnuson & Nikodem, 1986*), it has also been shown that its cell-type associated differences depend on the expression level of RXR alpha (*Hillgartner, Chen & Goodridge, 1992*; *Fang & Hillgartner, 2000*) suggesting that regulation by RXR has been conserved throughout metazoan evolution while additional regulation via thyroid hormone represents an innovation of Bilateria (*Wu, Niles & LoVerde, 2007*).

NRs form a network responding to 9-*cis*-RA

Since autoregulation and cross-regulation of NRs by their specific ligands is well documented for a large number of nuclear receptors (*Tata, 1994*), we searched if 9-*cis*-RA affects the expression of TaRXR mRNA relative to the other *T. adhaerens* NRs. Our *in vivo* experiments showed not only effects on specific gene expression in response to very low concentrations of 9-*cis*-RA (at 1 or 3 nM), but also an additional dose-dependent reverse effect of higher concentrations. This is likely to be in line with our binding experiments that suggested the possibility of an additional binding site or sites with higher capacity and lower affinity. We also cannot rule out that higher concentrations of 9-*cis*-RA affect some of the three remaining *T. adhaerens* NRs. Nevertheless, an inhibitory effect of 9-*cis*-RA on the expression of its cognate receptor at the protein level (through protein degradation) was reported (*Nomura et al., 1999*).

Although it is not clear if 9-*cis*-RA is the natural ligand for RXRs (*Wolf, 2006*; *Ruhl et al., 2015*) conserved in all metazoan phyla studied to date, we show not only that 9-*cis*-RA binds TaRXR with nanomolar affinity but also positively regulates its expression, which resembles auto-activation of several NRs in vertebrates (e.g., ER and TR (*Tata, 1994*; *Bagamasbad & Denver, 2011*)). Furthermore, three out of four NRs constituting the NR complement in *T. adhaerens* respond to treatment by 9-*cis*- RA at transcriptional level. Two NRs, RXR itself and ERR, respond positively to nanomolar concentrations of 9-*cis*-RA, while COUP-TF, which often acts as an inhibitor of specific gene expression (*Tran et al., 1992*), is regulated negatively by 9-*cis*-RA. COUP-TF was recently shown to be inactivated by small hydrophobic molecules (*Le Guevel et al., 2017*). The regulatory connections of *T. adhaerens* NRs places the autoregulation and cross-regulation of NRs to the base of metazoan evolution. The proposed regulatory network of *T. adhaerens* NRs is schematically represented in Fig. S5.

Food composition rather than quantity affects phenotype of *T. adhaerens*

At first glance, *T. adhaerens* seems to benefit from any source of biological material on surfaces that can be digested and absorbed by its digestive system (e.g., aquarium microorganisms and detritus). Feeding with certain live microorganisms in laboratory cultures, however, dramatically changes the dynamics of *T. adhaerens* cultures, such as shape, size, color, body transparency, growth and divisions of the animal. For example, we observed poor growth and reproduction rates of *T. adhaerens* fed solely on *Chlorella sp.* even at a relatively high density. In contrast, cultures fed with red pigment containing *Rhodomonas salina* showed much faster proliferation and led, in part, to the formation of giant animals, seeming to halt their division. Despite *Porphyridium cruentum* containing similar pigments as *Rhodomonas*, such as phycoerythrin, cultures grown with *Porphyridium* as the main nutrient source did not show phenotypical abnormalities but the addition of it to a culture with *Chlorella* and *Rhodomonas* resulted in an additive effect on reproduction rate.

Even though the growth of *T. adhaerens* seems to follow a simple program, it is likely to require strict regulatory mechanisms. Formation of specific cellular types is connected with phenotypic appearance of animals possessing larger proportions of certain cells, e.g., upper epithelium in balloon-like animals or larger proportion of peripheral regions containing stem cell-like cells in narrow or prolonged animals. Analysis of circularity as a measure of location specific cellular proliferation is in concordance with the observed culture characteristics and shows that lower isoperimetric values (less 'roundness') indicate higher reproduction rates.

Our experiments provide evidence that food composition is more important for *T. adhaerens* growth and propagation than its quantity, which is in line with the recent finding of phosphate and nitrate playing important roles determining the distribution of placozoans around the globe (*Paknia & Schierwater, 2015*). It indicates that food constituents, especially those present in the algae containing phycobilin based red pigments like *Rhodomonas salina* and *Porphyridium cruentum* might possess hormone-like molecules or molecules resulting in hormone-like metabolites in *T. adhaerens* that act through the

NR complement and, indeed, analysis of NRs in differently sized animals indicates impact of food composition on NR expression.

The high sensitivity of *T. adhaerens* to 9-*cis*-RA reflected by the transcriptional response to low nanomolar concentrations of 9-*cis*-RA but not all-*trans*-RA and the interference of 3.3 nM 9-*cis*-RA with the animal response to feeding together with the high affinity binding of 9-*cis*-RA by TaRXR suggests that the response of *T. adhaerens* to 9-*cis*-RA is mediated by TaRXR. It cannot be excluded that other *T. adhaerens* NRs, especially TaCOUP-TF and possibly also TaHNF4 may also be affected by 9-*cis*-RA. It seems possible that 9-*cis*-RA or similarly shaped molecules may be present in *T. adhaerens* food or can be formed from retinoids and other molecular components of food. Our data indicate that the sensitivity of *T. adhaerens* to 9-*cis*-RA depends on the actual feeding conditions and animal growth. There are several possible scenarios that may explain the high sensitivity of *T. adhaerens* to 9-*cis*-RA. The activation of RXR by 9-*cis*-RA or similar compounds has been documented in vertebrates (*Allenby et al., 1993*; *Ruhl et al., 2015*; *De Lera, Krezel & Ruhl, 2016*). The observation of 9-*cis*-RA induced growth arrest is similar as data reported on mammalian cells (e.g., *Wente et al., 2007*) however the concentration of 9-*cis*-RA used in our experiments is approximately 30 to 3,000 times lower than the levels reported in most mammalian systems. It seems likely that very low concentrations of natural ligands including 9-*cis*-RA or similarly shaped molecules or other molecules present in the algal food or produced from algal food as metabolites in *T. adhaerens* regulate the gene expression via RXR in *T. adhaerens*. This may be connected with *T. adhaerens* strong response to light exposure visible as coordinated relocations of animals inside laboratory culture containers and a strong influence of annual seasons on *T. adhaerens* propagation rates observed in laboratories localized in temperate geographical zones. The 9-*cis* conformation of RA is not only sensitive to light exposure with its reversal to all-trans conformation but it can also be formed by specific UV irradiation from all-trans conformation up to 10% as shown by Dr. Hans Cahnmann (*Cahnmann, 1995*).

Chlorophyll hydrophobic side chain which anchors the molecule to the chloroplast thylakoid membrane is metabolized to phytol that was shown to act as an RXR agonist (*Kitareewan et al., 1996*). Other molecules called rexinoids, which often contain aromatic rings in their structure act as RXR agonists or antagonists (*Dawson & Xia, 2012*). Lately, another group of ligands called organotins was shown to affect regulation by RXR (*Le Maire et al., 2009*). It has been proposed that RXRs can bind a larger group of polyunsaturated fatty acids (docosahexaenoic acid and arachidonic acid) and act as their sensors (*De Urquiza et al., 2000*; *Lengqvist et al., 2004*).

When viewed together, our work shows the presence of 9-*cis*- RA binding RXR in Placozoa and argues for the existence of ligand regulated NRs at the base of metazoan evolution. Our observations suggest the existence an endocrine-like regulatory network of NRs in *T. adhaerens* (schematically represented in Fig. S5). Endocrine, hormone-receptor regulations involving NRs may be viewed as specialized, very powerful yet not prevailing regulations transmitted by NRs. Increasingly larger numbers of non-hormonal ligands originating in environment, food or metabolism are emerging as regulatory molecules of NRs (*Holzer, Markov & Laudet, 2017*). Our data suggest that non-hormonal, environment

and food derived ligands are likely to be the first or very early ligands regulating the metazoan response to food availability and orchestrating growth of basal metazoans and necessary differentiation to specialized cell types. In this sense, NRs in *T. adhaerens* represent an endocrine-like system of ancestor NRs.

This work suggests that ligand regulated RXR is involved in the coordination of animal growth and development throughout the metazoan evolution. This also suggests that the regulation by liganded NRs evolved as an evolutionary need connected with heterotrophy and multicellularity.

In fact, despite fragments of NR domains being found in prokaryotes, no single full sized NR has been discovered in bacteria or archaea and the closest known relatives to metazoans, unicellular and colonial Choanoflagellates, lack nuclear receptors, as well as genes of several other regulatory pathways (*King et al., 2008*). On the other hand in fungi, the sister group of Holozoa, *Shalchian-Tabrizi et al., (2008)* transcription factors surprisingly similar to metazoan NRs evolved independently possibly for the regulation of metabolism and response to xenobiotics (*Thakur et al., 2008*; *Naar & Thakur, 2009*). Thus, the evolution of NRs seems to be associated with two key evolutionary features of metazoans: multicellularity and heterotrophy.

Ctenophores, a possible sister phylum to *Cnidaria*, do not contain classical NRs featuring both mechanistically critical domains of NRs, the DNA binding and ligand binding domains. Nevertheless, the ctenophore *Mnemiopsis* contains two orthologues of NR2A (HNF4) that lack the DNA binding domain (*Reitzel et al., 2011*).

Our observations of the exceptionally high sensitivity of *T. adhaerens* to 9-*cis*-RA imply the possibility that the originally very strong regulations mediated by NRs might have been softened or inhibited by additionally evolved mechanisms. To our knowledge, there are no reports of 100% lethal effects of exposure to low nanomolar levels of 9-*cis*-RA in any metazoan organism. It can be speculated that these mechanisms were likely to evolve to modulate 9-*cis*-RA's or similar ligand's regulatory potential further and might involve stronger regulations by heterodimerization partners of RXR and enzymatic or transport mechanisms regulating the availability of ligands in cells and tissues of more recent Metazoa.

In conclusion, the presence of functional nuclear receptors in *T. adhaerens* and their proposed regulatory network support the hypothesis of a basic regulatory mechanism by NRs, which may have been subspecialized with the appearance of new NRs in order to cope with new environmental and behavioral challenges during the course of early metazoan evolution and developmental regulatory needs of increasingly more complex metazoan species.

ACKNOWLEDGEMENTS

The databases of NCBI (*NCBI Resource Coordinators, 2017*) and Joint Genome Institute of United States Department of Energy (http://jgi.doe.gov/) (*Nordberg et al., 2014*) provided bioinformatics support for this study.

ADDITIONAL INFORMATION AND DECLARATIONS

Funding

The main funding sources were: 1/the European Regional Development Fund "BIOCEV—Biotechnology and Biomedicine Centre of the Academy of Sciences and Charles University in Vestec" (CZ.1.05/1.1.00/02.0109) (The Start-Up Grant to the group Structure and Function of Cells in Their Normal State and in Pathology—Integrative Biology and Pathology (5.1.10)); 2/ The grant PRVOUK-P27/LF1/1 from the Charles University; 3/The grants SVV 260377/2017, SVV260257/2016, SVV260149/2015 and SVV 260023/2014 from the Charles University. This work was supported by the research project PRVOUK—Oncology P27, awarded by Charles University in Prague and by the project OPPK No. CZ.2.16/3.1.00/24024, awarded by European Fund for Regional Development (Prague & EU—We invest for your future). PROGRES Q26/LF1. This work was also supported by the Ministry of Education, Youth and Sports of CR within the LQ1604 National Sustainability Program II (Project BIOCEV-FAR) and by the project "BIOCEV" (CZ.1.05/1.1.00/02.0109). The work of Radek Kaňa was further supported by GACR 16-10088S and by the institutional projects Algatech Plus (MSMT LO1416) and Algamic (CZ 1.05/2.1.00/19.0392) provided by the Ministry of Education, Youth and Sports of the Czech Republic. For getting the project started Bernd Schierwater received support from the German Science Foundation (DEG Schi 277/27-1 and Schi 277/29-1). Authors received monetary support of the work reported in this publication from MediCentrum Praha. Zdenek Kostrouch and Marta Kostrouchová contributed with personal funds to this work. The funders (except authors) had no role in study design, data collection and analysis, decision to publish, or preparation of the manuscript.

Grant Disclosures

The following grant information was disclosed by the authors:
European Regional Development Fund "BIOCEV—Biotechnology and Biomedicine Centre of the Academy of Sciences and Charles University in Vestec: CZ.1.05/1.1.00/02.0109.
Charles University: PRVOUK-P27/LF1/1, SVV 260377/2017, SVV260257/2016, SVV260149/2015, SVV 260023/2014.
PRVOUK—Oncology P27.
European Fund for Regional Development: OPPK No. CZ.2.16/3.1.00/24024.
Grant Agency of the Czech Republic: 16-10088S.
The Ministry of Education, Youth and Sports of the Czech Republic: CZ 1.05/2.1.00/19.0392.
German Science Foundation: DEG Schi 277/27-1 and Schi 277/29-1.

Competing Interests

Marta Kostrouchová is an Academic Editor for PeerJ. Authors declare there are no competing interests.

Author Contributions

- Jan Philipp Novotný, Ahmed Ali Chughtai, Markéta Kostrouchová, Veronika Kostrouchová and David Kostrouch conceived and designed the experiments, performed

the experiments, analyzed the data, wrote the paper, prepared figures and/or tables, reviewed drafts of the paper.

- Filip Kaššák conceived and designed the experiments, performed the experiments, analyzed the data, wrote the paper, reviewed drafts of the paper.
- Radek Kaňa conceived and designed the experiments, contributed reagents/materials/-analysis tools, wrote the paper, reviewed drafts of the paper.
- Bernd Schierwater analyzed the data, contributed reagents/materials/analysis tools, wrote the paper, reviewed drafts of the paper.
- Marta Kostrouchová and Zdenek Kostrouch conceived and designed the experiments, performed the experiments, analyzed the data, contributed reagents/materials/analysis tools, wrote the paper, prepared figures and/or tables, reviewed drafts of the paper, contributed with perosnal funds.

DNA Deposition

The following information was supplied regarding the deposition of DNA sequences:

The sequence has been deposited in GenBank (accession number: MF805762). The raw data has been submitted as Supplementary Files.

Data Availability

The following information was supplied regarding data availability:

The raw data has been submitted as Supplementary Files.

Supplemental Information

Supplemental information for this article can be found online at http://dx.doi.org/10.7717/peerj.3789#supplemental-information.

REFERENCES

Allenby G, Bocquel MT, Saunders M, Kazmer S, Speck J, Rosenberger M, Lovey A, Kastner P, Grippo JF, Chambon P, Levin AA. 1993. Retinoic acid receptors and retinoid X receptors: interactions with endogenous retinoic acids. *Proceedings of the National Academy of Sciences of the United States of America* **90**:30–34.

Bagamasbad P, Denver RJ. 2011. Mechanisms and significance of nuclear receptor auto- and cross-regulation. *General and Comparative Endocrinology* **170**:3–17 DOI 10.1016/j.ygcen.2010.03.013.

Baker ME. 2008. Trichoplax, the simplest known animal, contains an estrogen-related receptor but no estrogen receptor: implications for estrogen receptor evolution. *Biochemical and Biophysical Research Communications* **375**:623–627 DOI 10.1016/j.bbrc.2008.08.047.

Bell EA, Boehnke P, Harrison TM, Mao WL. 2015. Potentially biogenic carbon preserved in a 4.1 billion-year-old zircon. *Proceedings of the National Academy of Sciences of the United States of America* **112**:14518–14521 DOI 10.1073/pnas.1517557112.

Bridgham JT, Eick GN, Larroux C, Deshpande K, Harms MJ, Gauthier ME, Ortlund EA, Degnan BM, Thornton JW. 2010. Protein evolution by molecular tinkering:

diversification of the nuclear receptor superfamily from a ligand-dependent ancestor. *PLOS Biology* **8(10)**:e1000497 DOI 10.1371/journal.pbio.1000497.

Cahnmann HJ. 1995. A fast photoisomerization method for the preparation of tritium-labeled 9-cis-retinoic acid of high specific activity. *Analytical Biochemistry* **227**:49–53 DOI 10.1006/abio.1995.1251.

Dawson MI, Xia ZB. 2012. The retinoid X receptors and their ligands. *Biochimica et Biophysica Acta-Molecular and Cell Biology of Lipids* **1821**:21–56 DOI 10.1016/j.bbalip.2011.09.014.

De Lera AR, Krezel W, Ruhl R. 2016. An endogenous mammalian retinoid X receptor ligand, at last! *ChemMedChem* **11**:1027–1037 DOI 10.1002/cmdc.201600105.

De Urquiza AM, Liu S, Sjoberg M, Zetterstrom RH, Griffiths W, Sjovall J, Perlmann T. 2000. Docosahexaenoic acid, a ligand for the retinoid X receptor in mouse brain. *Science* **290**:2140–2144 DOI 10.1126/science.290.5499.2140.

Dozin B, Cahnmann HJ, Nikodem VM. 1985. Identification of thyroid hormone receptors in rat liver nuclei by photoaffinity labeling with L-thyroxine and triiodo-L-thyronine. *Biochemistry* **24**:5197–5202 DOI 10.1021/bi00340a036.

Dozin B, Magnuson MA, Nikodem VM. 1985. Tissue-specific regulation of two functional malic enzyme mRNAs by triiodothyronine. *Biochemistry* **24**:5581–5586 DOI 10.1021/bi00341a044.

Dozin B, Magnuson MA, Nikodem VM. 1986. Thyroid hormone regulation of malic enzyme synthesis. Dual tissue-specific control. *Journal of Biological Chemistry* **261**:10290–10292.

Egea PF, Klaholz BP, Moras D. 2000. Ligand-protein interactions in nuclear receptors of hormones. *FEBS Letters* **476**:62–67 DOI 10.1016/S0014-5793(00)01672-0.

Escriva H, Bertrand S, Laudet V. 2004. The evolution of the nuclear receptor superfamily. *Essays in Biochemistry* **40**:11–26 DOI 10.1042/bse0400011.

Escriva H, Delaunay F, Laudet V. 2000. Ligand binding and nuclear receptor evolution. *Bioessays* **22**:717–727 DOI 10.1002/1521-1878(200008)22:8<717::AID-BIES5>3.0.CO;2-I.

Escriva H, Langlois MC, Mendonca RL, Pierce R, Laudet V. 1998. Evolution and diversification of the nuclear receptor superfamily. *Annals of the New York Academy of Sciences* **839**:143–146.

Escriva H, Safi R, Hanni C, Langlois MC, Saumitou-Laprade P, Stehelin D, Capron A, Pierce R, Laudet V. 1997. Ligand binding was acquired during evolution of nuclear receptors. *Proceedings of the National Academy of Sciences of the United States of America* **94**:6803–6808.

Fang X, Hillgartner FB. 2000. Alterations in retinoid X receptor-alpha expression contribute to cell-type dependent differences in thyroid hormone regulation of malic enzyme transcription. *Molecular and Cellular Endocrinology* **164**:41–52.

Forman BM, Samuels HH. 1990a. Dimerization among nuclear hormone receptors. *New Biologist* **2**:587–594.

Forman BM, Samuels HH. 1990b. Interactions among a subfamily of nuclear hormone receptors: the regulatory zipper model. *Molecular Endocrinology* **4**:1293–1301 DOI 10.1210/mend-4-9-1293.

Guindon S, Dufayard JF, Lefort V, Anisimova M, Hordijk W, Gascuel O. 2010. New algorithms and methods to estimate maximum-likelihood phylogenies: assessing the performance of PhyML 3.0. *Systematic Biology* **59**:307–321 DOI 10.1093/sysbio/syq010.

Gutierrez-Mazariegos J, Schubert M, Laudet V. 2014. Evolution of retinoic acid receptors and retinoic acid signaling. *Subcellular Biochemistry* **70**:55–73 DOI 10.1007/978-94-017-9050-5_4.

Hillgartner FB, Chen W, Goodridge AG. 1992. Overexpression of the alpha-thyroid hormone receptor in avian cell lines. Effects on expression of the malic enzyme gene are selective and cell-specific. *Journal of Biological Chemistry* **267**:12299–12306.

Holzer G, Markov GV, Laudet V. 2017. Evolution of nuclear receptors and ligand signaling: toward a soft key-lock model? *Current Topics in Developmental Biology* **125**:1–38 DOI 10.1016/bs.ctdb.2017.02.003.

Issemann I, Green S. 1990. Activation of a member of the steroid hormone receptor superfamily by peroxisome proliferators. *Nature* **347**:645–650 DOI 10.1038/347645a0.

Jakob W, Sagasser S, Dellaporta S, Holland P, Kuhn K, Schierwater B. 2004. The Trox-2 Hox/ParaHox gene of Trichoplax (Placozoa) marks an epithelial boundary. *Development Genes and Evolution* **214**:170–175.

Kana R, Kotabova E, Lukes M, Papacek S, Matonoha C, Liu LN, Prasil O, Mullineaux CW. 2014. Phycobilisome mobility and its role in the regulation of light harvesting in red algae. *Plant Physiology* **165**:1618–1631 DOI 10.1104/pp.114.236075.

Kana R, Kotabova E, Sobotka R, Prasil O. 2012. Non-photochemical quenching in cryptophyte alga *Rhodomonas salina* is located in chlorophyll a/c antennae. *PLOS ONE* **7**:e29700 DOI 10.1371/journal.pone.0029700.

Kiefer JC. 2006. Emerging developmental model systems. *Developmental Dynamics* **235**:2895–2899 DOI 10.1002/dvdy.20900.

King N, Westbrook MJ, Young SL, Kuo A, Abedin M, Chapman J, Fairclough S, Hellsten U, Isogai Y, Letunic I, Marr M, Pincus D, Putnam N, Rokas A, Wright KJ, Zuzow R, Dirks W, Good M, Goodstein D, Lemons D, Li W, Lyons JB, Morris A, Nichols S, Richter DJ, Salamov A, Sequencing JG, Bork P, Lim WA, Manning G, Miller WT, McGinnis W, Shapiro H, Tjian R, Grigoriev IV, Rokhsar D. 2008. The genome of the choanoflagellate Monosiga brevicollis and the origin of metazoans. *Nature* **451**:783–788 DOI 10.1038/nature06617.

Kitareewan S, Burka LT, Tomer KB, Parker CE, Deterding LJ, Stevens RD, Forman BM, Mais DE, Heyman RA, McMorris T, Weinberger C. 1996. Phytol metabolites are circulating dietary factors that activate the nuclear receptor RXR. *Molecular Biology of the Cell* **7**:1153–1166.

Kostrouch Z, Kostrouchova M, Love W, Jannini E, Piatigorsky J, Rall JE. 1998. Retinoic acid X receptor in the diploblast, *Tripedalia cystophora*. *Proceedings of the National Academy of Sciences of the United States of America* **95**:13442–13447.

Kostrouch Z, Kostrouchova M, Rall JE. 1995. Steroid/thyroid hormone receptor genes in *Caenorhabditis elegans*. *Proceedings of the National Academy of Sciences of the United States of America* **92**:156–159.

Kostrouchova M, Kostrouch Z. 2015. Nuclear receptors in nematode development: natural experiments made by a phylum. *Biochimica et Biophysica Acta/General Subjects* **1849**:224–237 DOI 10.1016/j.bbagrm.2014.06.016.

Kumar R, Thompson EB. 1999. The structure of the nuclear hormone receptors. *Steroids* **64**:310–319 DOI 10.1016/S0039-128X(99)00014-8.

Laudet V. 1997. Evolution of the nuclear receptor superfamily: early diversification from an ancestral orphan receptor. *Journal of Molecular Endocrinology* **19**:207–226.

Le Guevel R, Oger F, Martinez-Jimenez CP, Bizot M, Gheeraert C, Firmin F, Ploton M, Kretova M, Palierne G, Staels B, Barath P, Talianidis I, Lefebvre P, Eeckhoute J, Salbert G. 2017. Inactivation of the nuclear orphan receptor COUP-TFII by small chemicals. *ACS Chemical Biology* DOI 10.1021/acschembio.6b00593.

Le Maire A, Grimaldi M, Roecklin D, Dagnino S, Vivat-Hannah V, Balaguer P, Bourguet W. 2009. Activation of RXR-PPAR heterodimers by organotin environmental endocrine disruptors. *EMBO Reports* **10**:367–373 DOI 10.1038/embor.2009.8.

Lengqvist J, Mata De Urquiza A, Bergman AC, Willson TM, Sjovall J, Perlmann T, Griffiths WJ. 2004. Polyunsaturated fatty acids including docosahexaenoic and arachidonic acid bind to the retinoid X receptor alpha ligand-binding domain. *Molecular & Cellular Proteomics* **3**:692–703 DOI 10.1074/mcp.M400003-MCP200.

Letunic I, Doerks T, Bork P. 2015. SMART: recent updates, new developments and status in 2015. *Nucleic Acids Research* **43**:D257–D260 DOI 10.1093/nar/gku949.

Markov GV, Laudet V. 2011. Origin and evolution of the ligand-binding ability of nuclear receptors. *Molecular and Cellular Endocrinology* **334**:21–30 DOI 10.1016/j.mce.2010.10.017.

Naar AM, Thakur JK. 2009. Nuclear receptor-like transcription factors in fungi. *Genes and Development* **23**:419–432 DOI 10.1101/gad.1743009.

NCBI Resource Coordinators. 2017. Database resources of the national center for biotechnology information. *Nucleic Acids Research* **45**:D12–D17 DOI 10.1093/nar/gkw1071.

Nomura Y, Nagaya T, Hayashi Y, Kambe F, Seo H. 1999. 9-cis-retinoic acid decreases the level of its cognate receptor, retinoid X receptor, through acceleration of the turnover. *Biochemical and Biophysical Research Communications* **260**:729–733 DOI 10.1006/bbrc.1999.0969.

Nordberg H, Cantor M, Dusheyko S, Hua S, Poliakov A, Shabalov I, Smirnova T, Grigoriev IV, Dubchak I. 2014. The genome portal of the Department of Energy Joint Genome Institute: 2014 updates. *Nucleic Acids Research* **42**:D26–D31 DOI 10.1093/nar/gkt1069.

Nowickyj SM, Chithalen JV, Cameron D, Tyshenko MG, Petkovich M, Wyatt GR, Jones G, Walker VK. 2008. Locust retinoid X receptors: 9-Cis-retinoic acid in embryos from a primitive insect. *Proceedings of the National Academy of Sciences of the United States of America* **105**:9540–9545 DOI 10.1073/pnas.0712132105.

Paknia O, Schierwater B. 2015. Global habitat suitability and ecological niche separation in the phylum placozoa. *PLOS ONE* **10**:e0140162 DOI 10.1371/journal.pone.0140162.

Paris M, Escriva H, Schubert M, Brunet F, Brtko J, Ciesielski F, Roecklin D, Vivat-Hannah V, Jamin EL, Cravedi JP, Scanlan TS, Renaud JP, Holland ND, Laudet V. 2008. Amphioxus postembryonic development reveals the homology of chordate metamorphosis. *Current Biology* **3;18(11)**:825–830 DOI 10.1016/j.cub.2008.04.078.

Petty KJ, Desvergne B, Mitsuhashi T, Nikodem VM. 1990. Identification of a thyroid hormone response element in the malic enzyme gene. *Journal of Biological Chemistry* **265**:7395–7400.

Petty KJ, Morioka H, Mitsuhashi T, Nikodem VM. 1989. Thyroid hormone regulation of transcription factors involved in malic enzyme gene expression. *Journal of Biological Chemistry* **264**:11483–11490.

Reitzel AM, Pang K, Ryan JF, Mullikin JC, Martindale MQ, Baxevanis AD, Tarrant AM. 2011. Nuclear receptors from the ctenophore Mnemiopsis leidyi lack a zinc-finger DNA-binding domain: lineage-specific loss or ancestral condition in the emergence of the nuclear receptor superfamily? *Evodevo* **2**:Article 3 DOI 10.1186/2041-9139-2-3.

Reitzel AM, Tarrant AM. 2009. Nuclear receptor complement of the cnidarian *Nematostella vectensis*: phylogenetic relationships and developmental expression patterns. *BMC Evolutionary Biology* **9**:Article 230 DOI 10.1186/1471-2148-9-230.

Robinson-Rechavi M, Escriva Garcia H, Laudet V. 2003. The nuclear receptor superfamily. *Journal of Cell Science* **116**:585–586 DOI 10.1242/jcs.00247.

Ruhl R, Krzyzosiak A, Niewiadomska-Cimicka A, Rochel N, Szeles L, Vaz B, Wietrzych-Schindler M, Alvarez S, Szklenar M, Nagy L, De Lera AR, Krezel W. 2015. 9-cis-13,14-dihydroretinoic acid is an endogenous retinoid acting as RXR ligand in mice. *PLOS Genetics* **11**:e1005213 DOI 10.1371/journal.pgen.1005213.

Schierwater, Holland PWH, Miller DJ, Stadler PF, Wiegmann BM, Wörheide G, Wray GA, DeSalle R. 2016. Never Ending Analysis of a Century Old Evolutionary Debate: "Unringing" the Urmetazoon Bell. *Frontiers in Ecology and Evolution* **4**:Article 5 DOI 10.3389/fevo.2016.00005.

Schierwater B, Kolokotronis SO, Eitel M, DeSalle R. 2009. The Diploblast-Bilateria Sister hypothesis: parallel revolution of a nervous systems may have been a simple step. *Communicative & Integrative Biology* **2**:403–405.

Schultz J, Milpetz F, Bork P, Ponting CP. 1998. SMART, a simple modular architecture research tool: identification of signaling domains. *Proceedings of the National Academy of Sciences of the United States of America* **95**:5857–5864.

Shalchian-Tabrizi K, Minge MA, Espelund M, Orr R, Ruden T, Jakobsen KS, Cavalier-Smith T. 2008. Multigene phylogeny of choanozoa and the origin of animals. *PLOS ONE* **3**:e2098 DOI 10.1371/journal.pone.0002098.

Sievers F, Wilm A, Dineen D, Gibson TJ, Karplus K, Li W, Lopez R, McWilliam H, Remmert M, Soding J, Thompson JD, Higgins DG. 2011. Fast, scalable generation of high-quality protein multiple sequence alignments using Clustal Omega. *Molecular Systems Biology* **7**:Article 539 DOI 10.1038/msb.2011.75.

Smith CL, Giordano H, Schwartz M, DeLotto R. 1995. Spatial regulation of Drosophila snake protease activity in the generation of dorsal-ventral polarity. *Development* **121**:4127–4135.

Smith CL, Varoqueaux F, Kittelmann M, Azzam RN, Cooper B, Winters CA, Eitel M, Fasshauer D, Reese TS. 2014. Novel cell types, neurosecretory cells, and body plan of the early-diverging metazoan *Trichoplax adhaerens*. *Current Biology* **24**:1565–1572 DOI 10.1016/j.cub.2014.05.046.

Srivastava M, Begovic E, Chapman J, Putnam NH, Hellsten U, Kawashima T, Kuo A, Mitros T, Salamov A, Carpenter ML, Signorovitch AY, Moreno MA, Kamm K, Grimwood J, Schmutz J, Shapiro H, Grigoriev IV, Buss LW, Schierwater B, Dellaporta SL, Rokhsar DS. 2008. The Trichoplax genome and the nature of placozoans. *Nature* **454**:955–960.

Stein DS, Stevens LM. 2014. Maternal control of the Drosophila dorsal-ventral body axis. *Wiley Interdisciplinary Reviews: Developmental Biology* **3**:301–330 DOI 10.1002/wdev.138.

Tata JR. 1994. Autoregulation and crossregulation of nuclear receptor genes. *Trends in Endocrinology and Metabolism* **5**:283–290.

Thakur JK, Arthanari H, Yang F, Pan SJ, Fan X, Breger J, Frueh DP, Gulshan K, Li DK, Mylonakis E, Struhl K, Moye-Rowley WS, Cormack BP, Wagner G, Naar AM. 2008. A nuclear receptor-like pathway regulating multidrug resistance in fungi. *Nature* **452**:604–609 DOI 10.1038/nature06836.

Tran P, Zhang XK, Salbert G, Hermann T, Lehmann JM, Pfahl M. 1992. COUP orphan receptors are negative regulators of retinoic acid response pathways. *Molecular and Cellular Biology* **12**:4666–4676.

Wente W, Brenner MB, Zitzer H, Gromada J, Efanov AM. 2007. Activation of liver X receptors and retinoid X receptors induces growth arrest and apoptosis in insulin-secreting cells. *Endocrinology* **148**:1843–1849 DOI 10.1210/en.2006-1247.

Wolf G. 2006. Is 9-cis-retinoic acid the endogenous ligand for the retinoic acid-X receptor? *Nutrition Reviews* **64**:532–538 DOI 10.1111/j.1753-4887.2006.tb00186.x.

Wu W, Niles EG, LoVerde PT. 2007. Thyroid hormone receptor orthologues from invertebrate species with emphasis on Schistosoma mansoni. *BMC Evolutionary Biology* **7**:150 DOI 10.1186/1471-2148-7-150.